Targeting MYC Function as a Strategy for Tumor Therapy

Hemmung der MYC-Funktion als Strategie für die zielgerichtete Tumortherapie

Doctoral thesis

for a doctoral degree

at the Graduate School of Life Sciences,

Julius-Maximilians-Universität Würzburg, Section Biomedicine

submitted by

Lisa Anna Jung

from Frankfurt am Main

Würzburg 2016

Submitted on:

Members of the Thesis Committee:

Chairperson: Prof. Dr. Manfred Gessler

Primary Supervisor: Prof. Dr. Martin Eilers

Second Supervisor: Prof. Dr. Caroline Kisker

Third Supervisor: Prof. Dr. Bernhard Lüscher

Fourth Supervisor: Prof. Dr. Stefan Gaubatz

Date of Public Defense:

Date of Receipt of Certificates:

Substantial parts of this thesis were published in the following article:

Jung, L.A., Gebhardt, A., Koelmel, W., Ade, C.P., Walz, S., Kuper, J., von Eyss, B., Letschert, S., Redel, C., d'Artista, L., Biankin, A., Zender, L., Sauer, M., Wolf, E., Evan, G., Kisker, C., Eilers, M. (2016). OmoMYC blunts promoter invasion by oncogenic MYC to inhibit gene expression characteristic of MYC-dependent tumors. Oncogene.

Table of Contents

Summary

A large fraction of human tumors exhibits aberrant expression of the oncoprotein MYC. As a transcription factor regulating various cellular processes, MYC is also crucially involved in normal development. Direct targeting of MYC has been a major challenge for molecular cancer drug discovery. The proof of principle that its inhibition is nevertheless feasible came from *in vivo* studies using a dominant-negative allele of MYC termed OmoMYC. Systemic expression of OmoMYC triggered long-term tumor regression with mild and fully reversible side effects on normal tissues.

In this study, OmoMYC's mode of action was investigated combining methods of structural biology and functional genomics to elucidate how it is able to preferentially affect oncogenic functions of MYC.

The crystal structure of the OmoMYC homodimer, both in the free and the E-box-bound state, was determined, which revealed that OmoMYC forms a stable homodimer, and as such, recognizes DNA via the same base-specific DNA contacts as the MYC/MAX heterodimer. OmoMYC binds DNA with an equally high affinity as MYC/MAX complexes. RNA-sequencing showed that OmoMYC blunts both MYC-dependent transcriptional activation and repression. Genome-wide DNA-binding studies using chromatin immunoprecipitation followed by high-throughput sequencing revealed that OmoMYC competes with MYC/MAX complexes on chromatin, thereby reducing their occupancy at consensus DNA binding sites. The most prominent decrease in MYC binding was seen at low-affinity promoters, which were invaded by MYC at oncogenic levels. Strikingly, gene set enrichment analyses using OmoMYC-regulated genes enabled the identification of tumor subgroups with high MYC levels in multiple tumor entities. Together with a targeted shRNA screen, this identified novel targets for the eradication of MYC-driven tumors, such as ATAD3A, BOP1, and ADRM1.

In summary, the findings suggest that OmoMYC specifically inhibits tumor cell growth by attenuating the expression of rate-limiting proteins in cellular processes that respond to elevated levels of MYC protein using a DNA-competitive mechanism. This opens up novel strategies to target oncogenic MYC functions for tumor therapy.

Zusammenfassung

Eine Vielzahl humaner Tumore entsteht durch die aberrante Expression des Onkoproteins MYC. Da MYC als Transkriptionsfaktor viele zelluläre Prozesse reguliert, ist er auch maßgeblich an der Entwicklung von normalem Gewebe beteiligt. Die direkte Hemmung von MYC stellt eine große Herausforderung für die Wirkstoffentwicklung dar. Studien mit dem dominant-negativen MYC-Allel namens OmoMYC belegten, dass MYC ein potenzieller Angriffspunkt für die zielgerichtete Tumortherapie ist. Die systemische Expression dieser MYC-Mutante löste eine dauerhafte Tumorregression aus und zeigte milde sowie vollständig reversible Nebenwirkungen. In der vorliegenden Arbeit wurde der molekulare Wirk-mechanismus von OmoMYC untersucht, wobei sowohl Methoden der Strukturbiologie als auch der funktionalen Genomik angewendet wurden.

Die Kristallstruktur des OmoMYC Proteins wurde im freien und E-Box-gebundenen Zustand bestimmt. Dadurch konnte gezeigt werden, dass OmoMYC ein stabiles Homodimer bildet. Als solches erkennt es DNA mittels derselben basenspezifischen Interaktionen wie der MYC/MAX-Komplex. Dabei bindet OmoMYC DNA mit einer ähnlichen Affinität wie das MYC/MAX-Heterodimer. Die genomweite Expressionsanalyse mittels RNA-Sequenzierung identifiziert eine Reduktion sowohl der MYC-abhängigen Transkriptionsaktiverung als auch der Transkriptionsrepression durch OmoMYC. Mittels Chromatin-Immunpräzipitation gefolgt von einer Hochdurchsatz-Sequenzierung wird gezeigt, dass OmoMYC mit MYC/MAX-Komplexen auf Chromatin konkurriert und so deren Besetzung global an Konsensus-Bindestellen verringert. Die stärkste Reduktion zeigt sich an Promoterregionen mit schwacher Affinität für die MYC-Bindung, welche durch onkogene MYC-Proteinmengen aufgefüllt werden. *Gene set enrichment*-Analysen unter Berücksichtigung von OmoMYC-regulierten Genen erlaubten die Identifizierung von Tumor-Subgruppen mit hohen MYC-Proteinmengen in zahlreichen Tumorentitäten. Zusammen mit einem fokussierten shRNA-Screen können so neue Zielproteine für die Bekämpfung von MYC-getriebenen Tumoren, wie zum Beispiel ATAD3A, BOP1 und ADRM1, identifiziert werden.

Zusammenfassend weisen die Ergebnisse darauf hin, dass OmoMYC spezifisch das Tumorzellwachstum inhibiert, indem es die Expression von zentralen Proteinen limitiert, welche durch erhöhte MYC-Proteinmengen reguliert werden. Somit können neue Strategien zur Tumortherapie identifiziert werden, die auf onkogene Funktionen von MYC zielen.

1 Introduction

1.1 From cytotoxic agents to targeted molecular cancer therapy

Since Ehrlich and Fleming created the basis of chemotherapy over 100 years ago, the development of tumor therapy has taken major steps from the treatment with nitrogen mustard discovered by Goodman and Gilman to rational cancer drug design initiated by Farber (Neidle, 2014; Strebhardt and Ullrich, 2008). Today, the scientific community is facing new advances in both cancer immune therapy and personalized cancer therapy fostered by an increasing, yet incomplete, understanding of the genetics, epigenetics, genomics and biochemistry of human cancers. Despite these efforts, cancer remains the second leading cause of death in developed countries such as Germany and the United States (Kaatsch et al., 2015; Siegel et al., 2015; Torre et al., 2015). Over 580,000 Americans die of cancer every year, and at least 100,000 cancer deaths alone are associated with aberrant expression of the oncoprotein MYC family (Siegel et al., 2015; Tansey, 2014). Hence, the development of new improved cancer therapies is urgently needed and many potential cancer targets are so far undrugged.

A new era of cancer drug development was initiated more than 30 years ago with the identification of cell signaling pathways and oncogenes allowing the design of targeted small molecule therapeutics by medicinal chemists and structural biologists (Neidle, 2014; Strebhardt and Ullrich, 2008). The first successful small molecule therapeutic for targeted cancer therapy was imatinib (Gleevec; STI-571) (Druker, 2002; Druker et al., 2006; O'Brien et al., 2003). The tyrosine kinase inhibitor targets the Abelson (ABL) kinase, which is aberrantly activated in chronic myeloid leukemia (CML) due to a chromosomal translocation creating a BCR (break point cluster)-ABL fusion protein. The tumor cells thus display a unique dependence on the ABL kinase. Imatinib has become the first-line therapy in CML and doubled the survival for patients with CML in less than 20 years (Siegel et al., 2015).

Kinase drug discovery has been very successful. With the help of structural biology and functional genomics, the mode of action and resistance of kinase inhibitors like imatinib and vemurafenib (Zelboraf, targeting the V600E variant of the serine/threonine kinase BRAF) are

understood and a large variety of new protein kinase inhibitors have been developed (Neidle, 2014; van Montfort and Workman, 2009). However, one of the major challenges in cancer drug discovery is still the design of small molecules inhibiting protein-protein and protein-nucleic acid interactions (PPI and PNI, respectively). This was regarded as less feasible since these interfaces are often large, flat, featureless, lacking obvious small molecule binding sites and display high binding energies (Arkin et al., 2014; Mullard, 2012; Wells and McClendon, 2007). Within the last 10-20 years, "hot spots" within large PPI surfaces were discovered by mutational analyses that defined a subset of residues that contributes to a large fraction of the binding free energy (Clackson and Wells, 1995; Guo et al., 2014b; Raj et al., 2013). Areas with a high density of "hot spots", so called "hot spot clusters", are now regarded to be targetable by small molecule inhibitors. Indeed, several protein interface-inhibiting drugs have made it to the clinic.

One example of clinically successful PPI inhibitors is the class of bromodomain inhibitors. Bromodomain proteins are epigenetic ''readers'' that recognize acetylated lysines on histones of active promoters. They play various roles in transcription, replication, epigenetic regulation and DNA repair (Wu and Chiang, 2007). The proof of principle that bromodomain proteins such as BRD4 (bromodomain-containing protein 4) are druggable and of interest for cancer therapy came from the study of (+)-JQ1 (Delmore et al., 2011; Filippakopoulos et al., 2010). JQ1 competitively binds to acetyl-lysine recognition motifs and can thus interfere with the BRD4/histone interaction. Several potent acetyl-lysine mimetic inhibitors have been tested in clinical trials for solid and hematopoietic malignancies, including MYC-associated cancers (e.g., I-BET762: ClinicalTrials.gov identifier NCT01587703; TEN-010: ClinicalTrials.gov identifier NCT01987362; OTX015: ClinicalTrials.gov identifier NCT01713582; CPI-0610: ClinicalTrials.gov identifier NCT01949883) (Filippakopoulos and Knapp, 2014).

Another example for a successful PPI is the novel BCL2 inhibitor venetoclax (ABT-199) (Arkin et al., 2014; Del Poeta et al., 2016; Mullard, 2016). It was approved by the United States Food and Drug Administration (FDA) in April 2016 for patients with chronic lymphocytic leukemia (CLL). Venetoclax is an inhibitor of the anti-apoptotic protein BCL2, which regulates the release of pro-apoptotic factors. Upon inhibitor treatment, cells undergo programmed cell death. This work proved that protein-protein interactions are viable drug targets for tumor therapy.

Despite well-established non-specific DNA-intercalating agents such as the topoisomerase II inhibitor doxorubicin, targeting protein-nucleic acid interactions for cancer therapy has been far less fruitful (Hurley, 2002; Liu, 1989). Only minor steps to clinical applications have been achieved so far. One example is the blockage of both PPI and PNI of the STAT3 (signal transducer and activator of transcription 3) transcription factor using the inhibitor S3I-201, which induced the regression of breast tumor xenografts in mice (Siddiquee et al., 2007).

Clearly, the concept of targeting protein-protein and protein-DNA interactions is on the rise, but still many targets remain undrugged. Many transcription factors fall into the group of proteins, which biophysically interact via both PPI and PNI, making them particularly interesting for discovery chemistry (Darnell, 2002).

One of the most attractive targets for cancer therapy is c-MYC. This oncogenic transcription factor is deregulated in the majority of tumors and its inhibition substantially affects tumor development and survival (Dang, 2012). High levels and/or aberrant expression of c-MYC are often correlated with high aggressiveness and poor prognosis (Albihn et al., 2010; Nesbit et al., 1999; Vita and Henriksson, 2006). Since c-MYC is rarely mutated, lacks enzymatic activity, and dominantly acts via protein-protein and protein-DNA interactions, it has long been regarded as undruggable (Dang, 2012). Yet, extensive research has been undertaken to therapeutically target MYC during the last decades (McKeown and Bradner, 2014; Vita and Henriksson, 2006).

In the following chapters, the oncoprotein c-MYC will be introduced. Specifically, I will describe its physiological role in transcriptional regulation, address the question why it is such an interesting yet challenging candidate for targeted tumor therapy, and outline strategies that have been attempted to target it.

1.2 The oncogenic transcription factor MYC

The *c-MYC* proto-oncogene was first described in the late 1970s as a cellular homolog of the viral oncogene *v-MYC* that causes myelocytomatosis (i.e., diffuse growth of myeloid cells) in fowl (Sheiness and Bishop, 1979; Vennstrom et al., 1982). The MYC protein family also includes N-MYC and L-MYC, which function in a similar manner, but differ i.a., in expression patterns (Legouy et al., 1987; Nau et al., 1985; Schwab et al., 1983; Strieder and

Lutz, 2002). N-MYC can functionally substitute for c-MYC (Malynn et al., 2000). The coding sequence of *c-MYC* is evolutionary highly conserved in vertebrates and has also been found in *Drosophila melanogaster* (Gallant et al., 1996).

Different c-MYC isoforms are generated due to alternative translation initiation start sites; p67 containing 454 amino acids and the predominant p64 isoform (hereafter referred to as MYC) encompassing 439 amino acids (Blackwood et al., 1994; Hann et al., 1988). Additional isoforms are the N-terminally shortened MYC-S (generated by downstream translation initiation) and MYC-nick, which is C-terminally truncated (generated due to calpain cleavage) (Conacci-Sorrell et al., 2010; Spotts et al., 1997). MYC-S, which lacks the first 100 N-terminal amino acids (including the first known structural element MYC box I, explained below), has been shown to act in a dominant-negative manner on MYC-dependent transcriptional activation, but is found in tumor cell lines and maintains the ability to stimulate proliferation (Spotts et al., 1997; Xiao et al., 1998).

1.2.1 MYC and MAX are b/HLH/Zip proteins

1.2.1.1 Domain architecture of MYC and MAX

The MYC protein topology can be divided into three highly conserved regions (Figure 1.1): a largely unstructured amino-terminal region involved in transcriptional regulation; a central portion containing nuclear localization sequences; and a carboxy-terminal DNA-binding and dimerization domain.

The MYC N-terminus contains several conserved sequence elements, termed MYC boxes (Mb). MbI and MbII are important for transcriptional co-factor recruitment and MYC protein turnover. MbI serves as a phosphodegron (a sequence that mediates phosphorylation-dependent degradation) as phosphorylation of T58 and S62 in MbI regulates proteasomal degradation of the MYC protein (Sears et al., 1999; Sears et al., 2000). Recently, Jaenicke et al. reported that T58 and S62 phosphorylation stimulates transient association with the PAF1 complex (PAF1C) (Jaenicke et al., 2016). In addition, the cyclin T subunit of the transcriptional elongation factor P-TEFb (consisting also of CDK9) binds to MbI and MbII (Eberhardy and Farnham, 2002). MYC box II is a hub for important protein-protein

interactions. The co-activator TRRAP (transformation/transcription domain associated protein), which recruits histone acetyl transferase (HAT) complexes, such as GCN5, PCAF and TIP60 (containing p400, TIP48 and TIP49) interacts with MbII (Frank et al., 2003; McMahon et al., 1998; McMahon et al., 2000).
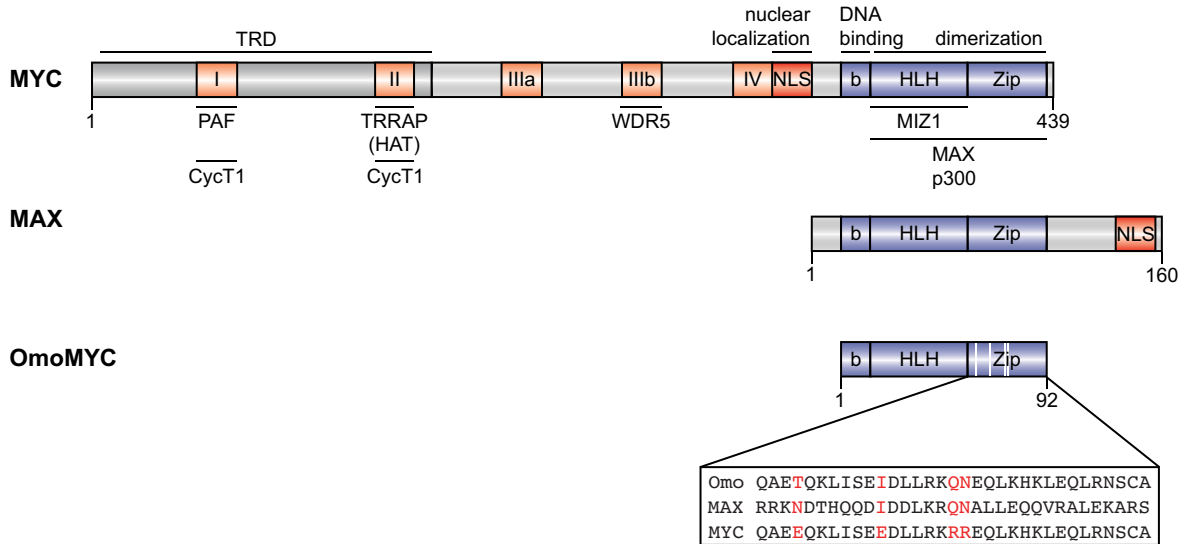
Figure 1.1: Schematic representation of the MYC, MAX and OmoMYC protein architecture
Abbreviations refer to: I-IV: MYC box I-IV; NLS: nuclear localization signal; b: basic region; HLH: helix-loop-helix domain; Zip: leucine zipper domain; TRD: transregulatory domain; CycT1: cyclin T1. Interaction sites of binding partners important for transcriptional regulation are shown below the MYC protein. HAT refers to histone acetyl transferases including GCN5 and TIP60, which are recruited via TRRAP binding.
Amino acid exchanges in OmoMYC are highlighted in white. The leucine zipper amino acid sequence of all three proteins is displayed in the box below and mutations in OmoMYC (Omo) are marked in red. Adapted from (Conacci-Sorrell et al., 2014).

MYC box IIIa, often referred to as MbIII, is not found in L-MYC. It mediates transcriptional repression via the recruitment of histone deacetylases (HDACs) and to inhibit apoptosis, thereby increasing MYC's transforming ability (Herbst et al., 2005; Kurland and Tansey, 2008). WDR5, a WD40-repeat protein interacting with MbIIIb (PDB entry 4Y7R), has recently been shown to be required for the recruitment of MYC to chromatin (Thomas et al., 2015). WDR5 is part of various chromatin regulatory complexes important for histone methylation and acetylation (Trievel and Shilatifard, 2009). An essential nuclear localization sequence (NLS) is found within MbIV, a second NLS is located in the basic region, which by itself only provides partial nuclear tethering in contrast to the first sequence (Dang and Lee, 1988).

The C-terminal region of MYC consists of a basic helix-loop-helix leucine zipper (b/HLH/Zip) domain, which functions as a DNA-binding and dimerization domain. This structural motif is found in the MYC family of b/HLH/Zip proteins containing (amongst others) MAX (MYC-associated factor X), MXD proteins (MAX dimerization proteins) and MondoA (Conacci-Sorrell et al., 2014). Also, many sequence-specific transcription factors, including MITF (microphthalmia-associated transcription factor) and SREBP-1 (sterol regulatory element-binding protein 1) share this conserved domain (Jones, 2004; Murre et al., 1989) (a sequence alignment can be found in (Ferre-D'Amare et al., 1993)).

MYC is thought to be unable to efficiently form homodimers at physiological concentrations *in vivo* (Dang et al., 1991; Marchetti et al., 1995). Dimerization with a 160 amino acid protein called MAX is essential for MYC's ability to bind to DNA and for most biological activities (Amati et al., 1993; Amati et al., 1992; Blackwood and Eisenman, 1991). MAX also belongs to the b/HLH/Zip family of transcription factors (Figure 1.1). However, it lacks transcriptional effector domains, which precludes MAX homodimers from activating transcription when bound to DNA.

MYC and MAX form a functional complex that recognizes hexanucleotide sequence elements termed "E-boxes" (enhancer box) in a sequence-specific manner via the basic region. Consensus E-box sequences encompass a palindromic CACGTG motif, which is bound by the MYC-MAX heterodimer with the highest affinity.

Several protein-protein interactions are additionally mediated via the MYC HLH/Zip domain: binding to the transcription factor MIZ1 (MYC-interacting zinc finger protein 1) and the HATs p300 and CBP (Herold et al., 2002; Peukert et al., 1997; Vervoorts et al., 2003).

1.2.1.2   Structural determinants for MYC/MAX dimer formation

The structures of the MAX homodimer and the MYC/MAX heterodimer bound to DNA enabled an analysis of the b/HLH/Zip domain topology of the proteins (PDB codes 1AN2, 1NKP; Figure 1.2 A and B) (Ferre-D'Amare et al., 1993; Nair and Burley, 2003). Each half of the respective dimer consists of two extended α-helices separated by a short loop region. The N-terminal helix encompasses the basic region and helix 1, while the C-terminal helix consists of helix 2 and the leucine zipper. Helix 1 and 2 form a parallel four-helix bundle and

the leucine zipper folds into a coiled-coil. Sequence-specific DNA-binding is ensured by interactions of the basic regions with the major groove, while the HLH/Zip motifs of MAX homodimers and MYC/MAX heterodimers mediate dimerization.
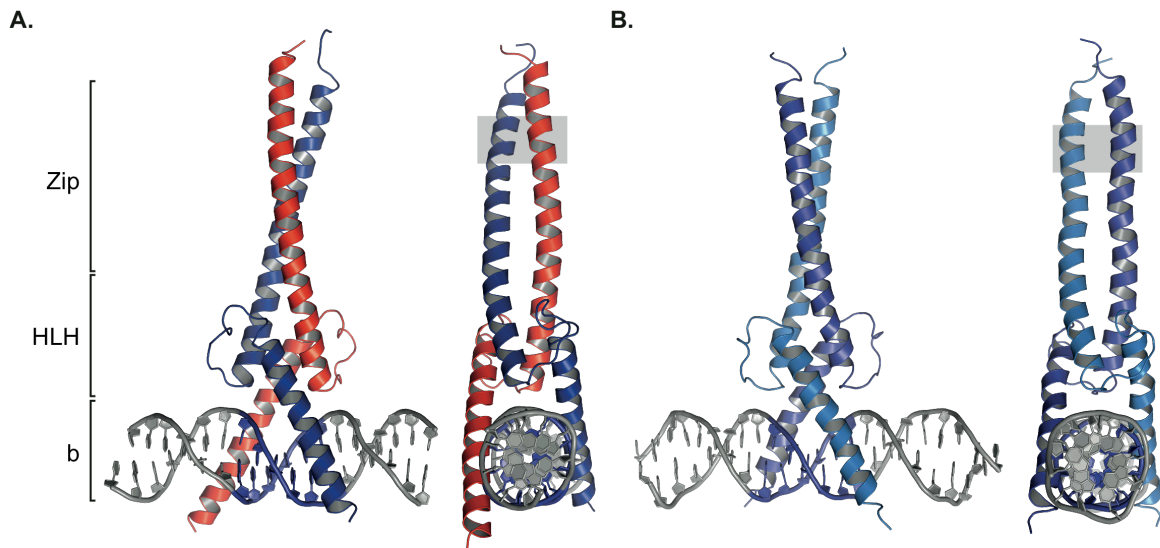
Figure 1.2: MYC and MAX homo- and hetero-complexes form a coiled-coil structure at the E-box motif
(A)   Schematic representation of the MYC/MAX/DNA co-crystal structure (PDB code 1NKP) (Nair and Burley, 2003). MYC is shown in red, MAX in blue. The consensus E-box motif (CACGTG) is colored in blue. Each image to the right shows a rotation of 90° around the y-axis. Here, regions contributing to dimerization specificity are highlighted in grey. Images were generated using PyMol. B: basic; HLH: helix-loop-helix; Zip: leucine zipper.
(B)   Crystal structure of the MAX homodimer b/HLH/Zip bound to DNA (PDB code 1AN2) (Ferre-D'Amare et al., 1993).

Extensive hydrophobic and polar interactions between the HLH/Zip interfaces stabilize the dimers. Yet, the crystal structures of these protein complexes suggest that only a minor part of the protein dimer interface contributes to the binding specificity. Detailed analysis of the structures revealed two amino acid residues within the leucine zipper that are critical for dimerization (Ferre-D'Amare et al., 1993; Nair and Burley, 2003). The C-terminal end of the homodimeric MAX leucine zipper comprises a Q91-N92-Q91*-N92* (an asterisk indicates residues belonging to the second monomer) tetrad that alters the packing scheme of the coiled-coil structure and accounts for a non-ideal flaring of the leucine zippers (Figure 1.2 B; grey highlight). In contrast, two positively charged guanidinium groups of arginine (R) residues are found at the equivalent position in MYC (amino acids 423 and 424; Figure 1.2 A; grey highlight). This specific pair of additional hydrogen bonds formed in the MYC/MAX heterodimer yield a more intimate dimer interface favoring MYC/MAX heterodimerization

over MAX homodimerization, while the tetrad of positively charged arginine residues disfavors MYC homodimerization, making it very difficult to occur *in vivo*.

1.2.2 MYC functions as a transcription factor

MYC is able to regulate transcription mediated by RNA Polymerase I, II and III, promoting messenger RNA (mRNA; by RNAPII), ribosomal RNA (rRNA; by RNAPI and RNAPIII), transfer RNA (by RNAPIII), lncRNAs (long non-coding RNA), snoRNAs (small nucleolar RNAs) and miRNA (micro RNA) transcription (Arabi et al., 2005; Gomez-Roman et al., 2003; Grandori et al., 2005; Grewal et al., 2005; Herter et al., 2015; O'Donnell et al., 2005; Steiger et al., 2008).

RNAPII-dependent transcription is characterized by a series of well-studied steps (reviewed in (Buratowski, 2009; Cheung and Cramer, 2012; Cole and Cowling, 2008; Jonkers and Lis, 2015)). First, RNAPII is recruited to the core promoter by general transcription factors (TFIIA, TFIIB, TFIID, TFIIE, TFIIF, TFIIH) resulting in the formation of a pre-initiation complex (PIC). The Mediator complex stimulates S5/S7 phosphorylation of the C-terminal domain (CTD) of RNAPII by the CDK7 subunit of TFIIH resulting in promoter clearance. During early elongation, RNAPII advances by producing short transcripts and pauses after 20-50 bp. At the pause site, RNAPII is stabilized by pausing factors: the negative elongation factor (NELF) and the DRB-sensitivity-inducting factor (DSIF). P-TEFb is then recruited and its CDK9 subunit subsequently phosphorylates DSIF, dissociating it from NELF and turning DSIF into a positive elongation factor. CDK9 also phosphorylates S2 of the CTD, which is required for the transition to productive elongation.

After RNAPII pause release, the production of mRNAs and lncRNAs starts. The RNA synthesis rate is enhanced during productive elongation via the PAF complex, as it mediates histone methylation and mRNA 3' end processing (Jaehning, 2010; Pavri et al., 2006; Qiu et al., 2012). DNA supercoiling is relieved via topoisomerase I stimulation by the transcription machinery in a BRD4-dependent manner (Baranello et al., 2016). Additionally, THIIS and the FACT complex help the polymerase during elongation by counteracting backtracking and arrests as well as by removing nucleosomes (Kim et al., 2010). During and after transcriptional termination, the CTD is dephosphorylated and a new cycle of transcription is

started (Buratowski, 2009; Cheung and Cramer, 2012; Cole and Cowling, 2008; Jonkers and Lis, 2015; Mayer et al., 2010).

1.2.2.1 MYC-mediated transcriptional activation

MYC plays an important role at various steps of the transcription cycle. MYC can stimulate transcriptional initiation, pause release and elongation, and is therefore a key element controlling global mRNA production.
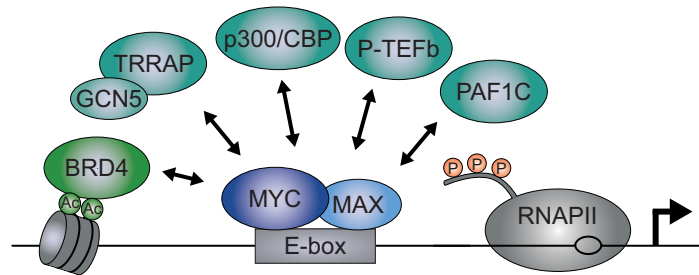
Figure 1.3: MYC-mediated transcriptional activation
Transactivation of target genes involves recruitment of co-activators and scaffold proteins (e.g., BRD4 and TRRAP) to promoter-bound MYC/MAX complexes. Histone acetylation (via TRRAP-associated HAT complexes including GCN5), chromatin remodeling (i.a., via TRRAP-associated complexes with ATPase activity), phosphorylation of the C-terminal domain of RNA polymerase II (i.a., via P-TEFb) and productive elongation (via PAF1C loading) are fostered by MYC.

MYC binds to promoters via both sequence-specific contacts to E-box-containing DNA and by interaction with proteins associating with the N-terminal domains of MYC, like WDR5 (Guo et al., 2014a; Thomas et al., 2015). Whether MYC is able to directly influence RNAPII loading to promoters (Bouchard et al., 2004; Walz et al., 2014) or if RNAPII is loaded on promoters before MYC binds has been discussed heavily (Guccione et al., 2006; Lin et al., 2012; Nie et al., 2012).

To further open the chromatin structure and enable transcriptional activation, MYC recruits chromatin modifying and remodeling complexes containing proteins with HAT and/or ATPase activity (see section 1.2.1.1 and Figure 1.3; e.g., p300, TRAPP/GCN5, TRAPP/TIP60; SWI/SNF (switch/sucrose nonfermentable) complex) (Bouchard et al., 2001; Cheng et al., 1999; Frank et al., 2003; McMahon et al., 1998; McMahon et al., 2000).

In addition, MYC is able to recruit RNAPII CTD kinases, such as CDK7 and CDK9/Cyclin T1, which are part of the TFIIH and the P-TEFb complex respectively, thus promoting both promoter clearance and pause release (Bouchard et al., 2001; Eberhardy and Farnham, 2002; Kanazawa et al., 2003; Rahl et al., 2010). BRD4 supports MYC by assisting with P-TEFb recruitment and S2 phosphorylation, thus enabling effective pause release (Baranello et al., 2016; Jang et al., 2005; Yang et al., 2005). This suggests that one of the key mechanisms by which MYC controls transcriptional activation is the support of RNAPII to overcome promoter-proximal pausing.

Finally, MYC also fosters the transition into productive elongation. MYC is suggested to interact with CDC73, a subunit of PAF1C (Jaenicke et al., 2016; Cornelia Redel, personal communication). Degradation of MYC promotes the transfer of this elongation factor to RNAPII thereby stimulating transcriptional elongation (Jaenicke et al., 2016).

1.2.2.2 MYC-mediated transcriptional repression

In addition to its role in transcriptional activation, MYC is also able to directly or indirectly repress gene transcription. It can recruit histone deacetylase 3 (HDAC3), which directly interacts with MYC box III, thereby reducing acetylation levels of histone H3 and H4 (Kurland and Tansey, 2008). Direct repression of target genes can also be induced by interactions with co-factors such as MIZ1 (MYC-interacting zinc finger protein 1) and SP1 (specificity protein 1) (Gartel et al., 2001; Peukert et al., 1997). These complexes recruit co-repressors such as DNA methyl transferases or HDACs (Brenner et al., 2005; Staller et al., 2001). Importantly, the MYC/MIZ1 ratio at the respective promoter determines if and to which degree transcription is activated or repressed (Walz et al., 2014). If MIZ1 levels outrank MYC levels, MIZ1 mediates the transcriptional response by activating genes containing a specific MIZ1 binding motif (Wolf et al., 2013). At a MYC/MIZ1 ratio of 1, E-box specific binding of the MYC-MIZ1 complex represses MYC-mediated gene regulation (Walz et al., 2014; Wiese et al., 2015; Wiese et al., 2013). MIZ1-mediated repression is especially required for the formation of MYC-driven lymphomas and medulloblastomas (van Riggelen et al., 2010a; Vo et al., 2016).

To repress transcription in an indirect manner, MYC is able to induce miRNAs such as the micro RNA cluster *miR17-92*. *miR17-92*, in turn, represses genes involved in chromatin modification and survival programs (Li et al., 2014).

1.2.3 MYC expression is deregulated in cancer

MYC is indispensable for embryonic development, as shown by mouse models with a homozygous deletion, conditional depletion or pharmacological inhibition of MYC (Davis et al., 1993; Dubois et al., 2008). Growth and proliferation of various cell types *in vivo* and in culture depends on MYC expression (Dubois et al., 2008; Muncan et al., 2006; Scognamiglio et al., 2016). MYC levels are low in quiescent cells, but upon exposure to growth stimuli, MYC expression is rapidly induced (Kelly et al., 1983; Marcu, 1987; Spencer and Groudine, 1991). MYC regulates a large spectrum of cellular processes by altering the transcription of target genes that execute diverse biological activities. Apart from its essential role in controlling cell proliferation, stimulating cell cycle progression, blocking differentiation and controlling metabolism, MYC has also been identified as an important factor to limit growth through the induction of apoptosis (reviewed in (Dang, 2012; Meyer and Penn, 2008)).

In non-transformed cells, MYC expression is tightly controlled. Physiological regulation of MYC levels is executed at (a) the transcriptional level by several upstream signaling pathways (e.g., Wnt-APC, Notch, MAPK), by non-B DNA structures close to the *MYC* promoter, including G-quadruplexes or FUSE (far upstream element); (b) at the level of translation, e.g., via eIF4A, which is directly regulated by mitogen-induced upstream pathways, or miRNAs (like miR-34b/c); and (c) at the level of posttranslational modifications, e.g., through phosphorylation and ubiquitination modulating turnover of the highly unstable protein (reviewed in (Dang, 2012; Tansey, 2014)).

During tumorigenesis, the tight control of MYC expression is disrupted. A majority of all human tumors display elevated levels of MYC protein. This occurs mainly as a consequence of mutations or alterations of upstream regulatory molecules controlling its expression or stability; but it is also due to genetic abnormalities, including translocations, mutations (as seen in Burkitt's lymphoma) or amplifications (found, i.a., in mammary carcinoma) (Albihn et al., 2010; Vita and Henriksson, 2006). MYC levels further increase during tumor progression, as seen for several tumor entities including colorectal carcinoma and lymphoma;

this supports the concept that elevated MYC levels are advantageous to cancer cells (Kress et al., 2011; Myant and Sansom, 2011; Sabò et al., 2014). That tumors depend on high levels of MYC has been shown in various transgenic mouse models in which MYC expression is conditionally activated (see section 1.2.4.1). There, suppression of MYC results in tumor regression in several tumor types (Felsher, 2010; Gabay et al., 2014).

Altered MYC expression can contribute to almost every aspect of tumor development and maintenance. It leads to uncontrolled cell proliferation and cell growth, genomic instability, increased ribosomal biogenesis and protein synthesis, and metabolic reprogramming. MYC induces changes on cell adhesion as well as the cytoskeleton; it modulates apoptotic response mechanisms, mediates angiogenesis and changes the tumor microenvironment and immune response (Dang, 2012; Rahl and Young, 2014; Vita and Henriksson, 2006).

Several models have been proposed to explain how elevated MYC levels are able to control these tumor-specific processes. Especially after it became clear that MYC binding is associated with histone marks of open chromatin and not restricted to a specific subset of promoters but found on virtually all promoters, thousands of enhancers and many distal sites in different cell types, the search for tumor-specific mechanisms of transcriptional regulation was started (Chen et al., 2008; Guccione et al., 2006; Guo et al., 2014a).

In these studies, MYC-dependent transcriptional regulation and MYC chromatin occupancy was analyzed at different protein levels. The first model suggested that MYC globally enhances transcription in a dose-dependent manner, both in tumor cells (a MYC-inducible B cell lymphoma cell line and SCLC cell lines) and in non-pathological settings, such as during lymphocyte activation and in embryonic stem cells. MYC binds to all transcriptionally active promoters. At high protein levels, MYC invades distal sites and enhancers. Inducible MYC overexpression (also indirectly via lipopolysaccharide stimulation) causes an increase in total RNA and mRNA levels, e.g., due to an increased RNAPII pause release. Thus, differential gene expression patterns result indirectly (e.g., through feedback loops) and are cell type specific. This has been termed the "amplifier model" (Lin et al., 2012; Nie et al., 2012). In the second model, MYC regulates a specific set of target genes, while other binding events are "non-productive" (i.e., not resulting in transcriptional activation). In this model of MYC-driven lymphomagenesis, RNA levels rise due to increases in cell growth of the B cells (Kress et al., 2015; Sabò et al., 2014).

A third set of studies connected both previously mentioned models. Using a MYC-inducible human osteosarcoma cell line (U2OS^{Tet-On}), expression signatures of MYC-amplified tumors can be recapitulated. In this system, the affinity of the respective promoter for MYC binding and therefore the change in occupancy upon MYC overexpression determines the response to MYC-mediated regulation. Promoters with high-affinity binding sites are saturated by levels found in proliferating non-transformed cells and therefore do not respond to further increases to supra-physiological MYC levels. This set of genes can be connected to physiological MYC functions, including protein biosynthesis, which are linked to cell growth. In contrast, low-affinity sites change in occupancy when MYC levels rise and display changes in gene expression. This group of genes is linked to oncogenic gene expression profiles, including processes such as nutrient transport and response to hypoxia (Lorenzin et al., 2016; Walz et al., 2014).

1.2.4 Targeting MYC

1.2.4.1 The challenge of inhibiting the transcription factor MYC

MYC has been regarded as the prototypical example for an "undruggable" target. Several reasons for this have been proposed: first, the MYC protein itself is rarely mutated in cancer; second, MYC is expressed in all proliferating cells, thus its inhibition could be associated with high toxicities; and third, MYC itself has no enzymatic activity and acts via PPIs and PNIs, which are difficult to target (Albihn et al., 2010; Lee et al., 2006). At the same time, there are plenty of arguments supporting the notion that MYC inhibition is feasible, offering a unique opportunity to address unmet medical needs.

Various *in vivo* mouse models demonstrate that both hematopoietic and solid tumors rely on (are "addicted" to) high levels of MYC (Felsher and Bishop, 1999; Flores et al., 2004; Jain et al., 2002; Marinkovic et al., 2004; Pelengaris et al., 2002; Shachaf et al., 2004). In these studies, discontinuation of high-level transgenic (not endogenous) MYC expression is associated with rapid tumor regression and/or apoptosis in lymphomas, osteosarcoma, papilloma, hepatocellular carcinoma, and insulinoma. As a majority of tumors express deregulated and/or elevated levels of MYC (Dang, 2012), MYC is the ideal candidate for

targeted tumor therapy. It thus has a broad area of application, as it is not limited to one specific tumor type, which shows unique mutations.

As most "normal" cells are non-proliferating and quiescent, toxicities of anti-MYC therapies might, at most, resemble those of non-targeted cytotoxic agents, e.g., hematopoietic and gastrointestinal side effects.

The argument that PPIs might be refractory to small molecule inhibition has been rebutted by several successful examples, as described above (section 1.1). With regard to the oncoprotein MYC, studies first showed that the leucine zipper mediates dimerization with MAX, both via hydrophobic interactions (Smith et al., 1990) as well as charged interactions (Amati et al., 1993). Comparison of the MYC/MAX crystal structure (PDB entry 1NKP) (Nair and Burley, 2003) with the MAX homodimer structure (PDB entry 1AN2) (Ferre-D'Amare et al., 1993) then revealed "hot spots" within the leucine zipper that specify heterodimerization of MYC with MAX. Specifically, a QN-QN tetrad induces a packing defect in the MAX/MAX leucine zipper, which is not visible in MYC/MAX (containing a QN-RR tetrad at this position) (see section 1.2.1.2) (Nair and Burley, 2003). Thus, the important interaction domain was found that could be further studied for cancer drug design.

1.2.4.2 Approaches to inhibit MYC using small molecule compounds

Various approaches have been undertaken to target the transcription factor MYC. In the following chapter, a selection of strategies that tackle MYC at the level of transcription, translation, mRNA and protein stability, dimerization and DNA-binding as well as downstream effectors will be highlighted (summarized in Table 1.1 and Figure 1.4).

Inhibition of MYC-dependent transcription

MYC induces transcriptional activation via the recruitment and assembly of transcriptional complexes and chromatin-modifying enzymes (see section 1.2.2). One of MYC's transcriptional co-activators is the bromodomain protein BRD4, which is a member of the bromodomain and extraterminal (BET) subfamily (see section 1.1). BRD4 interacts with acetylated chromatin and serves as a protein scaffold at promoters and so-called super-enhancers (Dey et al., 2000; LeRoy et al., 2008; Loven et al., 2013). Super-enhancers are large (up to 50 kb long) enhancer regions, which bind high levels of BRD4 and Mediator.

Inhibition of BRD4 selectively affects the transcription of a subset of genes, one of them being the *MYC* gene itself. One proposed mode of action of BRD4 inhibitors such as JQ1 is the depletion of BRD4 at super-enhancers driving *MYC* expression (Delmore et al., 2011; Loven et al., 2013). Targeting *MYC* transcription via BRD4 inhibition has been shown to be effective in a range of tumors, including Burkitt's lymphoma, multiple myeloma, acute myeloid leukemia (AML), and acute lymphoblastic leukemia (ALL), glioblastoma and medulloblastoma (Cheng et al., 2013; Dawson et al., 2011; Henssen et al., 2013; Mertz et al., 2011; Ott et al., 2012; Zuber et al., 2011).

Table 1.1: Small molecules linked to MYC inhibition
Compounds listed in this table are only a selection and various small molecules of the indicated classes exist but are omitted due to space restrictions.

Compound	Target	Class	References
JQ1, OTX015	BRD4, BRD3, BRD2	BET-bromodomain inhibitor	(Delmore et al., 2011; Filippakopoulos et al., 2010; Noel et al., 2013)
C646	p300/CBP	p300 HAT inhibitor	(Bowers et al., 2010)
Flavopiridol, SNS-032, THZ1	CDK2, CDK7, CDK9	CDK inhibitor	(Chen et al., 2005; Chipumuro et al., 2014; Walsby et al., 2011)
Triptolide	THIIH, XPB	TFIIH inhibitor	(Titov et al., 2011)
SGI-1776	PIM1	PIM kinase inhibitor	(Chen et al., 2009)
SAHA	HDAC1, HDAC3	HDAC inhibitor	(Richon et al., 1998)
GQC-05, TMPyP4	*MYC* promoter DNA	G-quadruplex stabilizer	(Brown et al., 2011; Grand et al., 2002)
OP449	SET	SET antagonist	(Christensen et al., 2011)
P22077	USP7	deubiquitination inhibitor	(Tavana et al., 2016)
Silvestrol	eIF4A	translation inhibitor	(Wiegering et al., 2015)
MLN8237, CD532	Aurora-A	Aurora-A/N-MYC complex disruptor	(Brockmann et al., 2013; Gustafson et al., 2014)
DFMO	ODC	ODC inhibitor	(Nilsson et al., 2005)
ON123300	i.a. ARK5, CDK4	multi-targeted kinase inhibitor	(Perumal et al., 2016)
BPTES, CB-839	Glutaminase	glutaminase inhibitor	(Gross et al., 2014; Le et al., 2012)
CX-5461	RNAPI	RNAPI inhibitor	(Bywater et al., 2012; Drygin et al., 2011)
10058-F4	MYC HLH/Zip	MYC/MAX dimerization inhibitor	(Yin et al., 2003)
NSC13728	MAX HLH/Zip	MAX homodimer stabilizer	(Jiang et al., 2009)

Recently, a novel strategy to chemically induce target protein degradation has been published by the Bradner laboratory (Winter et al., 2015). Using a JQ1-phthalimide-conjugate that degrades BET bromodomain proteins (dBET1), hijacking a cellular E3 ubiquitin ligase was shown to be a new approach to selectively reduce protein levels.

Other examples for inhibitors targeting transcriptional cofactors of MYC under preclinical and clinical investigation are the p300/CBP inhibitor C646 (Bowers et al., 2010), inhibitors of transcriptional kinases (CDK7, CDK8, CDK9), such as flavopiridol, SNS-032 and THZ1 (Chen et al., 2005; Chipumuro et al., 2014; Rahl et al., 2010; Walsby et al., 2011), the PIM1 inhibitor SGI-1776 (Chen et al., 2009), as well as HDAC and TFIIH inhibitors (Angela et al., 2016; Richon et al., 1998; Titov et al., 2011).

A distinct approach to target *MYC* gene transcription is the stabilization of G-quadruplex (G4) structures (Brown et al., 2011; Ou et al., 2007). These stacked nucleic acid structures are located downstream of the *MYC* promoter and alter DNA topology, thereby influencing transcription (Bochman et al., 2012). Compounds that stabilize these G4 structures have been shown to harbor *in vivo* antitumor activity (Brown et al., 2011; Grand et al., 2002; Panda et al., 2015; Siddiqui-Jain et al., 2002).

Modulation of MYC mRNA stability, translation and protein turnover

MYC is a highly unstable protein, which is rapidly turned over by the ubiquitin-proteasome system. Its protein half-life as well as protein-protein interactions are strongly regulated via various post-transcriptional modifications (Farrell and Sears, 2014; Sears, 2004). The phosphatase PP2A (protein phosphatase 2A) dephosphorylates MYC at serine 62 (S62), priming the protein for proteasomal degradation (Yeh et al., 2004). Targeting the PP2A inhibiting protein SET, which has been shown to be overexpressed in multiple tumor types (Westermarck and Hahn, 2008), is currently being investigated using an antagonistic peptide (OP449) (Christensen et al., 2011; Janghorban et al., 2014). SET inhibition decreased the growth of mammary gland xenografts through the alteration of post-transcriptional modification of MYC.

Several deubiquitinating enzymes, which antagonize ubiquitin-dependent protein degradation, have been reported for MYC proteins (Popov et al., 2007; Sun et al., 2015b; Tavana et al., 2016). Ubiquitin-specific proteases (USP; including USP28, USP36 and USP37) are highly expressed in human cancers (Diefenbacher et al., 2014; Pan et al., 2015; Sun et al., 2015a).

Small molecules targeting these cysteine proteases are currently under development (Martin Eilers, personal communication; Pal et al., 2014; Tavana et al., 2016). These studies suggest that therapeutically addressing post-translational modifications of MYC family proteins is a promising strategy of targeting MYC.

Recently, an approach to diminish MYC mRNA translation was shown to be effective against colon carcinoma (Wiegering et al., 2015). In this study, cap- and IRES-dependent translation (via the eukaryotic initiation factor-4A, eIF4A) was inhibited using silvestrol; this resulted in reduced MYC protein levels and cell proliferation *in vitro* and *in vivo*. Similar effects were shown using a T-ALL mouse model (Wolfe et al., 2014), confirming that MYC transcripts are particularly sensitive to silvestrol treatment.

Not only c-MYC, but also N-MYC protein turnover has been in the focus of drug discovery. *MYCN* amplification is found in neuroendocrine tumors, like neuroblastoma and medulloblastoma, together with various other tumor entities (Beltran, 2014). N-MYC associates with the Aurora-A kinase and is thus protected from Fbxw7-mediated proteasomal degradation. *MYCN* amplified neuroblastoma cells are highly dependent on increased levels of Aurora-A (Otto et al., 2009). The catalytic activity of the Aurora-A kinase is not required for N-MYC stabilization, but complex formation of N-MYC and Aurora-A is mediated via the kinase domain of Aurora-A (Otto et al., 2009) and distortion of the kinase domain impairs association with N-MYC (Sloane et al., 2010). Various small molecule inhibitors targeting the Aurora-A/N-MYC complex (i.a., MLN8237) have been tested in preclinical studies and clinical trials for example in neuroblastoma and neuroendocrine prostate cancer (Beltran et al., 2011; Brockmann et al., 2013). Because compounds like MLN8237 show little single-agent efficiency in patients (Mosse et al., 2012), new small molecules that more potently induce N-MYC degradation are under development (Gustafson et al., 2014) or combinations with other chemotherapeutic agents are tested (DuBois et al., 2016; Graff et al., 2016). A recently published study by the Zender laboratory shows that Aurora-A/N-MYC interaction inhibitors could also be applied for c-MYC-dependent tumors (Dauch et al., 2016).

Targeting MYC's downstream effectors

Innumerable pathways have been explored to inhibit downstream targets of MYC, including ODC, ARK5, and glutaminase, to name a few (Gross et al., 2014; Le et al., 2012; Liu et al., 2012; Nilsson et al., 2005; Perumal et al., 2016). Several of these target genes were selected as they were shown to be especially dependent on elevated MYC levels.

MYC plays a central role in regulating RNA Polymerase I (RNAPI) activity and ribosome biogenesis (van Riggelen et al., 2010b). Surprisingly, these "housekeeping" processes are accelerated in MYC-driven tumors, offering a considerable therapeutic window, i.e., demonstrating selectivity for malignant cells over normal cells (Barna et al., 2008; Ruggero, 2009). The RNA Polymerase I inhibitor CX-5461 demonstrated high *in vivo* efficacy in an Eμ-MYC-driven tumor model (Bywater et al., 2012) and is currently investigated in a Phase I/II study (ClinicalTrials.gov identifier NCT02719977).

Inhibition of MYC/MAX dimerization and stabilization of MAX homodimers

Since MYC's oncogenic activities require dimerization with MAX, interfering with MYC/MAX complex formation may be a rational approach to tumor therapy. In 2002, the first study identifying small molecule peptidomimetic inhibitors (i.e., IIA4B20) abrogating the interaction between the b/HLH/Zip domains of MYC and MAX was published (Berg et al., 2002). Subsequently, using a yeast two-hybrid screen, more potent compounds were found, including 10058-F4 and 10074-G5, which are still used for *in vitro* studies today (Yin et al., 2003). Further studies mapped the binding region of 10058-F4 and 10074-G5 within the HLH domain and the N-terminal moiety of the leucine zipper of MYC, a region with the highest density of hydrophobic residues. This hydrophobic segment could not be found in the MAX homodimer, providing an explanation for the specificity for MYC/MAX heterodimers over MAX homodimers (Cuchillo and Michel, 2012; Hammoudeh et al., 2009; Yap et al., 2013). These studies suggest that the above described inhibitors induce local conformational changes in the MYC protein, preserving its intrinsically disordered state and thus preventing dimerization with MAX. Even though the compounds induced G_0/G_1 arrest followed by apoptosis in various tumor cell lines *in vitro*, no significant effect on tumor growth has been demonstrated *in vivo* (Fletcher and Prochownik, 2015). Efficacy of 10058-F4 and 10074-G5 in mouse models was limited due to rapid metabolism and low intratumoral concentrations of the compounds (Clausen et al., 2010; Guo et al., 2009). In a recently published study, 10058-F4 was able to delay tumor growth accompanied with changes in lipid metabolism in a N-MYC driven mouse model (Zirath et al., 2013).

A second approach to inhibit MYC/MAX complex formation is the stabilization of the MAX homodimer preventing its dissociation and thus dimer exchange to MYC/MAX heterodimers. This idea is in line with studies demonstrating that MAX overexpression represses MYC-dependent transcription and tumorigenesis (Cogliati et al., 1993; Kretzner et al., 1992b;

Lindeman et al., 1995; Montagne et al., 2012). Using virtual ligand and fluorescence resonance energy transfer (FRET)-based compound screens, stabilizers of MAX homodimers (i.e., NSC13728) binding to the HLH/Zip region of MAX were identified. Treatment of a breast cancer cell line with NSC13728 resulted in growth inhibition (Jiang et al., 2009).

In summary, direct MYC/MAX inhibitors have failed to enter phase I clinical trials due to low *in vivo* efficacy and unfavorable pharmacokinetics. Clearly, new screening methods, including novel chemical libraries, are needed to identify new direct-acting MYC inhibitors, which can be applied in clinical trials.
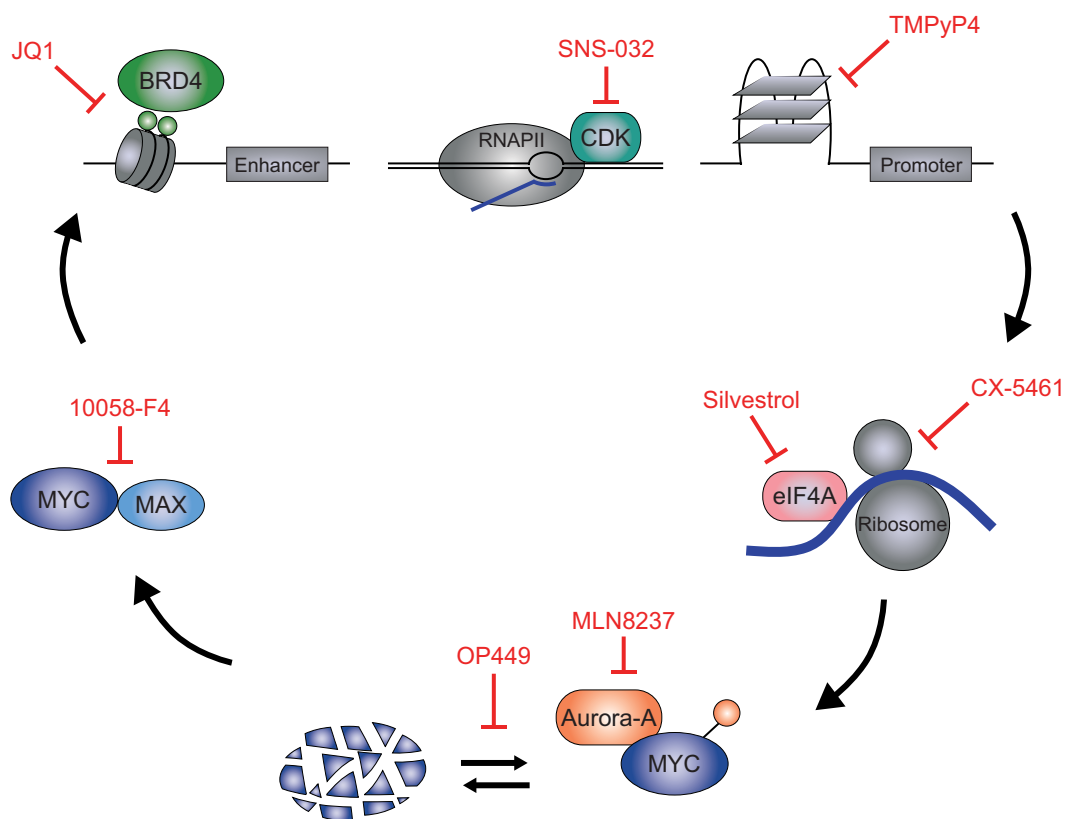
Figure 1.4: Targeting MYC at different stages of its life cycle
Starting with the upper left panel turning clockwise: Inhibition of *MYC* transcription using BET inhibitors interrupting BRD4/histone interaction preferably at super-enhancers (green circles represent acetyl-lysine modifications); Targeting transcriptional kinases, like cycline-dependent kinases (CDK); Stabilization of G-quadruplex structures close to the *MYC* promoter; Inhibition of MYC translation and ribosomal biogenesis; Modulation of MYC protein stability using Aurora-A inhibitors or compounds modulating MYC turnover (the orange circle represents a post-transcriptional modification, e.g., phosphorylation, ubiquitylation); Inhibition of MYC/MAX complex formation.

1.2.4.3   OmoMYC

Does OmoMYC expression show in vivo efficacy?

The final proof of principle that MYC inhibition is feasible came from *in vivo* studies using a dominant-negative allele of MYC, termed OmoMYC (Soucek et al., 2008). Expression of the OmoMYC transgene in *Kras^{G12D}*, *Haras^{V12}* and *SV40 T/t*-driven mouse models displayed rapid regression of different tumor entities, including lung adenocarcinoma, glioblastoma and pancreatic islet tumors (Annibali et al., 2014; Soucek et al., 2008; Soucek et al., 2013). Furthermore, OmoMYC prevented the formation of hyperproliferative lesions in the skin (pappilomatosis) in a MYC-driven mouse model (Soucek et al., 2004).

Surprisingly, systemic expression of OmoMYC induced only mild effects on tissues with high proliferative indices found in the skin, testes and intestine as well as the bone marrow. Thinning of the epidermis, hair re-growth defects, loss of spermatogonia and spermatocytes, reduced proliferation of intestinal crypts, abrasion of villi, anemia and leucopenia were observed, but the animals did not show signs of discomfort or weight loss. Importantly, upon discontinuation of OmoMYC expression, these effects were rapidly and fully reversed (Annibali et al., 2014; Soucek et al., 2008; Soucek et al., 2013). Furthermore, induced pluripotent and embryonic stem cell-derived cancers were responsive to OmoMYC treatment, while healthy iPS-derived tissues, important for regenerative medicine and tissue engineering, tolerated MYC inhibition (Oricchio et al., 2014).

More significantly, repeated cycles of short-term OmoMYC activation ("metronomic treatment") were sufficient to trigger long-term regression of p53-deficient and p53 wild type (WT) lung tumors. Response to MYC inhibition was also seen upon tumor recurrence and no resistances were acquired (Soucek et al., 2013). Crucially, the *in vivo* studies of the OmoMYC transgene (Annibali et al., 2014; Soucek et al., 2008; Soucek et al., 2013) extend and amend the investigations by the Felsher laboratory modeling MYC addiction (reviewed in (Felsher, 2010); see also 1.2.4.1). In contrast to their approach, OmoMYC is (a) expressed systemically; and (b) studied also in non-MYC-driven tumors, suggesting a universal effect on tumor development and maintenance.

Which effects are seen in vitro and in vivo?

A wide range of phenotypic changes upon OmoMYC activation was observed in *in vivo* and *in vitro* studies. OmoMYC blocked proliferation and induced an apoptotic response and/or cell cycle arrest in various cell lines, orthotopic xenografts and mouse models (Annibali et al., 2014; Fiorentino et al., 2016; Fukazawa et al., 2010; Oricchio et al., 2014; Savino et al., 2011; Soucek et al., 1998; Soucek et al., 2002; Soucek et al., 2004; Soucek et al., 2013). In cell lines derived from gliomas, this was explained by mitotic defects which resulted in the formation of multinucleated cells, presumably induced by a defective SUMOylation pathway (Annibali et al., 2014). A G_1 arrest was observed in a panel of SCLC cell lines harboring overexpressed c-MYC, N-MYC and L-MYC (Fiorentino et al., 2016).

Several publications highlighted OmoMYC-dependent changes on metabolic pathways (Oricchio et al., 2014; Savino et al., 2011). Additionally, the Nasi lab reported changes on the epigenetic marks of the tumor cells, accompanied by an increase of repressive histone modifications (especially on H3K9) when OmoMYC was expressed (Mongiardi et al., 2015; Savino et al., 2011).

In vivo, non-cell-autonomous effects on the microenvironment of pancreatic island tumors were observed (Sodir et al., 2011). Upon OmoMYC expression, the tumor vasculature resolved, macrophage and neutrophil recruitment was abrogated and chemokine and cytokine secretion modulated. This suggests that OmoMYC targets many hallmarks of MYC-driven tumors.

Tissue culture studies argue that OmoMYC expression has profound effects on MYC-dependent transcriptional regulation. This was shown for selected MYC target genes (Fiorentino et al., 2016; Mongiardi et al., 2015; Savino et al., 2011; Soucek et al., 1998; Soucek et al., 2002), but also using a microarray analysis of serum-stimulated fibroblasts (Savino et al., 2011). In all publications, OmoMYC inhibited MYC-dependent transcriptional activation. Reports on the impact of OmoMYC on repression differ: ranging from an increase, to no effect, to a decrease. A quantitative reverse transcriptase PCR (qPCR) analysis indicated that OmoMYC had no effects on a selected set of MYC target genes in cells lacking MYC (MYC-null Rat1 fibroblasts), suggesting that the transcriptional effects of OmoMYC are MYC-dependent (Savino et al., 2011). Yet, it has not been established that OmoMYC's genome-wide effects are MYC-specific and convincing global data on OmoMYC's influence on MYC's transcriptional regulation are lacking.

How was OmoMYC designed?

Soucek et al. designed a short MYC variant, only encompassing an altered b/HLH/Zip domain (Figure 1.1) (Soucek et al., 1998). Four point mutations (E410T, E417I, R423Q, R424N) were inserted into the leucine zipper. These amino acid substitutions were intended to remove repulsive interactions and facilitate homodimerization of the MYC b/HLH/Zip (see section 1.2.1.2 and Figure 1.2). The mutations were introduced at "hot spots" defining MYC/MAX dimerization specificity that were determined by analyzing published crystal structures of MYC/MAX and MAX/MAX dimers (PDB codes 1NKP and 1AN2) as well as mutational analyses of the leucine zipper (Amati et al., 1993; Nair and Burley, 2003).

How can OmoMYC's effects be explained on a molecular level?

On a molecular level, OmoMYC interacts with c-MYC (Fiorentino et al., 2016; Mongiardi et al., 2015; Savino et al., 2011; Soucek et al., 1998), MAX (Fiorentino et al., 2016; Savino et al., 2011; Soucek et al., 1998), N-MYC (Savino et al., 2011), L-MYC (Fiorentino et al., 2016), and MIZ1 (Savino et al., 2011) as demonstrated by co-immunoprecipitations (co-IPs), pull-down assays, and (less intriguingly) a chimeric repressor dimerization assay. OmoMYC was also suggested to form homodimers in a chimeric repressor dimerization assay (Soucek et al., 1998). A study published in parallel to our work indicated OmoMYC homodimerization using co-IPs (Fiorentino et al., 2016). No binding to MXD1 or other b/HLH proteins including ID1 or HIF1α was observed (Savino et al., 2011).

DNA binding of OmoMYC was shown in electrophoretic mobility shift assays (EMSAs) and chromatin immunoprecipitations (ChIPs) using reporter plasmids of selected MYC target genes (Savino et al., 2011; Soucek et al., 1998). MYC binding to DNA was reduced at the *Nucleolin* promoter in the presence of OmoMYC and in EMSAs using cell extracts (Savino et al., 2011; Soucek et al., 2002). Yet, it is not clear whether OmoMYC binds to DNA as a hetero- and/or homodimer, which binding sites it occupies on a genome-wide level, and which effect OmoMYC has on the chromatin occupancy of MYC.

Published data therefore cannot clearly elucidate by which mechanism(s) OmoMYC exceeds its effects. Several molecular modes of action could be possible: One in which the OmoMYC homodimer competes with MYC/MAX binding on DNA. However, a dominant role of the OmoMYC homodimer has been largely dismissed so far in the literature. A second possible mechanism could involve OmoMYC binding to MYC and/or MAX, preventing the

OmoMYC heterodimer(s) from binding to DNA. A third mode of action could be one in which an OmoMYC/MAX heterodimer binds promoter DNA and thereby inhibits transcriptional activation by MYC.

1.3 Objectives of the thesis

Most tumor cells harbor deregulated or elevated levels of the oncoprotein MYC. However, targeting this central oncogenic driver has been challenging and no direct MYC inhibitors have entered the clinic. Expression of a dominant-negative allele of MYC named OmoMYC has tremendous therapeutic benefit in various mouse models of tumorigenesis. These effects are currently not well understood on a structural and molecular level, such as specifically how it is able to discriminate physiological and oncogenic functions of MYC, impeding the design of a small molecule mimicking OmoMYC.

To date, no structural data on the OmoMYC protein-protein and protein-DNA interface is available. Global data on changes on the MYC-dependent transcriptome, especially in tumor cells, are lacking. It is therefore not known whether OmoMYC expression influences a specific subset or globally manipulates MYC target genes. It is further unclear, if OmoMYC is able to bind to chromatin and genome-wide DNA binding of MYC together with OmoMYC has not been studied.

To address these questions, three distinct objectives were pursued in this thesis: first, to structurally characterize OmoMYC; second, to understand its molecular mode of action in a cellular context; and third, to identify druggable OmoMYC target genes pinpointing critical oncogenic functions of MYC.

2 Materials

2.1 Primers and plasmids

2.1.1 Primers

DNA primers used in this study were purchased from Sigma-Aldrich, Invitrogen, or Eurofins MWG Operon (for: forward; rev: reverse). Universal ProbeLibrary by Roche, Primer3, or PrimerX were used for primer design. Primers for qPCR were designed to be intron spanning to avoid genomic DNA amplification. Oligonucleotides used to generate the targeted shRNA library were purchased from Integrated DNA Technologies.

Table 2.1: Primers used for cloning

Name	Application	Sequence (5' to 3')
TEV_5'rev_vec-linear (rev)	SLIC cloning	ggcgccctgaaaataaagattctc
pET/pBAD_vec-linear (for)	SLIC cloning	gacaagcttgcggccgcactcgag
Omo_TEV_pBad/pET (for)	SLIC cloning	ctttattttcagggcgccatggcgaccgagg agaatgtcaagaggcga
Omo_pBad/pET (rev)	SLIC cloning	gtgcggccgcaagcttgtcttattacgcaca agagttccgtagctgttcaagttt
pET_upstream_seq (for)	pETM11 sequencing	gatgcgtccggcgtagag
T7_terbis_seq (rev)	pETM11 sequencing	aaccccctcaagacccg
Myc aa 353-434_NcoI (for)	restriction cloning	tgtgcgaccatggccaatgtcaagaggcga
Myc aa 353-434_XhoI (rev)	restriction cloning	tcgtagctcgagtcatagctgttcaagtttgtg
HA-Omo/Myc_EcoRI (rev)	restriction cloning	agctcagaattcttacgcacaagagttccgta gctg
HA-Omo_BamHI (for)	restriction cloning	agctggatccatgtacccatacgatgttccag attacgccggcgcgtccaccgaggagaat
SFFV (for)	pLeGO sequencing	cttctgcttcccgagctcta
IRES (rev)	pLeGO sequencing	aggaactgcttccttcacga
pLeGO_HA-Omo_C89S (for)	mutagenesis	ctacggaactcttctgcgtaagaattc
pLeGO_HA-Omo_C89S (rev)	mutagenesis	gaattcttacgcagaagagttccgtag
OmoMYC_H906A (for)	mutagenesis	caagaggcgaacagccaacgtcttggag
OmoMYC_H906A (rev)	mutagenesis	ctccaagacgttggctgttcgcctcttg

OmoMYC_E910A,R914A (for)	mutagenesis	aacgtcttggctcgccagagggctaacgag ctaaaacgg
OmoMYC_E910A,R914A (rev)	mutagenesis	ccgttttagctcgttagccctctggcgagcca agacgtt
OmoMYC_H906A,E910A (for)	mutagenesis	caagaggcgaacagccaacgtcttggctcg ccagagg
OmoMYC_H906A,E910A (rev)	mutagenesis	cctctggcgagccaagacgttggctgttcgc ctcttg
OmoMYC_E910A (for)	mutagenesis	aacgtcttggctcgccagaggaggaacg
OmoMYC_E910A (rev)	mutagenesis	cgttcctcctctggcgagccaagacgtt

Table 2.2: Primers used for qPCR

Name	Sequence (5' to 3'); for	Sequence (5' to 3'); rev
B2M	gtgctcgcgctactctctc	gtcaacttcaatgtcggat
HA-OmoMYC	catacgatgttccagattacgc	ttagctcgttcctcctctgg
MYC	caccagcagcgactctga	gatccagactctgacctttgc
MYC+OmoMYC	gtcaagaggcgaacacacaa	gttttccaactccgggatct
CAMKV	tgatttgggacaggtcatca	tggaacttcttgcaggtgtg
ALDH3B1	aagccatcggagattagcaa	agcagctctggtccacgtat

Table 2.3: Primers used for qPCR after ChIP

neg.: intergenic negative region on chromosome 11

Name	Sequence (5' to 3'); for	Sequence (5' to 3'); rev
neg.	tttctcacattgcccctgt	tcaatgctgtaccaggcaaa
NPM1	cacgcgaggtaagtctacg	ttcaccgggaagcatgg
NCL	ctaccaccctcatctgaatcc	ttgtctcgctgggaaagg
FBXW8	gtgataggcagcagagctga	tgtacgcacgtggtggtc
CAMKV	attcagcttccaagccttca	cacctcccagcnggaacat
ARC	gctgggccaatgagaaac	agctctgcgctgagtcctg

Table 2.4: DNA-substrates used for EMSAs and protein crystallography (cryst)

Name	Sequence (5' to 3'); for	Sequence (5' to 3'); rev
CM-1 (EMSA)	cccccaccacgtggtgcctga	tcaggcaccacgtggtggggg
Max-Max (cryst)	gtgtaggccacgtgaccgggtg	cacccggtcacgtggcctacac
Myc-Max (cryst)	cgagtagcacgtgctactc	gagtagcacgtgctactcg

Table 2.5: Primers used for shRNA recovery and high-throughput sequencing

ampl.: amplification; NGS: next generation sequencing

Name	Sequence (5' to 3'); for	Sequence (5' to 3'); rev
shRNA ampl.	gtgactggagttcagacgtgtgctcttccgat ctgccgcctcgactagggataacagggtaa	acactctttccctacacgacgctcttccgatctt agccccttgaagtccgaggcagtagg
shRNA NGS	cccttgaagtccgaggcagtaggca	N/A

2.1.2 Plasmids

Plasmids used in this study are listed below. If not indicated otherwise, the plasmids were already available in the groups of Prof. Martin Eilers and Prof. Caroline Kisker.

Table 2.6: Empty vectors

Name	Characteristics	Reference/ Supplier
pETM-11	bacterial expression vector; N-terminal GST-tag; TEV cleavage site; T7 promoter; kanamycin resistance	EMBL Heidelberg
pGEX-4T1	bacterial expression vector; N-terminal His$_6$-tag; thrombin cleavage site; tac promoter; ampicillin resistance	GE Healthcare Life Sciences
pcDNA 3.1	eukaryotic expression vector; CMV promoter	Invitrogen
pLeGO-iG2-puro-IRES-GFP	lentiviral expression vector; SFFV promoter, puromycin resistance; eGFP	Boris Fehse, Hamburg-Eppendorf
RT3GEPIR	lentiviral shRNA expression vector; Tet-On all in one system; PGK promoter; puromycin resistance; eGFP (inducible)	Lars Zender, Tübingen

Table 2.7: Lentiviral packaging vectors

Name	Characteristics	Reference/ Supplier
psAX.2	plasmid for lentivirus production, encoding for virion packaging system	(Naldini et al., 1996)
pMD2.G	plasmid for lentivirus production, encoding for virion envelope	(Naldini et al., 1996)

Table 2.8: Expression vectors available in the group of Prof. Martin Eilers

Name	Characteristics
pGEX4T1_Max	bacterial expression vector; CDS of *MAX*

Table 2.9: Expression vectors generated for this study

Name	Characteristics
pETM-11_ OmoMYC	bacterial expression vector; CDS of *OmoMYC*
pETM-11_MYC	bacterial expression vector; CDS of *MYC* amino acids 353-434 (b/HLH/Zip)
pGEX4T1_ OmoMYC	bacterial expression vector; CDS of *OmoMYC*
pLeGO_HA- OmoMYC	eukaryotic expression vector; CDS of *OmoMYC*; N-terminal HA-tag

2.2 Chemicals

All chemicals and solutions were purchased from Roth, Sigma-Aldrich, Invitrogen Fluka, Hampton Research, Merck, Calbiochem or Applichem. Chemicals were of analytical grade or better, chemicals used for crystallization were of the highest available purity. If not indicated otherwise, solutions and buffers were prepared in ddH$_2$O.

2.3 Buffers and solutions

Table 2.10: Buffers and solutions used in this study

Name	Composition
Bacterial lysis buffer (GST-tagged proteins)	20 mM Tris-HCl pH 8.0 0.5 M NaCl + 1 Complete EDTA-free PI cocktail tablet (Roche) + 0.05-0.1 % DNase + 3 mM MgCl$_2$
Bacterial lysis buffer (OmoMYC)	20 mM Tris-HCl pH 8.0 0.5 M NaCl 10 mM Imidazole + 1 Complete EDTA-free PI cocktail tablet (Roche) + 0.05-0.1 % DNase + 3 mM MgCl$_2$
Bacterial lysis buffer (MYC)	20 mM HEPES pH 8.0 0.5 M NaCl 10 mM Imidazole + 1 Complete EDTA-free PI cocktail tablet (Roche) + 0.05-0.1 % DNase + 3 mM MgCl$_2$

Blocking solution for PVDF membranes	5 % (w/v) low fat powdered milk in TBS-T
Blocking solution for ChIP	5 mg/ml BSA in PBS
BCA buffer A	1 % (w/v) BCA-Na$_2$ 2 % (w/v) Na$_2$CO$_3$ x H$_2$O
BCA buffer B	4 % (w/v) CuSO$_4$ x 5 H$_2$O 0.16 % (w/v) Na-tartrate 0.4 % (v/v) NaOH 0.95 % (w/v) NaHCO$_3$
Bradford reagent	0.01 % (w/v) Coomassie Brilliant Blue G250 8.5 % (v/v) Phosphoric acid 4.75 % (v/v) Ethanol
ChIP elution buffer	50 mM Tris-HCl pH 7.5 1 mM EDTA 1 % (w/v) SDS, freshly added
ChIP lysis buffer I	5 mM PIPES pH 8.0 85 mM KCl 0.5 % (v/v) NP-40 0.1 % (v/v) Protease inhibitor cocktail (Sigma), freshly added
ChIP lysis buffer II / RIPA buffer	50 mM HEPES pH 7.9 140 mM NaCl 1 mM EDTA 1 % (v/v) Triton X-100 0.1 % (w/v) Na-deoxycholate 0.1 % (w/v) SDS 0.1 % (v/v) Protease inhibitor cocktail (Sigma), freshly added
ChIP wash buffer I	20 mM Tris-HCl pH 8.1 150 mM NaCl 2 mM EDTA 1 % (v/v) Triton X-100 0.1 % (w/v) SDS
ChIP wash buffer II	20 mM Tris-HCl pH 8.1 500 mM NaCl 2 mM EDTA 1 % (v/v) Triton X-100 0.1 % (w/v) SDS
ChIP wash buffer III	10 mM Tris-HCl pH 8.1 1 mM EDTA 250 mM LiCl 1 % (v/v) NP-40 1 % (w/v) Na-deoxycholate
Coomassie staining solution	50 % (v/v) Ethanol 10 % (v/v) Acetic acid 0.1 % (w/v) Coomassie brilliant blue R-250
Coomassie destain solution	10 % (v/v) Ethanol 5 % (v/v) Acetic acid

Crystal violet solution	0.1 % (w/v) Crystal violet 20 % (v/v) Ethanol
DNA annealing buffer	20 mM Tris-HCl pH 8.0 150 mM NaCl 5 mM MgCl$_2$ 1 mM EDTA autoclaved
DNA binding buffer (10 x)	100 mM Tris-HCl pH 8.0 500 mM KCl 50 mM MgCl$_2$ 10 mM EDTA
DNA loading buffer (6 x)	10 mM EDTA, pH 8.0 0.2 % (w/v) Orange G 40 % (w/v) Sucrose
GSH wash buffer	20 mM Tris-HCl pH 8.0 0.5 M NaCl
GSH elution buffer	20 mM Glutathione 500 mM NaCl 20 mM Tris-HCl pH 8.0
IEC high salt buffer (OmoMYC, MAX)	1 M NaCl 20 mM Tris-HCl pH 8.0
IEC high salt buffer (MYC)	1 M NaCl 20 mM HEPES pH 8.0
IEC low salt buffer 1 (OmoMYC, MAX)	75 mM NaCl 20 mM Tris-HCl pH 8.0
IEC low salt buffer 1 (MYC)	75 mM NaCl 20 mM HEPES pH 8.0
IEC low salt buffer 2 (OmoMYC)	250 mM NaCl 20 mM Tris-HCl pH 8.0
IEC low salt buffer 2 (MYC)	250 mM NaCl 20 mM HEPES pH 8.0
IEC no salt buffer (MAX)	20 mM Tris-HCl pH 8.0
Modified RIPA buffer	150 mM NaCl 50 mM Tris pH 8.0 25 mM Beta-glycerophosphate 100 mM Sodium fluoride 2 mM Sodium orthovanadate 10 mM Sodium pyrophosphate 2 mM EDTA 1 % (v/v) NP-40 1 mM Phenylmethylsulfonyl fluoride, freshly added 0.1 % (v/v) Protease inhibitor cocktail (Sigma), freshly added 10 mM N-ethylmaleimide, freshly added
Native acylamide gel (6%)	6 % Acrylamide / Bis-acrylamide 30 (37.5:1) 0.5 x TBE 0.2 % (w/v) APS 0.1 % (v/v) TEMED

Ni-NTA wash buffer (OmoMYC)	20 mM Tris-HCl pH 8.0 0.5 M NaCl 10 mM Imidazole
Ni-NTA wash buffer (MYC)	20 mM HEPES pH 8.0 0.5 M NaCl 10 mM Imidazole
Ni-NTA elution buffer (OmoMYC)	20 mM Tris-HCl pH 8.0 0.5 M NaCl 50 - 500 mM Imidazole
Ni-NTA elution buffer (MYC)	20 mM HEPES pH 8.0 0.5 M NaCl 50 - 250 mM Imidazole
PBS (1 x)	137 mM NaCl 2.7 mM KCl 10.1 mM Na_2HPO_4 1.76 mM KH_2PO_4 autoclaved
PEI transfection solution	450 µl PEI (10 %, MW 25,000 g/mol, Sigma) 150 µl HCl (2 N) 49.5 ml ddH_2O
Plasmid prep buffer 1	50 mM Tris-HCl pH 8.0 100 mM EDTA 100 µg/ml RNaseA
Plasmid prep buffer 2	200 mM NaOH 1 % (w/v) SDS 3.1 M potassium acetate pH 5.5
Protein loading buffer (3 x)	187.5 mM Tris-HCl pH 6.8 30 % (v/v) Glycerine 6 % (w/v) SDS 0.03 % (w/v) Bromphenol blue 2 M β-Mercaptoethanol
SDS running buffer	25 mM Tris base 250 mM Glycine 0.1 % (w/v) SDS
SDS separating gel (7.5-15 %)	7.5-15 % Acrylamide / Bis-acrylamide 30 (37,5:1) 375 mM Tris-HCl pH 8.8 0.1 % (w/v) SDS 0.1 % (w/v) APS 0.1 % (v/v) TEMED
SDS stacking gel (4 %)	4 % Acrylamide / Bis-acrylamide 30 (37,5:1) 125 mM Tris-HCl pH 6.8 0.1 % (w/v) SDS 0.1 % (w/v) APS 0.1 % TEMED
Silver stain fixing solution	50 % (v/v) Methanol 10 % (v/v) Acetic acid
Silver stain sensitization solution	0.02 % (w/v) Na_2SO_3 x 5 H_2O

Silver stain staining solution	0.2 % (w/v) AgNO$_3$ 0.075 % (v/v) Formaldehyde, added shortly before use stored protected from light
Silver stain developing solution	6 % Na$_2$CO$_3$ 0.05 % Formaldehyde, added shortly before use
Silver stain stopping solution	1 % (v/v) Acetic acid
Stripping buffer	2 M Glycin 1 % (v/v) Tween-20 0.1 % (w/v) SDS adjust pH to 2.3 with HCl
Superdex buffer (OmoMYC)	300 mM NaCl 20 mM Tris-HCl pH 8.0
Superdex buffer (MYC)	300 mM NaCl 20 mM HEPES pH 8.0
TAE	40 mM Tris base 0.114 % (v/v) Acetic acid 1 mM EDTA adjusted to pH 8.0
Tank blot buffer (1 x)	25 mM Tris base 192 mM Glycin 20 % (v/v) Methanol (will automatically reach pH 8.3)
TBE (5 x)	445 mM Tris base 445 mM Boric Acid 10 mM EDTA (will automatically reach pH 8.0)
TBS (20 x)	500 mM Tris base 2.8 M NaCl adjusted to pH 7.4
TBS-T	0.2 % (v/v) Tween-20 25 mM Tris base 140 mM NaCl adjusted to pH 7.4
TE	10 mM Tris 1 mM EDTA adjusted to pH 8.0
Trypsin solution	0.25 % Trypsin 5 mM EDTA 22.3 mM Tris base 125 mM NaCl adjusted to pH 7.4

2.4 Crystallization screens

Table 2.11: Crystallization screens used in this study

Crystallization screens were produced using the Lissy 2002 pipetting robot.

Name	Supplier
Index Screen	Hampton Research
Nucleix Suite	Qiagen
PEG Suite	Qiagen
Wizard Screen I/II	Emerald BioSystems

2.5 Strains and cell lines

2.5.1 Bacterial strains

Table 2.12: Bacterial strains (*E. coli*) used for plasmid amplification and protein expression in this study

Application	Strain	Genotype	Supplier
Plasmid amplification	DH5α	F-φ80dlacZΔM15 Δ(lacZYA-argF)U169 deoR recA1 endA1 hsdR17(rk-, mk+) phoA supE44 λ- thi-1 gyrA96 relA1	Invitrogen
Plasmid amplification	XL1-Blue	recA1 endA1 gyrA96 thi-1 hsdR17 supE44 relA1 lac [F′ proAB lacIqZΔM15 Tn10 (Tetr)]	Stratagene
Protein expression	BL21 (DE3)	B F–dcm ompT hsdS(rB–mB–) galλ(DE3)	New England Biolabs
Protein expression	Arctic express (DE3)RIL	B F– ompT hsdS(rB– mB–) dcm+ Tetr gal λ(DE3) endA Hte [cpn10 cpn60 Gentr] [argU ileY leuW Strr]	Stratagene

2.5.2 Cell lines

HEK293TN   human embryonic kidney cell line (ATCC)

U2OS (clone W11-1-4)   human osteosarcoma cell line (ATCC); stably transfected with a doxycycline-inducible two-vector system to overexpress human c-MYC (tet-on; Clontec Laboratories) (kindly provided by Elmar Wolf)

KPC   murine pancreatic adenocarcinoma cell line (Ptf1a+/Cre; Kras+/LSLG12D; p53loxP/R172H) (kindly provided by Jens Siveke, Technical University, Munich)

2.5.3 Media and antibiotics for bacterial cell culture

LB medium (plasmid amplification)

10 % (w/v) Bacto tryptone
0.5 % (w/v) Yeast extract
1 % (w/v) NaCl

LB medium (protein expression)

LB liquid medium (Lennox) (Carl Roth)

LB agar

LB-medium
1.2 % (w/v) Bacto-Agar
autoclaved, cooled down to 50 °C before adding the appropriate antibiotic, 20 ml poured into 10 cm dishes

Antibiotics

Depending on the resistance marker on the corresponding DNA plasmid, the following antibiotics were added to the LB-medium or LB-agar:

Table 2.13: Antibiotics for bacterial cell culture

Antibiotic	Stock	Final concentration
Ampicillin	100 mg/ml	100 mg/ml
Kanamycin	20 mg/ml	20 mg/ml
Gentamycin	10 mg/ml	20 mg/ml

2.5.4 Media for mammalian cell culture

Basal medium

DMEM containing 4.5 g/l glucose and 0.584 g/l L- glutamine (Sigma)

10 % (v/v) FBS (Biochrom, heat inactivated for 30 min at 56 °C before usage)
1 % (v/v) Penicillin / streptomycin (Sigma)

Transfection medium

DMEM containing 4.5 g/l glucose and 0.584 g/l L-glutamine (Sigma)
2 % (v/v) FBS (Biochrom, heat inactivated for 30 min at 56 °C before usage)

Freezing medium

10 % (v/v) DMSO
40 % (v/v) Basal medium
50 % (v/v) FBS

2.5.5 Antibiotics and supplements for mammalian cell culture

Table 2.14: Antibiotics and supplements for mammalian cell culture

Antibiotic	Stock	Final concentration	Supplier
Puromycin	10 mg/ml	0.5-2 µg/ml	InvivoGen
Doxycyclin	1 mg/ml in EtOH	1 µg/ml	Sigma
Polybrene	4 mg/ml	4 µg/ml	Sigma

2.6 Inhibitors

Table 2.15: Inhibitors for in vitro application

Inhibitor	Vehicle / Solvent	Source
Benzylserine (BenSer)	DMEM basal medium	Sigma
2-Aminobicyclo[2.2.1]heptane-2-carboxylic acid (BCH)	DMEM basal medium	Sigma
Difluoromethylornithine (DFMO)	PBS	Sigma
Tigecycline	DMSO	Sigma
CX-5461	DMF	Selleck Chemicals
RA 190	DMSO	Xcessbio Biosciences Inc.

2.7   Standards, enzymes and kits

2.7.1   Standards and Thermofluor dye

DNA marker	Gene Ruler 1 kb Plus DNA ladder (Thermo Scientific)
Protein marker	PageRuler prestained protein ladder (Thermo Scientific)
Thermofluor dye	SYPRO Orange protein gel stain (Invitrogen)

2.7.2   Enzymes

DNase	Applichem
M-MLV Reverse Transcriptase	Promega
Phusion High Fidelity DNA polymerase	Thermo Scientific
Restriction endonucleases	Thermo Scientific, New England Biolabs (NEB)
RNase-free DNase	Qiagen
RNaseA	Roth
SYBR Green qPCR Master Mix	Thermo Scientific
T4 DNA ligase	Thermo Scientific
Thrombin	GE Healthcare

2.7.3   Kits

Experion DNA 1K Analysis kit	Bio-Rad
Experion RNA StdSense Analysis Kit	Bio-Rad
GeneJET Gel Extraction Kit	Thermo Scientific
GeneJET PCR Purification Kit	Thermo Scientific
Immobilon Western HRP Substrate	Millipore
MinElute PCR Purification Kit	Qiagen
NEBNext ChIP-Seq Library Prep Master Mix Set for Illumina	NEB
NEBNext Multiplex Oligos for Illumina (Index Primer Set 1+2)	NEB
NEBNext Multiplex Oligos for Illumina (Dual Index Primers Set 1)	NEB

NEBNext Poly(A) mRNA Magnetic Isolation Module   NEB

NEBNext Ultra RNA Library Prep Kit for Illumina   NEB

PureLink HiPure Plasmid Maxiprep Kit   Invitrogen

QIAquick PCR Purification Kit   Qiagen

QIAquick Gel Extraction Kit   Qiagen

Quanti-iT PicoGreen dsDNA Assay Kit   Thermo Scientific

RNeasy Mini Kit   Qiagen

2.8 Antibodies and sera

2.8.1 Primary antibodies

All primary antibodies were diluted in 5 % (w/v) BSA in TBS-T.

Table 2.16: List of primary antibodies

ChIP: Chromatin Immunoprecipitation; IB: Immunoblot

Antibody	Host / Isotype	Application	Supplier / Source
CDK2	rabbit, polyclonal IgG	IB	M2, Santa Cruz, sc-163
HA-tag	rabbit, polyclonal IgG	ChIP, IB	Abcam, ab9110
MAX	rabbit, polyclonal IgG	EMSA	C17 X, Santa Cruz, sc-197 X
MYC	mouse, monoclonal IgG$_1$	IB	9E10, produced by AG Eilers
MYC	mouse, monoclonal IgG$_1$	EMSA	9E10 X, Santa Cruz, sc-40 X
MYC	rabbit, polyclonal IgG	IB	N-262, Santa Cruz, sc-764
MYC	rabbit, polyclonal IgG	ChIP, EMSA	N-262 X, Santa Cruz, sc-764 X
MYC	rabbit, polyclonal IgG	IB	Y69, Abcam, ab32072
OmoMYC	rabbit, polyclonal IgG	EMSA	Laura Soucek, Barcelona
VINCULIN	mouse, monoclonal IgG$_1$	IB	V9131, Sigma-Aldrich

2.8.2 Secondary antibodies

All secondary antibodies were diluted in 5% (w/v) low fat powdered milk in TBS-T.

Table 2.17: List of secondary antibodies used for immunoblots

Antibody	Host / Isotype	Supplier / Source
anti-mouse IgG-HRP	donkey	sc-2314, Santa Cruz
anti-rabbit IgG-HRP	donkey	sc-2313, Santa Cruz

2.8.3 Control sera for ChIP

Table 2.18: Control sera for ChIP

Antibody	Host / Isotype	Supplier / Source
IgG	polyclonal mouse serum	Sigma
IgG	polyclonal rabbit serum	GE Healthcare

2.9 Consumables

Consumables such as cell culture dishes, reaction tubes, crystallization plates, concentrators and other disposable plastic items were purchased from the companies Applied Biosystems, Eppendorf, Greiner, Kimberley- Clark, Nunc, Sarstedt and VWR.

2.10 Equipment

Table 2.19: Technical equipment used in this study

Application	Specification	Supplier
Automated Electrophoresis	Experion Automated Electrophoresis System	Bio-Rad
Chemiluminescence imaging	LAS-4000 mini	Fujifilm
Cell culture incubator	BBD 6220	Heraeus
Cell Counter	CASY cell counter	Innovatis
Centrifuges (AG Eilers)	Avanti J-26 XP 5417 R/ 5425 / 5430 Galaxy MiniStar Multifuge 1S-R	Backman Coulter Eppendorf VWR Heraeus

Centrifuges (AG Kisker)	Avanti J-26S XP / J-HC	Beckmann Coulter
	5415 D / 5415R / 5417R /	Eppendorf
	5810R	
	Heraeus Multifuge X3R Fiber	Thermo Scientific
	Lite F12-8x50C	
	Biofuge 13R No. 3757	Heraeus Kendro
Columns for manual affinity chromatography	Econo-Column 1.5x20 cm	Bio-Rad
	Econo-Column 0.7x20 cm	
Columns for FPLC systems	GSTrap HP	GE Healthcare
	HiTrap Benzamidine FF	
	MonoQ 5/50 GL	
	MonoQ 10/100 GL	
	MonoS 10/100 GL	
	HiLoad 16/60 Superdex 200 pg	
	Superdex 75 10/300 GL	
	Superdex 200 10/300 GL	
Cryo loop	Crystal CapTM hT (Spine)	Hampton Research
Crystallization robot	Honey Bee 963	Zinsser Analytic
Deep-sequencer	Genome Analyzer IIx	Illumina
	NextSeq500	
Fast protein liquid chromatography systems (FPLC)	ÄKTA pure M1	GE Healthcare
	ÄKTAxpress	
Fluorescence Imager	Molecular Imager Pharos (FX) System	BioRad
Gel-drying device	Heto-Dry gD-1	Heto Lab Equipment
Heating block	Dry Bath System	Starlab
	Thermomixer comfort	Eppendorf
Heat Sealing	ALPTM 50V	Thermo Scientific
Homogenizer	Cell Disruptor M-110P	Microfluidics
Incubator shaker	G25	New Brunswick Scientific
	ISF-1-W/ ISF-1-X / LT-X	Kühner
	Certomat U	B. Braun
Microscopes	Axiovert 40 CFL, HXP 120 (AG Eilers)	Zeiss
	Stemi 2000-C, KL 2500 LCD, AxioCam MRC (AG Kisker)	
PCR thermal cycler	Mastercycler pro S	Eppendorf
Photometer	Multiscan Ascent	Thermo Labsystems
	Ultrospec 3100 pro UV/Visible	Amersham Biosciences
	NanoDrop 1000	Thermo Scientific
	Bio-Photometer	Eppendorf
Pipetting robot	Lissy 2002	Zinsser Analytic
Power supplies	Power Pac	Bio-Rad
	Consort EV231/EV243	Roth
PVDF transfer membrane	Immobilon-P transfer membrane	Millipore

Quantitative RT-PCR machine	Mx3000P Mx3005P	Stratagene
Resins	Ni-NTA Agarose Glutathion Sepharose 4B	Qiagen GE Healthcare
SDS-PAGE system	Mini-PROTEAN Tetra Cell	Bio-Rad
Sealing robot	RoboSeal	Zinsser Analytic
Sterile bench	HeraSafe	Heraeus
Ultrasonifier	Digital Sonifier W-250 D	Branson
UV fluorescent table	Maxi UV fluorescent table	Peqlab
Vortex mixer	Vortex-Genie 2	Scientific Industries
Water bath	ED-5M water bath Memmert waterbath	Julabo Memmert
Immunoblot transfer chamber	PerfectBlue Tank Electro Blotter Web S	Peqlab
Whatman filter paper	Gel Blotting Paper	Schleicher and Schuell
X-ray detector	R-Axis IV++ R-Axis hTC	Rigaku
X-ray generator	Ultra X18 MicroMax-007 hF	Rigaku

2.11 Software, databases and online programs

Table 2.20: Software, databases and online programs used in this study

Name	Supplier / Reference
Acrobat Professional	Adobe Systems
ApE – A plasmid Editor	http://biologylabs.utah.edu/jorgensen/wayned/ape/
bcl2fastq	Illumina
BEDtools	(Quinlan and Hall, 2010)
Bioconductor incl. the following packages: - biomaRt - edgeR - GenomicAlignments - GenomicFeatures - GenomicRanges - limma - Rsamtools	(Huber et al., 2015) http://www.bioconductor.org (Durinck et al., 2009) (Robinson et al., 2010) (Lawrence et al., 2013) (Lawrence et al., 2013) (Lawrence et al., 2013) (Ritchie et al., 2015) Martin Morgan, Herve Pages, Valerie Obenchain, Nathaniel Hayden
BLAST	http://blast.ncbi.nlm.nih.gov/Blast.cgi
Bowtie versions 1 and 2	(Langmead, 2010) www.bowtie-bio.sourceforge.net
CASAVA	Illumina

CCP4 program suite incl. e.g. - AIMLESS - Coot - MATTHEWS_COEF - POINTLESS - PHASER	(Winn et al., 2011) http://www.ccp4.ac.uk (Evans, 2011) (Emsley and Cowtan, 2004) (Matthews, 1968) (Evans, 2011) (McCoy et al., 2007)
Clustal Omega	(Sievers et al., 2011)
ClustalW	(Thompson et al., 1994)
Compusyn	ComboSyn
DAVID	(Huang da et al., 2009a, b) http://david.abcc.ncifcrf.gov/
dGidb	(Griffith et al., 2013) http://dgidb.org/
EndNote X7	endnote.com / Thomson Reuters
ExPASY Proteomics Server	http://www.expasy.ch/
FastQC	http://www.bioinformatics.babraham.ac.uk/projects/fastqc/
Galaxy	(Blankenberg et al., 2010; Giardine et al., 2005) (Goecks et al., 2010) https://main.g2.bx.psu.edu/
GEO	(Edgar et al., 2002) http://www.ncbi.nlm.nih.gov/geo/
Gibthon ligation calculator	http://www.gibthon.org/ligate.html (discontinued)
Illustrator	Adobe Systems, Inc
ImageJ	(Schneider et al., 2012) http://imagej.nih.gov/ij/
Integrated Genome Browser	(Nicol et al., 2009)
Java Treeview	(Saldanha, 2004)
Mac OS X	Apple Inc.
MACS v1.4.2	(Zhang et al., 2008)
MEME suite	(Bailey et al., 2009) http://meme-suite.org
MolProbity	(Chen et al., 2010)
Multi Gauge	Fujifilm
MSigDB 5.0 / GSEA	(Subramanian et al., 2005) www.broadinstitute.org/gsea/msigdb/index.jsp
MxPro qPCR Software	Stratagene
National Center for Biotechnology Information	http://www.ncbi.nlm.nih.gov/
Office 2011 Mac	Microsoft Inc.
Papers	Mekentosj
Photoshop	Adobe Systems, Inc.
PDB - RCSB Protein Data Bank / PDBe	Velankar et al., 2012
PDBePISA	(Krissinel and Henrick, 2007)
PHENIX.refine	(Adams et al., 2010)
Phyre[2] Server	(Kelley and Sternberg, 2009)

Primer3	Rozen & Skaletsky, 2000 http://frodo.wi.mit.edu/
PrimerX	http://www.bioinformatics.org/primerx/
Prism6	GraphPad Software Inc.
ProtParam	(Gasteiger et al., 2003)
PyMOL/ X11 Hybrid	(Schrodinger, 2015) https://www.pymol.org
PubMed	http://www.ncbi.nlm.nih.gov/pubmed
R 3.1.1	R foundation
RTA v2	Illumina
Samtools	(Li et al., 2009) http://samtools.sourceforge.net/
SeqMiner v1.3.3	(Ye et al., 2011)
SnapGene Viewer 2.6.2	http://www.snapgene.com/
UCSC Genome Bioinformatics	http://genome.ucsc.edu
XDS	(Kabsch, 2010)

3   Methods

3.1   Molecular biology methods

3.1.1 Transformation of *E. coli* cells with plasmid DNA and plasmid amplification

A ligation mixture (3.1.3) or 1 µg plasmid DNA (Table 2.6-Table 2.9) were added to 50 µl chemically competent *E. coli* (*Escherichia coli*) cells (listed in Table 2.12) thawed on ice, and incubated for 30 min on ice, followed by a heat shock for 90 s at 42 °C. The mixture was cooled on ice for 1 min before 800 µl of LB medium without antibiotics were added. Subsequently, the bacterial suspension was incubated at 37 °C while shaking before plating on LB-agar containing the appropriate antibiotic (Table 2.13) for selection. To this end, cells were pelleted, the supernatant was carefully decanted and the bacterial pellet resuspended in the remaining LB medium. The LB-agar plates were incubated over night at 37 °C.

Single colonies were transferred to LB-medium with the appropriate antibiotics. The cultures were incubated over night while shaking at 200 rpm and 30-37 °C. Cells were harvested by centrifugation at 4 °C.

3.1.2   Isolation of plasmid DNA from bacteria

3.1.2.1 Analytical preparation of plasmid DNA from bacteria (Miniprep)

Plasmid DNA was extracted using alkaline lysis. 1-2 ml bacterial overnight culture was spun down and the bacteria were resuspended in 200 µl plasmid prep buffer 1. To denature protein components, 200 µl plasmid prep buffer 2 was subsequently added and the mixture was inverted 10 times. Lysis was stopped by adding 200 µl plasmid prep buffer 3 and samples were spun down (13,000 rpm, 5 min, room temperature). To precipitate the plasmid DNA, the supernatant was mixed with 600 µl isopropanol, incubated at -20 °C for 30 min, and then

pelleted through centrifugation (13,000 rpm, 20 min, 4 °C). The DNA was washed once with 500 µl 70 % ethanol, air-dried and solubilized in 30 µl Ampuwa water (aqua ad iniectabilia, Fresenius Kabi).

3.1.2.2 Preparative isolation of plasmid DNA from bacteria (Maxiprep)

Large-scale purification of plasmid DNA was performed using the PureLink HiPure Plasmid Maxiprep Kit (Life Technologies) from 200 ml over night bacterial culture according to the manufacturer's instructions. The purified plasmid was dissolved in Ampuwa water and the DNA concentration was adjusted to 1 µg/µl.

3.1.3 Cloning techniques

3.1.3.1 Cloning using restriction enzymes

Cloning using restriction enzymes (restriction endonucleases) involves a restriction digest of both the vector as well as the insert DNA followed by a purification step (see 3.1.4 and 3.1.5) and a subsequent ligation reaction.

Sequence-specific DNA fragmentation using restriction endonucleases (Fermentas, New England Biolabs) was achieved according to the manufacturers instructions and as described in Table 3.1 and incubated for one hour at 37 °C. This recipe was upscaled for a preparative restriction digest and incubation time was prolonged.

Table 3.1: Recipe analytical restriction digest

Component	Amount
Plasmid DNA	1 µg
Restriction endonuclease 1	0.5 µl
Restriction endonuclease 2	0.5 µl
10 x reaction buffer	2 µl
Ampuwa water	ad 20 µl

Thereafter, vector and insert DNA were purified preferably via agarose gel electrophoresis and subsequent gel extraction (see 3.1.4 and 3.1.5). If a single site was used for restriction cloning, the vector was dephosphorylated via addition of 1 µl alkaline phosphatase (Thermo Scientific) directly to the restriction digest mixture and incubation for 10 min at 37 °C to prevent re-ligation of the vector DNA.

Ligation of the insert into the linearized vector was catalyzed using a T4 DNA ligase (Thermo Scientific). The insert DNA was used in 10 x molar excess (calculated using the Gibthon ligation calculator) or 2 x/100 x absolute excess to the linearized vector. The reaction was carried out for two hours at room temperature or 16 °C over night according to the recipe in Table 3.2. The mixture was then transformed into chemically competent *E. coli* cells according to 3.1.1.

Table 3.2: Recipe ligation of DNA fragments

Component	Amount
Linearized plasmid DNA	100 ng
Insert DNA	x ng
T4 DNA ligase buffer	2 µl
T4 DNA ligase	1 µl
Ampuwa water	ad 20 µl

3.1.3.2 Sequence and ligation independent cloning (SLIC)

Sequence and ligation independent cloning (SLIC) makes use of *in vitro* homologous recombination of overlapping single-stranded complementary overhangs on the target vector and a PCR-generated insert (Li and Elledge, 2007, 2012).

In the first step, vector and insert DNA fragments with overlapping ends were produced by PCR (see and Table 2.1 and 3.1.10). Template DNA was removed via addition of 10 U of DpnI enzyme to the PCR mixture and incubation for one hour at 37 °C. DNA was purified using the Gene Jet Gel Extraction Kit (Fermentas). Exonuclease treatment (incubating T4 DNA polymerase without dNTPs) induces the formation of 5' single-stranded overhangs. To this end, 3 µg of vector and insert DNA were treated separately with 1 µl of T4 DNA polymerase (New England Biolabs), supplemented with 1 µg BSA in 1 x NEB buffer 2. The mixture was incubated at room temperature for 30 min. The reaction was stopped adding 1/10

of the total reaction volume 10 mM dCTP on ice. Annealing of the fragments (1:1 molar ratio) is achieved via incubation 500 ng of the vector DNA in 1 x T4 ligase buffer (New England Biolabs) for 30 min at room temperature and subsequent transformation into chemically competent DH5α cells (as described in 3.1.1).

3.1.3.3 Site-directed mutagenesis

Site-directed mutagenesis was performed using PCR-driven overlap extension (Heckman and Pease, 2007) as illustrated in Figure 3.1. A mutated fragment is produced by two successive rounds of PCR (see 3.1.10) followed by restriction digest cloning into the target vector (as described in 3.1.3.1). Primers are listed in Table 2.1.
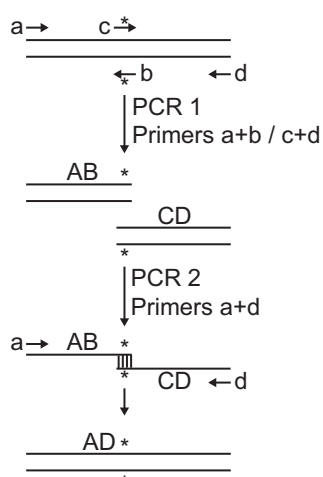
Figure 3.1: PCR-mediated overlap extension for site-directed mutagenesis
Schematic illustrating a PCR of overlapping gene segments to introduce mutations. Primers containing the desired sequence changes to generate mutated residues (b, c) as well as flanking primers (a, d) are used to generate the first PCR products AB and CD separately. These are used as templates for a second PCR, in which the overlapping, complementary regions containing the desired mutation (indicated by *) anneal and the flanking primers generate the final product AD (adapted from (Heckman and Pease, 2007)).

3.1.4 Separation of DNA fragments via agarose gel electrophoresis

DNA fragments were separated via agarose gel electrophoresis according to their negative charge. Depending on the size of the DNA fragment 1-2 % agarose gels prepared in TAE buffer with 0.3 μg/ml ethidium bromide were used. Samples were mixed with DNA loading buffer and loaded using the pockets of the gels previously generated by combs. In addition, a

DNA marker (Thermo Scientific, 2.7.1) was loaded to determine the size of the DNA fragment. Separation was carried out at 120 V for one hour. The ethidium bromide-nucleic acid complex was visualized using a UV transilluminator.

3.1.5 DNA extraction and purification

The DNA fragments of interest were excised from the agarose gel and extracted using silica-based membrane spin columns (GeneJET Gel Extraction Kit, Thermo Scientific) according to the manufacturer's instructions. PCR products were similarly purified (GeneJET PCR Purification Kit, Thermo Scientific) following the manufacturer's instructions.

3.1.6 Nucleid acid quantification

3.1.6.1 Nanodrop

Nucleid acid as well as protein concentrations were determined via UV/VIS spectrophotometry using the NanoDrop 1000 system (PeqLab). For nucleic acid quantification, absorbance at 260 nm was measured. For nucleic acid purity, the ratio of sample absorbance at 260 and 280 nm was determined. At a ratio of ~1.8 (for DNA) and ~2.0 (for RNA) the samples were considered as pure. Protein concentration was measured at 280 nm.

3.1.6.2 Picogreen

To quantify low amounts (pg) of double-stranded DNA (dsDNA), usually obtained when performing ChIPs for sequencing, the Quant-iT PicoGreen dsDNA reagent was used according to the manufacturer's instructions. The fluorescent dye intercalates into dsDNA and the fluorescence intensity can be determined using a fluorescence microplate reader at ~480 nm (excitation wavelength) and ~535 nm (emission wavelength).

3.1.6.3 Automated electrophoresis

For sizing and quantification of RNA used for RNA-sequencing library preparation, as well as DNA libraries for deep sequencing, the Experion Automated Electrophoresis System (Bio-Rad) was applied with the appropriate analysis kit (2.7.3) according to the instructions given by the manufacturer.

3.1.7 Hybridization of DNA oligonucleotides

To generate double-stranded DNA oligonucleotides for electrophoretic mobility shift assays (EMSA) as well as co-crystallization of proteins with DNA fragments the reverse-complimentary oligonucleotides were mixed in equal amounts in DNA annealing buffer and incubated for 5 min at 95 °C in a Thermomixer heating block. Subsequently, the heating was turned off and samples were left to slowly cool overnight in the apparatus. Annealing of the oligonucleotides was verified using native PAGE followed by silver staining (see 3.3.5).

3.1.8 RNA Isolation

3.1.8.1 RNA isolation with TriFAST reagent

To isolate total RNA from mammalian cells the peqGOLD TriFast reagent (Peqlab) was normally used (for RNA isolation for RNA-sequencing see 3.1.8.2). To this end, the cell culture medium was aspirated from adherent cells and the cells were lysed directly on the cell culture plate adding 1 ml TriFast reagent, scraping and transferring the mixture to a reaction tube. 200 μl chloroform was added and the suspension was vortexed for 15 s. The reactions were centrifuged for 10 min at 14,000 rpm (room temperature) to separate the phases. The upper aqueous phase containing the RNA (~500 μl) was subsequently transferred into a new reaction tube. 500 μl isopropanol and 1 μl GlycoBlue co-precipitant (15 μg/μl stock solution, Thermo Scientific) were added to precipitate the RNA. The mixture was incubated on ice for 15 min followed by centrifugation for 15 min (14,000 rpm at 4 °C). The RNA pellet washed twice with 75 % ethanol, air-dried and solubilized in 20-50 μl Ampuwa water, quickly frozen

in liquid nitrogen, thawed again to aid the solubilization. The RNA was used for cDNA synthesis or stored at -80 °C.

3.1.8.2 RNA isolation for deep sequencing

RNA utilized for RNA-sequencing (RNA-seq) was isolated using the RNeasy Mini Kit and on-column DNase I digestion according to the manufacturer's protocol. mRNA was enriched by poly(A) selection using the NEBNext Poly(A) mRNA Magnetic Isolation Module. Library preparation is described in section 3.3.14.2.

3.1.9 cDNA synthesis

In order to analyze transcript levels of individual genes, complementary DNA (cDNA) was reverse transcribed from previously extracted total RNA (3.1.8.1 and 3.1.8.2) using the reverse transcriptase and random hexanucleotide primers. 0.5-2 µg total RNA was diluted with Ampuwa water up to 10 µl, incubated for 2 min at 65 °C to dissolve secondary structures and finally quickly cooled down. For each sample two different reactions were set up: 40 µl cDNA synthesis mix was added either containing reverse transcriptase or not to detect genomic DNA contaminations. The mixtures were incubated for 10 min at 25 °C, at 37 °C for 50 min and 70 °C for 15 min. The cDNA was used for quantitative reverse transcriptase PCR (qPCR, see 3.1.11) reaction or stored at -80 °C.

Table 3.3: Recipe cDNA synthesis mixture

Component	Amount
5x First strand reaction buffer (Promega)	10 µl
dNTPs (10 mM, Roth)	1.25 µl
Random Primer p(dN)6 (2 mg/ml, Roche)	2 µl
Riboloc (Fermentas)	0.2 µl
M-MLV, Reverse Transcriptase (200 U/µl, Invitrogen)	1 µl
Ampuwa water	ad 40 µl

3.1.10 Polymerase chain reaction (PCR)

To generate new cDNA expression vectors, insert mutations, add new restriction sites and tags to the gene of interest, polymerase chain reaction (PCR) was used.

Table 3.4: Recipe PCR reaction mixture

Component	Amount
cDNA template	1-50 ng
5x Phusion HF buffer (Fermentas)	10.0 µl
forward primer (10 µM)	2.5 µl
reverse primer (10 µM)	2.5 µl
dNTPs (10 mM)	1.0 µl
DMSO (optional)	2.5 µl
Phusion High Fidelity DNA Polymerase	1.0 µl
Ampuwa water	ad 50.0 µl

Table 3.5: Standard PCR thermal cycling profile

Cycle step	Temperature	Time	Cycles
Initial denaturation	98 °C	30 s	1
Denaturation	98 °C	10 s	
Annealing	55-72 °C	30 s	25-30
Extension	72 °C	15-30 s per kb	
Final extension	72 °C	5 min	1

3.1.11 Quantitative reverse transcriptase PCR (qPCR)

To quantify nucleic acids - mRNA as cDNA (see 3.1.8 and 3.1.9) or genomic DNA fragments after chromatin immunoprecipitation (see 3.3.13) quantitative reverse transcriptase PCR was applied. A short specific part of the template DNA (amplicon) is exponentially amplified, the amplified DNA is fluorescently labeled and fluorescence is monitored during the PCR process in real time.

Table 3.6: Recipe qPCR reaction mixture

Component	Amount
diluted cDNA / chromatin	1 μl / 10 μl
SYBRGreen Mix (Thermo Scientific)	10 μl
forward primer	5 pmol
reverse primer	5 pmol
Ampuwa water	ad 20 μl

Table 3.7: qPCR thermal cycling profile

Cycle step	Temperature	Time	Cycles
Initial denaturation	95 °C	15 min	1
Denaturation	95 °C	30 s	
Annealing	60 °C	20 s	38
Extension	72 °C	15 s	
Melting curve	95 °C	1 min	
	60 °C	30 s	1
	95 °C	30 s	

qPCR was used determine steady-state mRNA levels of a specific gene across several samples and compare it to levels of another mRNA. For calculation, the threshold cycle (CT) of the specific sample at which the fluorescence signal reached above the background fluorescence was used and normalized to the CT of the housekeeping gene *β2-MICROGLOBULIN* (b2M). The following equations were used for the calculation of relative gene expression according to the delta-delta CT method (Livak and Schmittgen, 2001):

Fold change (FC) $= 2^{-\Delta\Delta CT} =$ [(CT gene of interest - CT b2M) sample A – (CT gene of interest - CT b2M) sample B]

To quantify ChIP DNA, the results were presented as % of input and calculated as followed (usually 1 % input was taken):

% of input $= 2^{CT(1\% \ Input) - CT(IP)}$ x 1 %

The qPCR measurements was performed in triplicates and average and standard deviation were calculated according to the following equation:

$$\text{standard deviation (SD)} = \sqrt{\frac{\Sigma(X-\overline{X})^2}{(n-1)}}$$

3.2 Cell biology methods

3.2.1 Cultivation of eukaryotic cell lines

Eukaryotic cell lines used in this study (see 2.5.2) were grown and maintained in a cell incubator at 37 °C, 5 % CO_2 and a relative humidity of 95 %. All cell culture work was carried out under aseptic conditions using a cell culture hood.

3.2.1.1 Passaging of cells

Adherent cell lines were subcultured every second to third day. For this, the cultivation medium was removed, cells were washed with PBS and dissociated from the cell culture dish adding trypsin and incubating for 2-10 min in the incubator. When the cells had detached, they were resuspended in pre-warmed fresh basal medium (2.5.4) and pelleted at 1200 rpm for 5 min. The cell pellet was resuspended and the cells were replated with pre-warmed fresh basal medium at the desired density on a new cell culture dish. To plate a specific cell number, the cells were counted in suspension using a Neubauer counting chamber (S1 and S2) or a CASY cell counter (S1).

3.2.1.2 Freezing and thawing cells

For long-term storage, cells were cryopreserved in liquid nitrogen. Cells were detached from the cell culture dish (as described in 3.2.1.1) and resuspended in freezing medium (2.5.4), transferred to cryo vials and slowly frozen by reducing the temperature at approximately 1 °C per min in a cryo-freezing container (such as Mr.Frosty, Nalgene) at -80 °C. Once frozen, the vials were transferred to liquid nitrogen storage tanks.

To thaw cells, the vials were rapidly heated in a 37 °C water bath. The cell suspension was diluted 1:10 with pre-warmed fresh basal medium, cell were pelleted at 1200 rpm for 5 min, and resuspended in basal medium before plating on a new cell culture dish.

3.2.2 Transfection of plasmid DNA

Mammalian cells were transfected with plasmid DNA using the PEI method. To this end, cells were plated 24 h before transfection in basal medium at the appropriate density. At least 2 h before the start of the transfection, the basal cell culture medium was replaced by transfection medium (2.5.4). 5-15 µl of plasmid DNA was diluted in 250 µl Opti-MEM. In a second reaction tube, 24 µl PEI (1 µg/µl) were mixed with 250 µl Opti-MEM. Both tubes were incubated for 5 min at room temperature and subsequently mixed by carefully adding the DNA mixture to the PEI mixture drop by drop. After 20 min of incubation, the final transfection mix was added dropwise to the cells. 4-6 h later, the medium was changed to basal medium.

3.2.3 Production of lentiviral particles

For lentivirus production, 293TN cells were transfected with a lentiviral expression plasmid (e.g. pLeGO), the packaging vector psPAX2 and the envelope vector pMD2.G. For this, $5x10^6$ cells were plated on a 10 cm cell culture dish one day before the transfection. Transfection was carried out as described in 3.2.2 with 8 µg lentiviral expression plasmid, 4 µg psPAX2, and 1.25 µg pMD2.G. After the first medium change, lentivirus-containing supernatant was harvested every 12 h for 3 times. Supernatants were pooled, filtered with a 0.45 µm syringe filter and stored at -80 °C.

3.2.4 Infection of mammalian cells

To stably introduce a transgene of interest into mammalian cells, the construct of interest as well as a packaging and a envelope plasmid were transfected into HEK 293TN cells as described in 3.2.3 and the resulting lentivirus added to the target cell line. For a 10 cm cell

culture dish, 3 ml of lentivirus-containing supernatant (for transgene overexpression) were mixed with 3 ml of basal medium and 12 µl polybrene (4 mg/ml) and added to the cells. 24 h after infection, the medium was changed and 48 h post-infection selection antibiotics were added (see 2.5.5).

3.2.5 Hydrogen peroxide treatment

Treatment of adherent cells with hydrogen peroxide (H_2O_2) was performed as described in (Danciu and Whitman, 2010). In preparation for the treatment, the cells were rinsed twice with PBS and subsequently briefly maintained in serum- and antibiotic-free DMEM. After addition of H_2O_2 to the medium, cells were incubated at 37 °C for 5 min and then immediately washed twice with ice cold PBS. In order to prepare cell extracts for immunoblots (for detailed information see sections 3.3.9, 3.3.10, 3.3.11), cells were lysed in modified RIPA buffer containing 10 mM N-ethylmaleimide to prevent disulfide bond formation during cell extract preparation. Samples were divided in two and subjected to protein loading buffer in the presence or absence of 100 mM dithiothreitol (DTT; which was added instead of β-Mercaptoethanol as a reducing agent).

3.2.6 Colony formation assay

To determine the growth and survival behavior of adherent cell lines, cells were grown on 6-10 cm cell culture dishes and stained with crystal violet. Cells were fixed by adding 1/10 of the medium volume formaldehyde (37 %) directly to the medium and incubating at room temperature for 10 min. The dishes were dried thoroughly and crystal violet solution was added for at least 1 h. Spare dye was washed away rigorously with desalted water and the dishes were dried at room temperature.

3.2.7 Cumulative growth curve

To analyze the growth characteristics of a cell line a cumulative growth curve was established. Equal cell numbers (50,000 for U2OS) were plated on 6-well plates. Every

second day the cells were detached via trypsinization, counted, and the initial cell number was replated (50,000 for U2OS). This way, it was ensured the cells grow at a uniform cell density and do not exhibit any contact inhibition at a high density. From the acquired data, a fold increase in cell number (R) (R=X/50,000; X being the total viable cell count) could be calculated. The cumulative cell number (Y) of each passage (p) was determined ($Y_p = Y_{p-1}$ x R) and plotted.

3.2.8 MTT assay, IC_{50} determination and CI analysis

To assay cell proliferation and cytotoxicity in a 96-well format, the MTT assay was applied (Mosmann, 1983). In this colorimetric assay, the yellow tetrazolium salt MTT (3-(4,5-dimethylthiazol-2-yl)-2,5-diphenyltetrazolium bromide) is reduced by metabolically active cells to its purple formazan. The purple insoluble salt is solubilized and the absorbance is measured by spectrophotometric means. To this end, 1,000 KPCs were seeded into 96-well plates (with 100 µl basal medium), 24 h later treated with inhibitors and 48-72 h after inhibitor treatment analyzed using the MTT assay. A MTT working solution (0.25 mg/ml MTT in PBS) was freshly prepared and filtered through a bottle-top vacuum filter (0.2 µm pore size). 100 µl of this solution was added to the cell culture dishes after removal of the growth medium and purple formazan crystals were formed after incubation for 1-2 h in the incubator. Subsequently, 50 µl of the MTT supernatant is removed and 200 µl of DMSO is added and the mixture is resuspended to solubilize the crystals. Absorbance is measured at 550 nm using a plate reader. Background absorbance is subtracted (from blank wells containing medium only) and the effect of the compounds on cell viability was calculated relative to control wells containing vehicle control.

IC_{50} values were fitted by non-linear regression using Prism. For combination index (CI) analysis, fixed-ratio combination experiments using the Chou-Talalay method (Chou and Talalay, 1984) in twofold dilutions were carried out and CI scores were calculated using the Compusyn software (ComboSyn, Inc.).

3.2.9 Pooled negative-selection shRNA screening

Target selection

A custom shRNA library targeting 27 druggable OmoMYC-regulated genes was constructed. The following criteria for target selection from RNA-sequencing data were included: Genes annotated by Ensembl bearing a unique HGNC (Human Genome Organization Gene Nomenclature Committee) symbol had to be significantly OmoMYC-repressed (in the +MYC +OmoMYC situation; q-value <0.05) and at the same time significantly MYC-activated (q-value <0.05). This primary selection resulted in a list of 91 genes, which were further filtered for druggability using the drug-Gene interaction database (dGidb) (Griffith et al., 2013) or manual literature search for published small molecule inhibitors using the PubMed search engine. A table of all 27 target genes containing information about their druggability can be found in Table 7.6. Dr. Carsten Ade constructed the final shRNA library using 5 shRNAs per target.

shRNA library generation

To this end, 135 miR-E based oligonucleotides (a complete list of sequences can be found in the supplementary material of (Jung et al., 2016)) were PCR amplified and pool-cloned into the RT3GEPIR vector, enabling lentiviral transduction and doxycycline-induced shRNA expression (Fellmann et al., 2011). Additionally, 5 shRNAs targeting MYC and 8 shRNAs targeting *Renilla* luciferase were added as positive and negative controls, respectively. Single-stranded oligonucleotides were PCR amplified and ligated into the shRNA expression vector using *Xho*I and *Eco*RI restriction enzymes (see section 3.1.3.1). After transformation into *E.coli* cells (XL1-Blue; see section 3.1.1), >50,000 colonies were pooled and plasmid DNA isolated (see section 3.1.2.2). Subsequently, lentivirus from the pooled shRNA library was produced, as described in section 3.2.3.

Viral transduction and cell sampling

The final lentiviral library was transduced into KPC cells using conditions that predominantly resulted in a single stable shRNA integration per cell (MOI of <0.1). To this end, a total of 10^7 cells were infected and selected for two days using 2 µg/ml puromycin in four biological replicates (n=4). At each passage more than 340,000 cells were maintained to preserve library representation throughout the experiment. Cells of each replicate were either treated with

1 µg/ml doxycycline or ethanol and cultured for four days, representing about seven population doublings.

shRNA recovery and sequencing library preparation

Cells were harvested, genomic DNA was isolated and purified by phenol-chloroform extraction and ethanol precipitation (see section 3.3.13). The shRNA sequences were recovered from the genomic DNA of each sample in two subsequent amplification steps. First, multiple parallel PCRs were done using a standard PCR reaction mixture (see section 3.1.10) with 1 µg genomic DNA and a custom primer pair (listed in Table 2.5).

Table 3.8: PCR thermal cycling profile for shRNA recovery

Cycle step	Temperature	Time	Cycles
Initial denaturation	98 °C	2 min	1
Denaturation	98 °C	10 s	
Annealing	65 °C	20 s	24
Extension	72 °C	30 s	
Final extension	72 °C	5 min	1

PCR products from the first amplification step were gel purified (see section 3.1.5) and used as template for the subsequent PCR. The final library was amplified using commercial index primers (NEBNext Multiplex Oligos for Illumina (2.7.3)) that added barcodes for multiplexing and adaptors suitable for Illumina sequencing. This second PCR was done according to the manufacturer's instructions with 12 denaturation/ annealing/ extension cycles. Libraries were size-selected by excision from an agarose gel (3.1.4) followed by gel extraction with the GeneJET Gel Extraction Kit. The Experion system (3.1.6.3) was used for sizing and quantification. The libraries were sequenced on a Illumina GAIIx platform with a custom sequencing primer (listed in Table 2.5) generating more than 450,000 reads per sample. Bioinformatics analysis of the data is described in section 3.3.14.6.

3.3 Protein biochemistry methods

3.3.1 Protein expression in *E. coli*

For recombinant protein expression, the plasmid containing the protein-encoding sequence (listed in Table 2.8 and Table 2.9) was transformed into Arctic Express or in case of MAX into BL-21 cells (Table 2.12) as described in 3.1.1. 200 ml LB medium (in a 500 ml Erlenmeyer flask) were inoculated with a single colony obtained after transformation. Cells were grown at 37 °C (200 rpm) overnight. Antibiotics suitable for the respective strain-plasmid combination (2.5.3) were added to LB agar plates and liquid medium. Note that only precultures containing Arctic express cells were supplemented with gentamycin. For large-scale expression, 2 l of LB medium (in 5 l Erlenmeyer flasks each; in total 16 l of LB medium per batch) were inoculated with 20 ml of the preculture and grown at 37 °C (200 rpm) until an OD_{600} (optical density measured spectrophotometrically at a wavelength of 600 nm) of 0.8 (for BL21 0.6) was reached. For Arctic Express cells, the temperature was lowered to 14 °C and protein expression was induced by adding 100 µM of IPTG and protein expression was conducted for 18 h. In BL21 cells, protein expression was accomplished at 30 °C for 4 h. Cells were harvested by centrifugation at 5,000 g and 4 °C for 12 min. MYC and OmoMYC proteins did not tolerate freezing of the bacterial pellet, thus cell lysis was performed immediately following the cell harvest.

3.3.2 Recombinant protein purification

Proteins used in this study were purified under native conditions using a series of chromatography steps after cell lysis.

3.3.2.1 Cell lysis

Cell pellets were resuspended in 5-10 ml bacterial lysis buffer per g bacterial pellet (different recipes for hexahistidine- (His_6-; MYC and OmoMYC protein) or glutathione-S-transferase-tagged proteins (GST; e.g. MAX protein: see Table 2.10) and homogenized using the cell

disruptor at 1.3-1.5 kbar, which was cooled with ice. Cell debris was removed via centrifugation (50,000 g, 4 °C, 1 h) and the supernatant was used for the next purification step.

3.3.2.2 Affinity chromatography

His$_6$-tagged proteins

Immobilized metal ion affinity chromatography (IMAC) was performed manually using gravity flow columns as a first purification step of N-terminally His$_6$-tagged proteins after cell lysis. To this end, the cleared lysate was loaded at least twice onto Econo columns with Ni-NTA agarose slurry (1 ml slurry = 0.5 ml bed volume/15 g cell pellet; pre-equilibrated with Ni-NTA wash buffer). Unbound protein was washed off 3 times with 5-6 bed volumes of Ni-NTA wash buffer. OmoMYC was eluted 8 times with 3 ml Ni-NTA elution buffer containing 100 mM imidazole followed by 8 elution fractions with 3 ml of Ni-NTA elution buffer containing 500 mM imidazole. For the MYC protein, the first 8 elution fractions were performed with 50 mM imidazole followed by 8 elution fractions with 250 mM imidazole. Fractions were collected manually and analyzed by SDS-PAGE followed by Coomassie staining (described in 3.3.3 and 3.3.4).

GST-tagged proteins

GST-tagged proteins were affinity-purified using glutathione (GSH) sepharose in gravity flow columns as a first purification step as well as using pre-packed affinity columns (GSTrap HP). Gravity flow columns were manually packed with GSH sepharose (1 ml slurry per 3 g cell pellet), washed extensively with GSH wash buffer and the supernatant after cell lysis was then loaded onto the column. The beads were washed 3 times with 5 ml GSH wash buffer per 1 ml slurry. Protein was eluted 6 times with 3 ml of GSH elution buffer and fractions were collected manually. Beads were washed again 3 times with 5 ml wash buffer and all fractions were analyzed by SDS-PAGE and Coomassie staining of the gel. Pre-packed affinity columns were applied as a polishing step after thrombin cleavage to remove the GST protein tag according to the manufacturer's instructions.

3.3.2.3 Thrombin cleavage

Expression of GST-tagged proteins using the pGEX4T1 vector allowed cleavage of the tag after affinity chromatography. The pooled peak fractions obtained by GSH-affinity chromatography were incubated with 1 U thrombin (dissolved in PBS at 1 U/µl) per mg protein either at 4 °C or room temperature overnight. Thrombin was removed using pre-packed HiTrap Benzamidine affinity columns according to the protocol provided by the manufacturer. The protein was eluted in 10 ml GSH wash buffer and used for ion exchange chromatography.

3.3.2.4 Ion exchange chromatography

Ion exchange chromatography (IEC) was performed using ÄKTA FPLC systems together with columns of the MonoQ (anion exchange) and MonoS (cation exchange) series. Buffers and columns applied for the FPLC run are listed in Table 3.9. Protein samples were diluted to reduce the salt concentration. MAX could be diluted to a final salt concentration of 75 mM, but MYC and OmoMYC only tolerated reduction of the salt concentration to 250 mM and 150 mM respectively. The protein solution was filtered using syringe filters (0.2 µm pore size) and buffers (see Table 2.10; note that different buffer compositions were used for each protein) were filtered (0.2 µm bottle top filter) and degassed prior to the chromatography run. The column was equilibrated with 5 column volumes of buffer A at a flow rate of 3 ml/min. IEC was performed using an injection flow rate of 2 ml/min and elution of the protein was achieved by increasing the salt concentration with a linear gradient over 20 column volumes (start concentration = 0 % high salt buffer (buffer B)) at a flow rate of 3 ml/min. Elution was monitored by measuring absorbance at 280, 260 and 220 nm using the UV/Vis detector (ÄKTAxpress system only 280 nm). The elution fractions as well as the flow through were analyzed via SDS-PAGE and Coomassie staining. Note that MYC did not bind to neither the MonoS nor the MonoQ column but was found quite purely in the flow through of the MonoQ column − as the protein contaminations mostly bound to the column and were eluted in the fraction collector this step could still be considered as a purification step.

Table 3.9: Protein purification via ion exchange chromatography

	His$_6$-OmoMYC	**His$_6$-MYC**	**GST-MAX**
Theoretical PI	9.3	10.0	6.0
Column	MonoS	MonoQ	MonoQ
Dilution buffer	IEC low salt buffer 1	IEC low salt buffer 1	IEC no salt buffer
Buffer A (low salt)	IEC low salt buffer 2	IEC low salt buffer 2	IEC low salt buffer 1
Buffer B (high salt)	IEC high salt buffer	IEC high salt buffer	IEC high salt buffer

3.3.2.5 Size-exclusion chromatography

Size-exclusion chromatography (SEC) was performed on ÄKTA systems using Superdex columns either as a final polishing step or for analytical reasons. The protein solution was concentrated and particles were removed via centrifugation (16,000 g, 4 °C, 10 min) or sterile filtration. Buffers were filtered and degassed. SEC was performed using a flow rate of 1 ml/min (HiLoad column) or 0.5 ml/ml (analytical column) via an isocratic elution over 1 CV using the Superdex buffer (Table 2.10).

3.3.3 SDS polyacrylamide gel electrophoresis (SDS-PAGE)

For analytical protein separation, SDS polyacrylamide gel electrophoresis (SDS-PAGE), a discontinuous denaturing system, was applied (Laemmli, 1970). Recombinant protein solutions (as generated in 3.3.2) or crude cell lysates (see as well 3.3.9) were boiled for 5 min in 3x protein loading buffer at 95 °C and spun down. Polyacrylamide gels consisting of a 7.5-18 % resolving gel and a 4 % stacking gel were placed in a electrophoresis cell, SDS running buffer was added and samples were loaded together with a protein marker. Electrophoresis was carried out at 80 V for 15 min followed by 120 V for 60-90 min to separate the proteins according to their molecular weight.

3.3.4 Coomassie staining

After SDS-PAGE, proteins were visualized via incubation of the gel in Coomassie staining solution under gentle shaking for 15 min followed by repeated incubation in fresh Coomassie destain solution to remove excess dye in the background.

3.3.5 Silver staining

To visualize proteins or nucleic acids after PAGE with a high sensitivity (np-pg range) gels were silver stained. To this end, the gel was bathed under gentle shaking with fixer solution for 1 h, washed once with water and three times with 50 % ethanol for 20 min, and subsequently incubated for 1 min with sensitization solution. After quickly washing the gel three times with water, it was incubated for 20 min in staining solution and the washing was repeated. After this, the gel was incubated in developing solution until the bands were stained to the desired degree. The reaction was stopped adding stopping solution.

3.3.6 Fluorescence-based thermal shift assay

To optimize buffer conditions in a high-throughput approach in order to improve protein stability the fluorescence-based thermal shift assay (Thermofluor assay) was applied (Ericsson et al., 2006; Pantoliano et al., 2001). The protein solution is heated stepwise together with Sypro Orange, a fluorescence dye that is highly fluorescent in non-polar environments. During thermally-induced protein unfolding or melting, florescence is monitored in real time using a qPCR cycler and melting curves are generated from which the melting temperature (T_m) can be deduced based on the infliction point. T_m values were determined in various buffer compositions and positive shifts in T_m were considered to show an increase in protein stability.

0.5-2 µg of protein were heated with 1 µl 2.5 % (v/v) Sypro Orange solution in 100 mM buffer from a buffer screen in duplicates in a 96-well plate (the screen setup can be found in Table 7.1). The mixtures were heated starting at room temperature with a temperature

increase of 1 °C per min to 95 °C. Analysis was performed using an Excel script provided by the Structural Genomics Consortium as described in (Niesen et al., 2007).

3.3.7 Electrophoretic mobility shift assay (EMSA)

To detect protein-DNA interactions the electrophoretic mobility shift assay (EMSA) was used (Hellman and Fried, 2007). Binding reactions were performed with 5'CY3-labled double stranded DNA substrates (listed in Table 2.4; previously annealed according to 3.1.7) and increasing concentrations of recombinant protein at 12 °C for 20 min followed by 25 min at 4 °C in DNA binding buffer in the presence of 10 mM dithiothreitol (DTT) if not indicated otherwise. To induce heterodimer formation, proteins were mixed and pre-incubated for 20 min at 12 °C. If not indicated differently, proteins were mixed at a molar ratio of 3 (MYC) to 1 (MAX or OmoMYC). For supershift assays, antibodies (listed in Table 2.16) were added for 30 min prior to DNA addition. The reaction mixture together with DNA loading buffer was loaded onto a 6 or 8 % native polyacrylamide gel. Electrophoresis was carried out for 1 h at 100 mA and 4 °C in 0.5 x TBE. Gels were imaged using a PHAROS FX fluorescent imager. Dissociation constants were calculated determining the fraction of protein-bound DNA for each protein concentration (from the background-subtracted signal intensities using ImageJ) and fitting the data using non-linear regression (standard four parameter fitting algorithms using Prism).

3.3.8 Protein crystallization

Three-dimensional structures of macromolecules were determined in this study using X-ray crystallography. This involved a series of steps including generation of pure soluble protein (described in 3.3.1 and 3.3.2), growing of protein crystals, data collection, and structure determination as explained in (Blow, 2002; Chayen and Saridakis, 2008; Rhodes, 2006; Rupp, 2010).

3.3.8.1 Crystallization screening

Sample preparation

A concentrated, pure solution of soluble protein was generated (see sections 3.3.1 and 3.3.2). His$_6$-OmoMYC protein was used in 20 mM Tris-HCl pH 8.0, ~500 mM NaCl (as eluted from the IEC column) at a concentration of ~2.9 mg/ml (~ 205 µM). The protein was thawed on ice and debris was removed via centrifugation (16,000 x g, 25 min, 4 °C).

For protein-DNA co-crystallization, DNA oligonucleotides (listed in Table 2.4) were annealed as described in section 3.1.7 to obtain double-stranded DNA (dsDNA) fragments at a final concentration of 250 µM. Protein and dsDNA were mixed at a 1:1.2 molar ratio and incubated for 1 h at 20 °C followed by a concentration step using spin columns (Vivaspin 20, MWCO 10,000) to reduce the sample volume by half. The mixture was again cleared by centrifugation (16,000 x g, 25 min, 4 °C) and used for high-throughput crystallization screens.

High-throughput crystallization screening

Crystallization screens were performed in a high-throughput format using the crystallization robot (Honeybee) and different commercially available sparse-matrix screens (listed in Table 2.11). This permitted the analysis of the protein in several hundred crystallization conditions (varying in buffer composition, pH, addition of precipitants and other additives).

0.3 µl of protein were added to 0.3 µl of reservoir solution to form a crystallization droplet next to 40 µl of reservoir solution in a sitting drop vapor diffusion setup using 96-well crystallization plates (Greiner). The plates were sealed using the sealing robot, stored at 20 °C, and crystal formation was examined using light microscopy at several time points. During incubation, the droplet and the reservoir solution equilibrated by vapor diffusion and the protein and precipitant concentration gradually increased in the droplet thus aiding nucleation and crystal growth. Manual optimization screening was not required since crystals suitable for X-ray diffraction analysis were formed in the initial high-throughput screens. The crystals were removed from the droplet utilizing CryoLoops (used in various sizes according the size of the crystal and attached to Crystal Cap Spine HT, Hampton Research) and cryoprotected by immersion into a solution corresponding to the reservoir solution supplemented with 20 % glycerol. Crystals were stored in liquid nitrogen.

3.3.8.2 Data collection

A three-dimensional electron density map of the crystal is generated analyzing an X-ray diffraction pattern using X-ray crystallography (described in detail in (Blow, 2002; Rhodes, 2006; Rupp, 2010)). This map can serve as a basis to create a three-dimensional model of the protein structure.

For data collection, a crystal is mounted between an X-ray source and an X-ray detector and atoms within the crystal reflect the electromagnetic waves, the reflected waves interfere with waves emitted by other atoms causing a specific diffraction pattern on the detector. The crystal is then rotated around the phi axis to obtain a useful data set for the entire crystal. The position and intensity of each reflection is used for further analysis.

Data collection was performed at synchrotron facilities such as the Berliner Elektronen Speicherring Gesellschaft für Synchrotronstrahlung (BESSY II, in Berlin) or the European Synchrotron Radiation Facility (ESRF, in Grenoble, France) at 100 K. Synchrotron radiation was used at a wavelength of 1.06448 Å (OmoMYC apo data set, ESRF) and 0.91841 Å (DNA-bound OmoMYC data set, BESSY) and data were recorded using charge-coupled device (CCD) or hybrid photon counting (e.g. PILATUS) detectors.

3.3.8.3 Data processing, structure determination and refinement

During data analysis the two-dimensional diffraction patterns are converted to three-dimensional electron density maps using Fourier transformations. Wolfgang Kölmel performed data processing, structure determination and refinement.

Data sets were indexed, integrated and scaled using XDS (Kabsch, 2010) thus identifying the dimensions of the unit cell as well as the symmetry and mosaicity of the crystal and merging the data into a single file with an optimized intensity scale. To estimate the Laue group and space group, POINTLESS (CCP4 suite, (Evans, 2011) was used. Data were reduced with AIMLESS (CCP4 suite), (Evans, 2011) depending on the given data quality indicators (i.e., R_{merge} as a measure of internal consistency, R_{meas} which is multiplicity weighted, $R_{p.i.m.}$ as the precision indicating merging R factor, $<I/\sigma(I)>$ indicating the signal-to-noise ratio at the cut-off level, $CC_{1/2}$ as the Pearson correlation coefficient between random half datasets; (Diederichs and Karplus, 1997; Weiss, 2001; Weiss and Hilgenfeld, 1997)). The Matthews

coefficient was calculated with MATTHEWS_COEF (CCP4 suite) (Matthews, 1968) to determine the number of molecules present in the asymmetric unit.

The apo OmoMYC structure was solved by molecular replacement using PHASER (CCP4 suite) (McCoy et al., 2007)) and the published structure of the DNA-bound MYC/MAX heterodimer (PDB entry 1NKP, (Nair and Burley, 2003)) as a search model. This apo structure was used as a phasing model for structure determination of the DNA-bound OmoMYC structure. Molecular replacement gives incomplete estimates of phases. Phases can be improved by structure refinement. For this, an initial model is built manually into the first electron density map. During various rounds of model building and automated refinement, the electron density map is optimized. In this study, manual structure building was performed with the molecular graphics program Coot (CCP4 suite) (Emsley and Cowtan, 2004; Emsley et al., 2010) and refinement was done with PHENIX.refine (Adams et al., 2010).

Refinement is usually continued until the differences between the measured diffraction intensities and the intensities predicted by the refined model are minimal. As criteria for model quality, further R-factors, R_{work} and R_{free}, are calculated. R_{free} is calculated using a subset of random chosen intensities excluded from the refinement process and only used for cross-validation. The R_{free} factor measures how well the model predicts this subset of measured intensities, while R_{work} assessed the agreement between the model and the entire dataset (Brunger, 1992). The structure was validated using MolProbity (Chen et al., 2010). All images or figures of crystal structures were generated using PyMOL (Schrodinger, 2015).

3.3.9 Generation of whole cell protein extracts

To generate whole cell protein lysates, cell culture dishes were washed with PBS, cells were collected by scraping and pelleted (400 x g, 4 °C, 5 min). The cell pellet was lysed by resuspension in RIPA buffer containing protease inhibitors and incubation on ice for 30 min. Cell debris was removed via centrifugation (18,000 x g, 4 °C, 10 min) and the soluble protein fraction in the supernatant was used for protein quantification (3.3.10) and immunoblot analysis or stored at -80 °C.

3.3.10 Protein quantification using colorimetric assays

3.3.10.1 Bradford assay

Whole cell protein lysates (3.3.9) were quantified according to (Bradford, 1976). 1-2 µl of protein lysate were mixed with 100 µl 150 mM NaCl and 900 µl Bradford reagent. Absorbance was measured at 595 nm using a reference containing lysis buffer instead of protein lysate and protein concentrations were determined using a standard curve generated with different concentrations of a BSA solution.

3.3.10.2 Bicinchoninic acid assay (BCA) assay

As second way to determine the protein concentration of protein lysates, the bicinchoninic acid (BCA) assay was applied. A BCA solution mix was prepared consisting of 49 parts of BCA buffer A and 1 part BCA buffer B. 4 µl sample or lysis buffer (as a blank) were mixed with 200 µl of BCA solution mix, incubated for 20 min at 37 °C and absorbance was measured at 550 nm and protein concentrations were determined using a BSA standard curve.

3.3.11 Immunoblot

To specifically detect a protein of interest in a protein mixture an immunoblot (also referred to as western blot) was generated. For this, proteins were separated via SDS-PAGE (as described in 3.3.3) and in the next step transferred electrophoretically to a polyvinylidene difluoride (PVDF) membrane using the tank blot method. The gel was equilibrated in cold tank blot buffer and the membrane was prepared via a 1 min incubation in methanol followed by a 1 min incubation in desalted water and a 5 min incubation in tank blot buffer. The gel sandwich was assembled putting the membrane and the gel between 4 pieces of blot adsorbent filter paper (Whatman paper, previously soaked with tank blot buffer) and placed into a tank blot transfer system. The transfer tank was placed on a magnetic stirplate in the cold room (4 °C) and the transfer was carried out at 300 mA for 2 h (depending on the size of the protein). The membrane was subsequently incubated while shaking gently for 1 h at room

temperature in blocking solution. After optional cutting of the membrane, it was incubated in 5-10 ml primary antibody solution overnight. For this, the antibody (listed in Table 2.16) was dissolved in 5 % (w/v) BSA in TBS-T. The membrane was washed 5 times for 10 min in TBS-T and incubated in 5 ml secondary antibody in blocking solution (listed in Table 2.17) for 1 h and subjected to 5 further washing steps with TBS-T. Chemiluminescence was used for detection, applying Immobilon Western HRP Substrate according to the manufacturer's instructions as well as a chemiluminescence imager.

3.3.12 Stripping antibodies from PVDF membranes

Antibodies were removed from PVDF membranes via incubation in stripping buffer for 20 min. Subsequently, the membranes were washed 5 times in TBS-T and the immunoblot procedure (3.3.11) was re-started by blocking the membrane in blocking buffer.

3.3.13 Chromatin immunoprecipitation (ChIP)

To investigate protein-DNA interactions, the chromatin immunoprecipitation (ChIP) technique was applied. Briefly, DNA and associated proteins were crosslinked, DNA was sheared and fragments associated with a specific protein were enriched by immunoprecipitation. Finally, DNA fragments were purified and enrichments were quantified using qPCR.

Chromatin preparation

To this end, cell culture dishes were incubated with formaldehyde (1 % final concentration in cell culture medium) for 10 min on a platform shaker at room temperature. Fixation was stopped adding 1 ml 1 M glycine solution and incubating for 5 min. The cells were washed twice with ice cold PBS and cells were removed from the dishes by scraping into PBS containing a protease inhibitor cocktail on ice. Cells of up to 10 dishes were pelleted by centrifugation (800 x g, 5 min, 4 °C), resuspended in 3 ml ChIP lysis buffer I, and incubated 20 min on ice to induce cell swelling. Nuclei were pelleted (800 x g, 5 min, 4 °C) and resuspended in 2 ml ChIP lysis buffer II 10 min before sonification. Sonification was carried out well cooled usually at 20 % amplitude for 15-25 min (10 s pulse, 20 s pause). Sonification

time was determined empirically for every cell line – U2OS cells were sonified for 20 min – to reach a fragment size between 200 and 500 bp.

Chromatin quality control

Chromatin fragment size was determined diluting 25 µl of sample with 475 ml of TE buffer after sonication. After addition of 16 µl 5 M NaCl and 5 µl RNase A (10 mg/ml stock solution), the samples were incubated for 2 h at 37 °C followed by 6 h at 65 °C while shaking. 7 µl 0.5 M EDTA and 10 µl proteinase K (10 mg/ml stock) were subsequently added and incubated for 2 h at 45 °C. This procedure allowed reversion of the protein-DNA crosslink as well as digestion of both RNA and proteins in the sample. The DNA was purified by phenol-chloroform extraction and ethanol precipitation (as described below). The purified DNA (in 25 µl Ampuwa water) was loaded on a 2 % agarose gel (see 3.1.4) for size determination or DNA was quantified using Nanodop (3.1.6.1). After successful size-control, the sonified chromatin was cleared by centrifugation and the supernatant transferred to a new reaction tube. Protein concentration was determined using the Bradford method (3.3.10.1).

Coupling of the antibody to magnetic beads

20 µl of a 1:1 mixture of protein A and G Dynabeads (Invitrogen) were used per immunoprecipitation (IP). The beads were washed three times in 1 ml blocking solution for ChIP. After the last washing step, 1 ml blocking solution and 2 µg antibody (Table 2.16) or control serum (Table 2.18) were added to the beads and the mixture was kept an a rotating wheel at 4 °C for 6 h. Subsequently, the beads were washed three times with 1 ml and resuspended in 30 ml blocking solution.

Immunoprecipitation

Equal amounts of chromatin (usually 200-400 µg of protein as determined by the Bradford assay) were used for the immunoprecipitation (IP), added to the prepared magnetic beads, and rotated on a wheel at 4 °C overnight. 1 % of the chromatin used for the IP was taken and stored at -20 °C as an input reference. The beads were washed three times each with cold ChIP wash buffer I, II, and III followed by a single washing step with TE buffer while the beads where transferred to a new reaction tube.

Elution and de-crosslinking

After the IP, the protein-DNA complexes were eluted from the magnetic beads by rotating the beads twice in 150 μl ChIP elution buffer on a rotating wheel at room temperature. The eluates were pooled and inputs were replenished to a volume of 300 μl with ChIP elution buffer. For de-crosslinking, both samples and inputs were supplemented with 16 μl 5 M NaCl and 5 μl RNase A and incubated for 2 h at 37 °C followed by 6 h at 65 °C while shaking vigorously. 7 μl 0.5 M EDTA and 10 μl proteinase K were additionally added and heated for 2 h at 45 °C while shaking.

DNA purification and qPCR

The DNA was purified using phenol-chloroform extraction followed by ethanol precipitation. In detail, 300 μl of a phenol-chloroform-isoamyl alcohol mixture (50:48:2) was added to the samples and inputs and vortexted for 15 s. The tubes were centrifuged for 18,000 g and 5 min at room temperature to separate the phases. ~ 280 μl of the upper phase were transferred to a new reaction tube and mixed with 1 ml 100 % ethanol (ice-cold), 50 μl 3 M sodium acetate pH 5.2 and 1 μl GlycoBlue co-precipitant (15 μg/μl stock solution, Thermo Scientific). After at least 30 min at -20 °C, the DNA was pelleted by centrifugation (16,000 x g; 20 min; 4 °C), the pellet washed with 500 μl 70 % ethanol, and resuspended in 50 μl Ampuwa water after air drying. For qPCR reactions (3.1.11), the DNA was further diluted 1:10 with Ampuwa water and 10 μl of this dilution were used for each reaction. qPCRs were carried out in technical triplicates using primers designed for specific chromosomal regions (listed in Table 2.3; including an intergenic negative region) to analyze local binding enrichments of the protein of interest.

3.3.14 Next-generation sequencing

3.3.14.1   Sample preparation for ChIP-sequencing

To identify protein-DNA interactions in a genome-wide manner, a ChIP followed by deep sequencing (ChIP-sequencing or ChIP-seq) was performed.

ChIP for deep sequencing

To this end, the standard ChIP protocol was carried out (see section 3.3.13) except cell, antibody and magnetic bead amounts were increased fivefold and the purified DNA was solubilized in 30 μl Ampuwa water. DNA was quantified using the Picogreen reagent (3.1.6.2).

Library preparation

Library preparation (including end repair, 5' phosphorylation, dA-tailing, adaptor ligation, U excision) was performed using the NEBNext ChIP-Seq Library Prep Master Mix Set for Illumina and NEBNext Multiplex Oligos for Illumina (2.7.3). Clean up steps were done using the QIAquick PCR Purification Kit. Libraries were size-selected using an agarose gel (3.1.4) followed by gel extraction with the QIAquick Gel Extraction Kit. All kits were applied using the manufacturer's instructions. Libraries were PCR-amplified with 16-18 denaturation/ annealing/extension cycles. The Experion system (3.1.6.3) was used for sizing and quantification. The libraries were sequenced with the Illumina Genome Analyzer IIx or the Illumina NextSeq 500.

3.3.14.2   Sample preparation for RNA-sequencing

mRNA fragmentation and cDNA synthesis for RNA-sequencing

Total RNA prepared as described in 3.1.8.2 was analyzed using the automated electrophoresis system (3.1.6.3) together with the Experion RNA StdSens Analysis Kit. The level of RNA degradation was estimated automatically and a RNA quality indicator (RQI) was given ranging from 1 (degraded RNA) to 10 (intact RNA). RNA with RQIs above 9 was considered suitable for further processing. mRNA was isolated from 1 μg total RNA using the NEBNext Poly(A) mRNA Magnetic Isolation Module. All kits were used following the manufacturer's protocol.

Library preparation

Libraries suitable for RNA-sequencing (RNA-seq) were prepared using the NEBNext Ultra RNA Library Prep Kit for Illumina (including 12 PCR cycles) as well as NEBNext Multiplex Oligos for Illumina. Purification and size-selection was performed using Agencourt AMPure

XP Beads (Beckman Coulter). Quantification and size determination was done using the Experion system. All kits were applied following the manufacturer's instructions. The libraries were sequenced with the Illumina Genome Analyzer IIx or the Illumina NextSeq 500.

3.3.14.3   Bioinformatic analysis of sequencing data

Analysis of sequencing raw data was performed using the programs and sources cited below. Further analyses and statistical tests were performed using Microsoft Excel and R if not indicated otherwise. Dr. Carsten Ade, Dr. Susanne Walz, and Dr. Elmar Wolf performed bioinformatic analyses of deep sequencing data for this study.

Base calling and quality scoring were performed on the Illumina sequencing system using the integrated analysis software (RTA v2). Fastq files were generated either using the CASAVA software or the bcl2fastq Conversion Software only considering high quality PF-clusters and quality control was performed using the FastQC script.

3.3.14.4   Bioinformatic analysis of ChIP-seq data

ChIP-sequencing reads were mapped to the human reference genome (*Homo sapiens* UCSC assembly 19, hg19) using Bowtie v1.1.1. with default parameters (Langmead, 2010), converted to .bam files using SAMtools (Li et al., 2009) and normalized to the sample containing the least mapped reads. Peak calling was performed with MACS v1.4.2. (Zhang et al., 2008) with default parameters and using a p-value cut-off of 1×10^{-6}. The input sample served as a control. .wig files were visualized with the Integrated Genome Browser (IGB) (Nicol et al., 2009) and heat maps were generated using SeqMiner (50 bp resolution, $\pm$ 5 kb window around the MYC peak) (Ye et al., 2011) and visualized using Java Treeview (Saldanha, 2004). To intersect or merge .bed files defining genomic regions, BEDtools was used (Quinlan and Hall, 2010). To calculate MYC recruitment, the number of tags in a region of $\pm$ 100 bp around the summit of the MYC peak were counted with SeqMiner, input counts were subtracted and fold changes (+Dox vs. –Dox) were calculated. For OmoMYC binding motif discovery, DREME analysis using the MEME suite (Bailey et al., 2009) was performed. 100 bp surrounding the center of the OmoMYC peak were entered and the analysis was

performed with default settings. Comparison of identified motifs against a database of known motifs (JASPAR database) was performed using Tomtom (MEME suite).

3.3.14.5 Bioinformatic analysis of RNA-seq data

RNA-sequencing reads were mapped to the human reference genome (*Homo sapiens* UCSC assembly 19, hg19) using Bowtie2 v2.2.4 (Langmead, 2010) using default parameters. The resulting file was converted from a SAM format to a BAM format with SAMtools (Li et al., 2009) and used for downstream analysis with R and various Bioconductor packages. Read counts for all genes were extracted using the summarizeOverlaps function (Genomic Ranges package). After removal of weakly expressed genes (with mean CPM over all samples < 1) and normalization, differentially expressed genes were called using the edgeR package (Robinson et al., 2010).

Functional analyses were performed using GSEA and DAVID tools. The Database for Annotation, Visualization and Integrated Discovery (DAVID) tool (Huang da et al., 2009a, b) was used for gene ontology (GO) analysis using standard settings. Gene Set Enrichment Analysis (GSEA) (Subramanian et al., 2005) was performed applying C2 and C5 gene sets from the Molecular Signature Database (MSigDB) using the signal2noise metric and 1,000 permutations.

3.3.14.6 Bioinformatic analysis of shRNA screening data

Reads of recovered guide-stem sequences were aligned to a reference file containing guide-sequences of all 148 shRNAs included in the library using Bowtie v0.12.8 (Langmead, 2010). The total number of library-specific reads was used for normalization of reads per shRNA between different samples. Only shRNAs represented by >0.01 % of all normalized reads in the initial untreated population were included in the primary analysis. Fold changes (FC) of shRNA abundance between untreated and doxycycline-treated samples at the end of the screen were generated by calculation a ratio of the means of the normalized reads of all four replicates. Z-scores were calculated for each $\log_2$FC based on the observed distribution of negative control shRNAs (targeting *Renilla* luciferase). shRNAs with z-scores <(-3) (implicating a depletion of more than 3 standard deviations below the mean of the negative

control shRNAs) were defined as "scoring" shRNAs. A gene was defined as a "hit" in the screen if more than 50 % of all analyzed shRNAs targeting this gene "scored" in the analysis. A complete table of the results from the shRNA screen can be found in the supplementary material of the related publication (Jung et al., 2016).

3.3.14.7   Statistics

If not indicated otherwise, data were expressed as means ± standard deviation. After testing if the data was normally distributed using the Shapiro-Wilk test, statistical significance was calculated with a two-tailed Student's t-test. For box plots, p-values were determined using non-parametric two-tailed Wilcoxon-Mann-Whitney tests, the horizontal line within the box indicates the median and whiskers extend to 1.5x interquartile range. q-values were estimated by correction of p-values for multiple testing via the Benjamini-Höchberg procedure (false discovery rate). If data was binned, the binned data was sorted using independent experiments and the mean of each bin was plotted. Regression analysis was performed using linear models, p-values were obtained using two-tailed Student's t-tests and analysis of covariances (ANCOVA) was performed.

4 Results

4.1 OmoMYC forms a stable homodimer that strongly binds to DNA

X-ray crystallographic data on MYC/MAX and MAX/MAX-DNA bound complexes has profoundly aided in explaining how homodimer and heterodimer binding within the MYC/MAX family of proteins is guided and how sequence-specific DNA-recognition is achieved (PDB (protein data bank) entries 1NKP and 1AN2, respectively; see also section 1.2.1.2) (Ferre-D'Amare et al., 1993; Nair and Burley, 2003). Yet protein-protein and protein-DNA interfaces of the mutant MYC allele OmoMYC have not been structurally characterized and affinities for protein-DNA binding have not been determined, thereby hindering an in-depth analysis of the influences of mutations introduced to MYC when generating OmoMYC.

To understand the structural properties of OmoMYC as a first step on the way to determine the protein's mode of action, DNA-binding affinities of recombinant OmoMYC, MYC and MAX protein complexes were determined using electrophoretic mobility shift assays, and crystallization of OmoMYC alone and in complex with E-box-containing DNA was pursued. For this, OmoMYC was expressed in *E. coli* and purified to homogeneity. In parallel, MAX and the b/HLH/Zip domain of MYC were purified.

4.1.1 Recombinant expression and native purification of OmoMYC

For recombinant expression of an N-terminally hexahistidine- (His$_6$-) tagged OmoMYC protein, *E. coli* cells were transformed with the pETM11 expression plasmid. To prevent protein insolubility and misfolding, the cells were grown at 14 °C and a modified bacterial strain, Arctic Express (DE3) RIL, was used, because it co-expresses cold-adapted chaperonins improving protein folding at low temperatures.
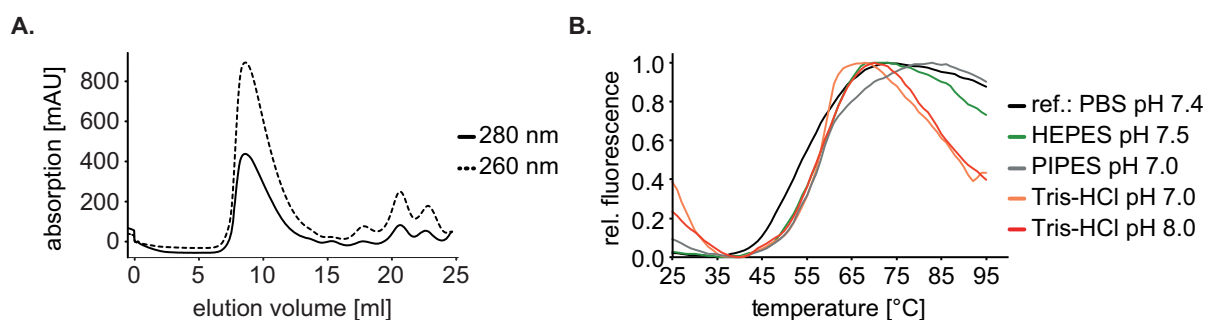
Figure 4.1: OmoMYC protein purification optimization
(A) Preparative size-exclusion chromatography (SEC) profile of His$_6$-OmoMYC (Superdex 200 column).
(B) Selected thermal unfolding profiles of the OmoMYC Thermofluor buffer screen. Changing the buffer from PBS pH 7.4 (black; T_m =51 °C) to Tris-HCl pH 8.0 (red; T_m =56 °C) resulted in a strong melting temperature (T_m) shift and thus an increase in protein stability.

Using a purification protocol consisting of a Ni-affinity chromatography, followed by a preparative size-exclusion chromatography step (SEC; Figure 4.1 A), protein aggregation as well as massive nucleic acid contamination was observed. The OmoMYC protein was found in the main peak, which eluted with low retention time/elution volume typical for high molecular weight aggregates. The high 260 nm/280 nm ratio in the chromatogram indicates a strong nucleic acid contamination. A fluorescence-based thermal shift assay (Thermofluor buffer screen) was performed to elucidate whether a change in the buffer composition might prevent protein aggregation (Figure 1.1Figure 4.1 B). Tris-HCl pH 8.0 was found to be more suitable for purification as it stabilized the protein (shown in red).

The final two-step purification protocol combined immobilized metal affinity (IMAC, Figure 4.2 A) with ion exchange chromatography (IEC, Figure 4.2 B and C). The latter step was used to remove DNA as an additional cause for protein aggregation. This optimization allowed large-scale expression and purification of soluble, natively folded OmoMYC protein. The protein was concentrated after IEC to 2.9 mg/ml (extinction coefficient calculated using ProtParam) and then flash frozen for storage at -80 °C. 16 litres of bacterial culture yielded around 38 mg of purified protein (2.375 mg of protein per liter). Mass spectrometry confirmed the identity of OmoMYC, as well as MYC and MAX recombinant protein (see below). Analytical SEC (Figure 4.2 D and E) indicated that OmoMYC formed a dimer or a tetramer in solution.

A.

B.

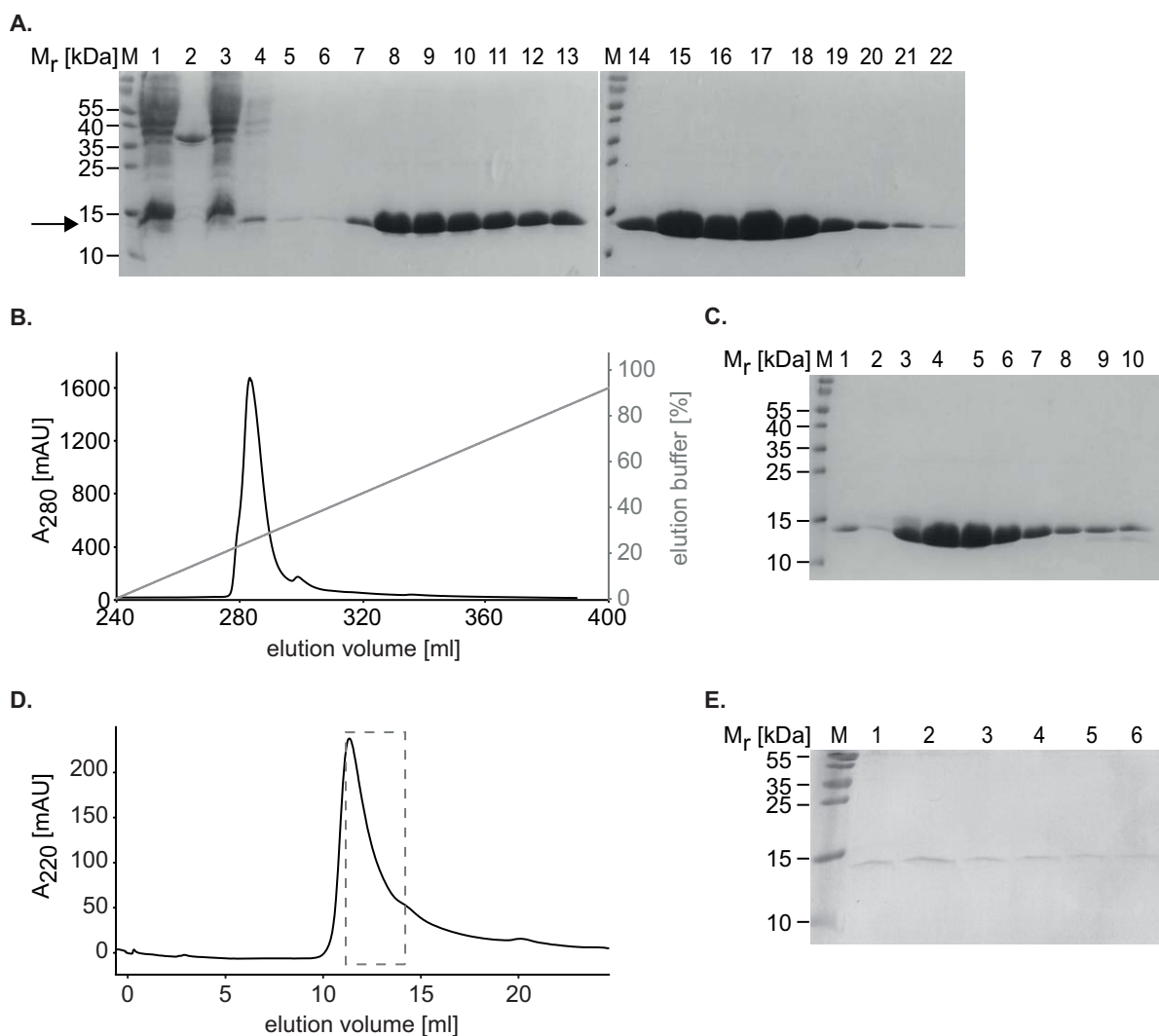**C.**

D.

E.

Figure 4.2: Large-scale purification and analytical SEC of natively folded OmoMYC

(A) Coomassie-stained SDS-PAGE gel of OmoMYC protein expression and initial purification. Shown are samples of whole cell lysate (lane 1 = supernatant; lane 2 = pellet), which was enriched for His-tagged OmoMYC protein via manual Nickel-affinity chromatography (lane 3 = unbound lysate; lane 4-6 = wash fractions). Representative elution fractions are depicted as well (fractions 7-13 = 100 mM imidazole; fractions 14-22 = 500 mM imidazole; M = marker).

(B) Cation exchange chromatogram using a MonoS column.

(C) SDS-PAGE followed by Coomassie staining of the peak fractions corresponding to the IEC shown in (B). OmoMYC protein can be found purely in the main peak (lane 1 = load; lanes 2-10 = elution fractions; M = marker). Fractions 3-8 were pooled and used further.

(D) Chromatogram of the analytical SEC of the purified OmoMYC protein. The elution volume corresponds to the expected size of a homodimer or -tetramer. The dashed frame indicates peak fractions analyzed by SDS-PAGE in (E). For analytical SEC chromatography with lower concentrations of protein, absorption was recorded at 220 nm to monitor the absorbance of the peptide backbone as the protein does not contain any tryptophans.

(E) Fractions of the indicated peak area of the SEC chromatogram shown in (D) separated by SDS-PAGE and Coomassie-stained.

4.1.2 Recombinant expression and native purification of MYC (b/HLH/Zip)

To recombinantly express and natively purify the MYC protein, only a fragment of MYC comprising the b/HLH/Zip domain (amino acids 353-434, as described in (Nair and Burley, 2003)) with an N-terminal His$_6$-tag was used. In contrast to previously published protocols (Farina et al., 2004; Gaubatz et al., 1995; Guo et al., 2014a; Hu et al., 2005; Lebel et al., 2007; Lin et al., 2012; McDuff et al., 2009; Nair and Burley, 2003; Park et al., 2004; Watt et al., 1985), which majorly pursued strategies involving *in vitro* re-folding of the protein after isolation from inclusion bodies under denaturing conditions, MYC was natively purified from the soluble fraction of the *E.coli* lysate.
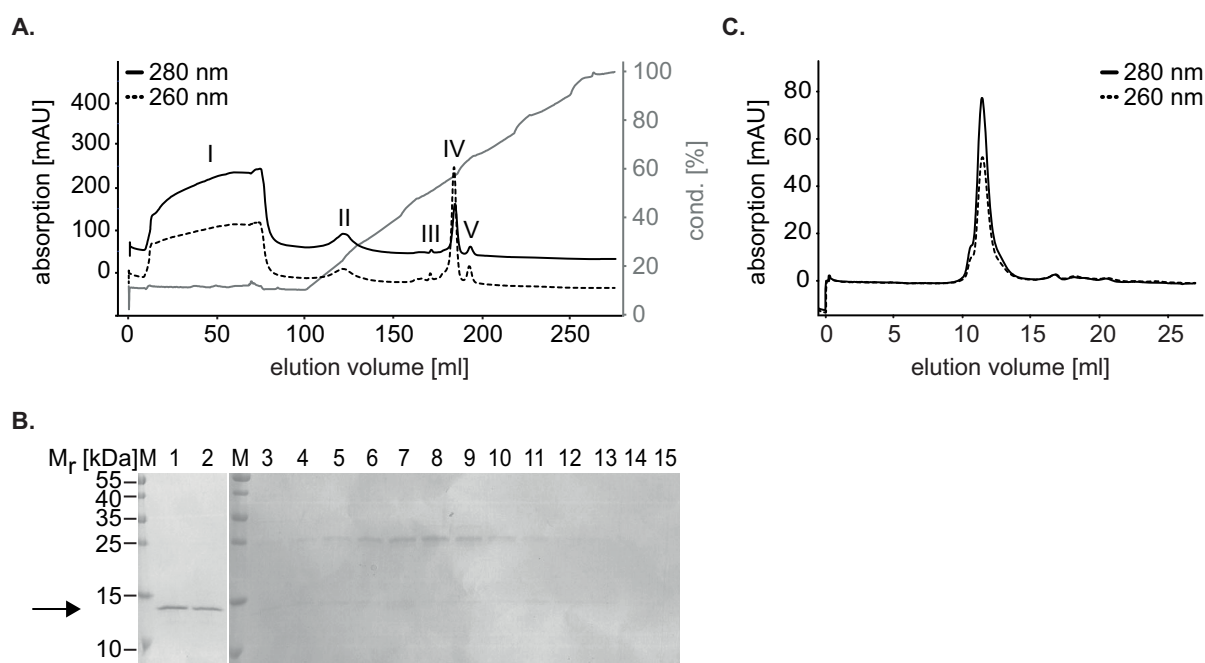
Figure 4.3: Chromatographic His$_6$-MYC protein purification and analytical SEC
(A) IEC (ion exchange chromatography) of MYC using a MonoQ column. Peak I indicates the flow through fractions.
(B) Coomassie-stained SDS-PAGE showing characteristic peak fractions of the chromatogram shown in (A): peak I = flow through/void volume (1-2); peak II (3-12); peak III-V (13-15); M = marker. MYC protein can be found in the unbound protein fractions (1-2).
(C) Size-exclusion profile of the purified MYC protein. 25 µM of the purified MYC protein were loaded on a Superdex 75 column. MYC protein eluted in a single peak at a position corresponding to the expected size of a monomer.

The MYC expression and purification protocol was established following the OmoMYC purification protocol. Likewise, Arctic Express cells were grown at 14 °C and IMAC was

used as the first purification step. Thermofluor assays revealed that buffers containing HEPES pH 8.0 were most suitable for MYC purification. Subsequently, IEC was applied to remove DNA contaminations (Figure 4.3 A, B). In contrast to OmoMYC, MYC neither bound to a cation nor an anion exchange resin. It eluted in the void volume of the anion exchange column (MonoQ) and could thus be separated from further impurities, which largely bound to the column. MYC purification yielded about 2 mg of purified protein per liter of bacterial culture. The protein was concentrated after IEC to 0.6 mg/ml (extinction coefficient calculated with ProtParam), flash frozen and then stored at -80 °C. Analytical size-exclusion chromatography (Figure 4.3 C) indicated a monomeric state of the recombinant protein.

4.1.3 Recombinant expression and native purification of MAX

Full-length MAX protein was expressed as a GST fusion protein with a thrombin-cleavage site at the N-terminus. After affinity purification using glutathione (GSH) sepharose beads and elution with reduced glutathione, the GST-tag was cleaved overnight using thrombin. Thrombin was subsequently removed using benzamidine sepharose-packed columns and the protein solution was subjected to IEC for intermediate purification and DNA removal. Remaining GST impurities were eliminated using GSH sepharose columns. The protein was concentrated to 7.6 mg/ml and then flash frozen for storage at -80 °C. This purification protocol yielded about 3 mg of purified protein per liter of bacterial culture.
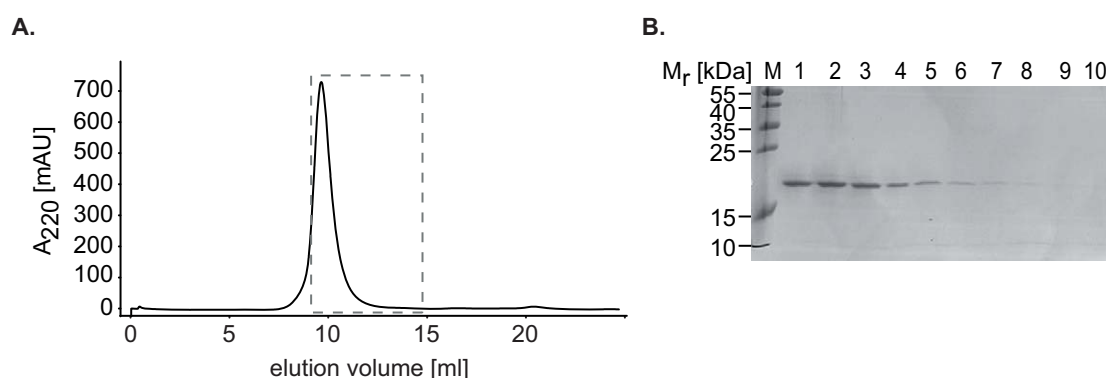

Figure 4.4: Final size-exclusion chromatogram and SDS-PAGE showing peak fractions of purified MAX protein
(A) Approximately 25 μM of MAX protein was loaded onto an analytical Superdex 75 column. Untagged MAX elutes at a position corresponding to a relative molecular mass of approximately 30 kDa, the expected size of a homodimer.
(B) Representative fractions from the elution (indicated in (A) by a dashed frame) shown on a Coomassie-stained SDS-PAGE gel.

To determine the subunit composition, analytical SEC was performed, which suggested that the purified MAX protein forms a stable homodimer (Figure 4.4 A and B).

In summary, the MYC b/HLH/Zip fragment together with full-length OmoMYC and MAX proteins were expressed and natively purified from the soluble fraction to yield proteins of high purity suitable for further crystallographic and biochemical experiments (Figure 4.5).
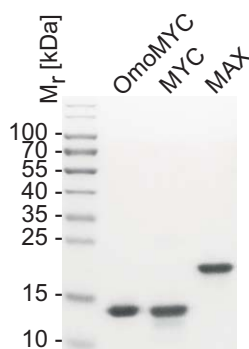

Figure 4.5: Purified recombinant OmoMYC, MYC and MAX proteins[1]
Coomassie-stained SDS-PAGE gel of purified recombinant OmoMYC, MYC, and MAX protein.

4.1.4 OmoMYC strongly binds to E-box-containing DNA *in vitro*

To study the DNA binding properties of all three purified proteins, electrophoretic mobility shift assays (EMSAs) were performed using a fluorescently labeled dsDNA oligonucleotide carrying a central consensus E-box motif (Blackwell et al., 1990).

OmoMYC bound to the probe producing a discrete protein-DNA complex that migrated slower than free DNA (Figure 4.6 A), which was consistent with a previously published result using crudely purified GST-tagged OmoMYC (Soucek et al., 1998). This was also the case for MAX and MYC proteins (Figure 4.6 B and C). MYC displayed only weak binding to the probe. Micromolar concentrations of this protein were required to observe protein-DNA complex formation, in contrast to OmoMYC and MAX, which formed complexes at 10-fold less protein concentrations.

---

[1] This Figure was submitted for publication in similar form in (Jung et al., 2016) (see also following pages).
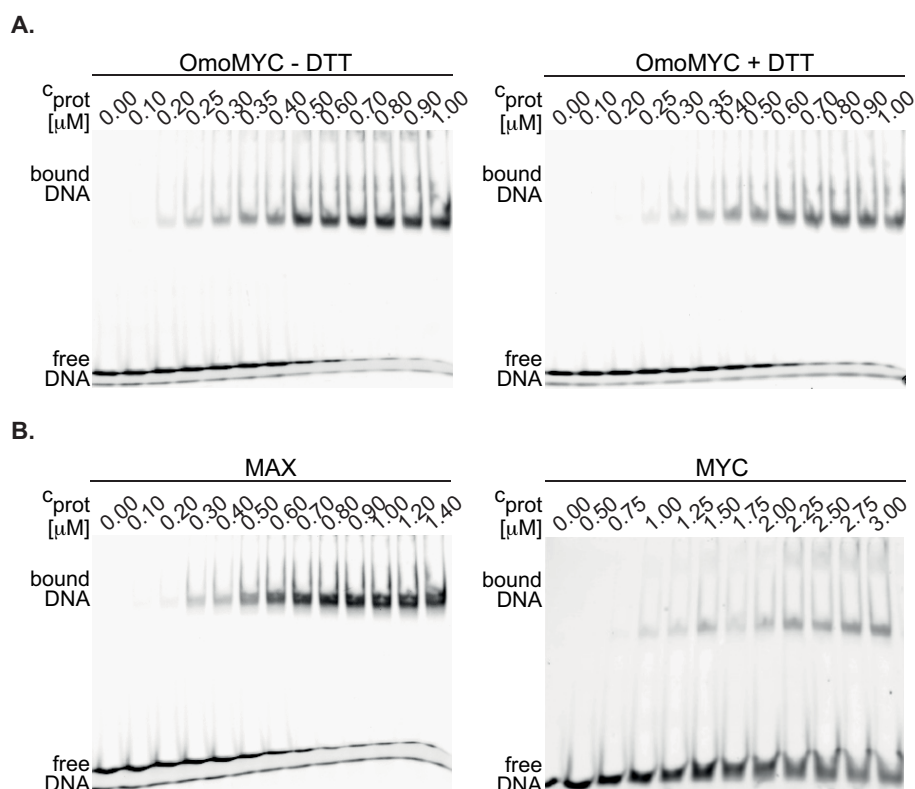
Figure 4.6: Electrophoretic mobility shift assays (EMSAs) of OmoMYC, MYC and MAX proteins as well as their heterodimers[1]

(A)   Representative EMSAs of rising concentrations of OmoMYC protein (c_{prot}; indicated for dimers) with a consensus E-box containing oligonucleotide (5' CY3-labeled, CM1 (Blackwell et al., 1990)) in the presence or absence of the reducing agent dithiothreitol (DTT, as indicated). Gels were imaged using a PHAROS FX scanner (n ≥ 3; n indicates the number of independent replicates).

(B)   EMSAs with MAX and MYC (no DTT added) protein as described in (A) (n ≥ 3).

Additionally, possible heterodimer/DNA complexes were reconstituted *in vitro*. The heterodimer ratio was established using a constant amount of one protein (e.g. MAX or OmoMYC) and titrating increasing amounts of the partner protein (e.g. MYC). This revealed that MYC and MAX as well as MYC and OmoMYC cooperated in DNA binding (Figure 4.7 A). At 3-fold molar excess, no further increase in band intensity was seen, suggesting complete heterodimer formation (Figure 4.7 A). Thus, this setting was chosen for further experiments. Both proteins of the respective heterocomplex were confirmed to be part of the protein-DNA complex using supershift assays with several antibodies (Figure 4.7 B).
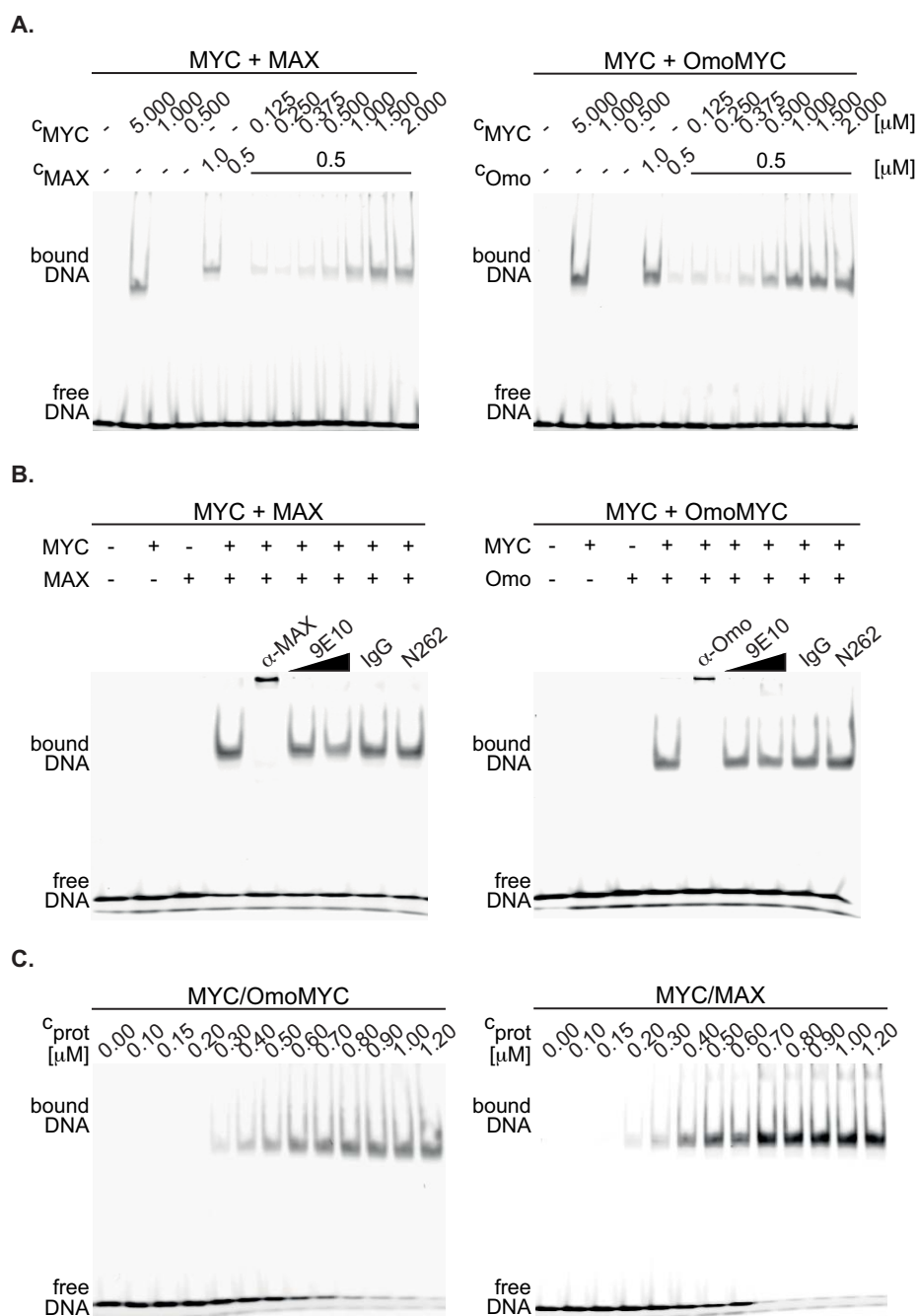
Figure 4.7: EMSA analysis of heterodimer DNA-binding *in vitro*[1]

(A) EMSAs demonstrating cooperative DNA-binding of MYC and OmoMYC as well as MYC and MAX proteins. Titration of MYC and MAX or MYC and OmoMYC proteins are shown (note that protein concentrations (c_{prot}) of the respective monomers are given here) (n = 2).

(B) EMSAs demonstrating the presence of both proteins in the respective complex. 0.5 μM MAX or OmoMYC protein (monomeric concentration) was incubated with a 3-fold molar excess of MYC (1.5 μM; monomeric concentration) where indicated. Adding increasing amounts of α-MYC antibody (9E10) reduced DNA-binding by 44 % for MYC/MAX and 32 % for MYC/OmoMYC (n = 2). The α-MYC antibody N262 recognizes the N-terminus of MYC not present in the recombinant proteins used here and thus serves as a negative control together with IgG.

(C) EMSAs with MYC/OmoMYC and MYC/MAX heterodimers as in (Figure 4.6 A) in the presence of DTT (n $\geq$ 3).

81

MYC/MAX and OmoMYC/MYC heterodimers showed strong binding to the E-box containing probe (Figure 4.7 C). In the case of OmoMYC/MAX, EMSAs did not convincingly establish whether the main DNA binding species is indeed a heterodimer (data not shown).

To determine the dissociation constants (K_d) for DNA binding, titrations of increasing amounts of protein with constant amounts of labeled DNA were carried out (as shown in Figure 4.6 A-B and Figure 4.7 C). Recombinant full-length MAX protein bound to the E-box oligonucleotide with slightly lower affinity than MYC/MAX heterodimers as reported previously (Fieber et al., 2001; Guo et al., 2014a; Hu et al., 2005; Park et al., 2004) (Figure 4.8). No binding affinities have been published so far for OmoMYC. Soucek et al. observed a weak binding of GST-OmoMYC to the probe, which could be due to incomplete protein purification as co-purified DNA was not reported to be removed by IEC or other methods (Soucek et al., 1998). In the current study, OmoMYC bound the DNA with an affinity higher than that of MAX (Figure 4.8), both in the presence and absence of a reducing agent (dithiothreitol, DTT). OmoMYC/MYC heterodimers exhibited an intermediate DNA binding affinity (Figure 4.8).
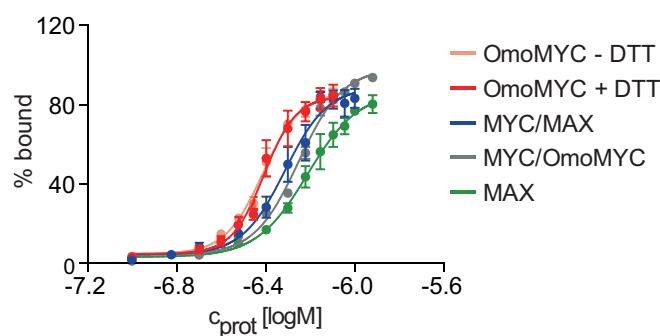
	log Kd [M]	Kd [nM]	95 % CI
Omo + DTT	-6.408	391	-6.446 to -6.371
Omo - DTT	-6.413	386	-6.441 to -6.384
MYC/MAX	-6.314	485	-6.362 to -6.265
MYC/Omo	-6.252	560	-6.272 to -6.233
MAX	-6.213	612	-6.263 to -6.163

Figure 4.8: OmoMYC strongly binds to DNA[1]
Fractions of bound DNA (% bound, deduced from gel shifts as shown in Figure 4.6 and Figure 4.7 C; ImageJ was used for quantification) were plotted against the respective logarithmic protein concentration (c_{prot}) (n ≥ 3). Error bars indicate the standard error of the mean (SEM). Dissociation constants (K_d) of the protein-DNA complexes obtained by a four parameter non-linear fit using Prism are shown in the table to below. Omo: OmoMYC; CI: confidence interval.

4.1.5 OmoMYC forms a tight homodimer that recognizes E-boxes in a base-specific manner

To understand protein-protein and protein-DNA interactions on a structural level, OmoMYC was crystallized in the presence and absence of double-stranded DNA. His$_6$-OmoMYC apo crystals were grown using the vapor diffusion method in sitting drops, and the structure was solved by molecular replacement using the structure of the MYC/MAX heterodimer bound to DNA (PDB code 1NKP; (Nair and Burley, 2003)) as a search model to a resolution of 1.95 Å (Figure 4.9 A, Figure 4.10 A and Table 7.2). OmoMYC was subsequently co-crystallized with an E-box-carrying double-stranded oligonucleotide (as used in (Ferre-D'Amare et al., 1993); Figure 4.9 B and Table 7.2). Wolfgang Kölmel performed data processing, structure determination and refinement and participated in the subsequent analysis.
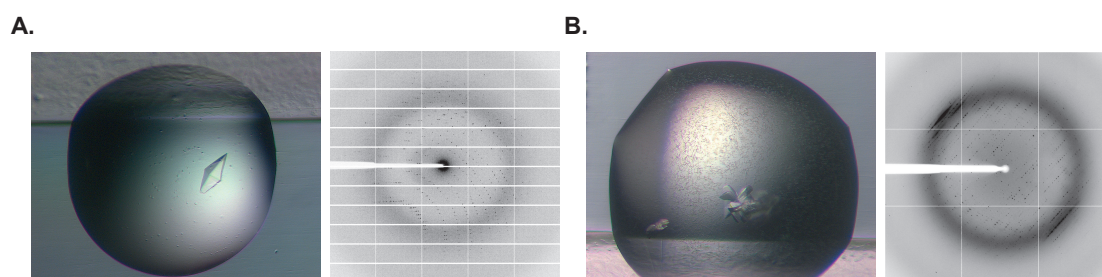

Figure 4.9: Crystallization and data collection of OmoMYC apo crystals and OmoMYC/DNA co-crystals
(A)   The OmoMYC apo crystal was grown using the sitting drop vapor diffusion method in a reservoir solution containing 100 mM MES pH 6.0, 1 M potassium sodium tartrate (left panel). The image was captured using a light microscope at 50 x magnification. Diffraction pattern of the protein crystal (right panel).
(B)   OmoMYC/DNA co-crystals were grown with 50 mM MES pH 5.6, 10 mM magnesium sulfate, 200 mM potassium chloride, and 10 % PEG 400 as precipitating agent (left; 50 x magnification as in A). The corresponding diffraction pattern (right) shows characteristic reflections of helical DNA with strong meridional intensity at 3.4 Å.

In the apo structure, the leucine zipper and the HLH region could be modeled as a coiled coil and four-helix bundle respectively (Figure 4.10 A). In the absence of DNA, the basic region is unstructured and flexible and thus cannot be modeled in the crystal structure. This also holds true for other known b/HLH/Zip apo structures (Figure 4.10 B and C) (Pogenberg et al., 2012; Sauvé et al., 2004). The OmoMYC apo structure clearly revealed the formation of a homodimer even in the absence of DNA. This dimerization was mediated by the leucine zipper and was independent of DNA-binding.

Elucidating this high-resolution apo structure enabled an in-depth analysis of the protein-protein interface. Multiple interactions stabilized the OmoMYC homodimer (Figure 4.10 A, Figure 4.11 A, and Table 7.3). Three out of four mutations introduced into OmoMYC led to stabilizing interactions between the two monomers. Hydrogen bonds were formed between threonines at position 63 (T63) as well as asparagines at position 77 (N77) of each monomer, with an additional intrastrand interaction between N77 and lysine 81 (K81, Figure 4.10 A). Both T63 residues also contributed to interstrand hydrophobic interactions to leucine 66 (L66) of both chains. Additional hydrophobic interactions were observed between both isoleucines 70 (I70) and between I70 and L66. Unexpectedly, one of the mutated residues in OmoMYC, glutamine 76, faced away from the interface.
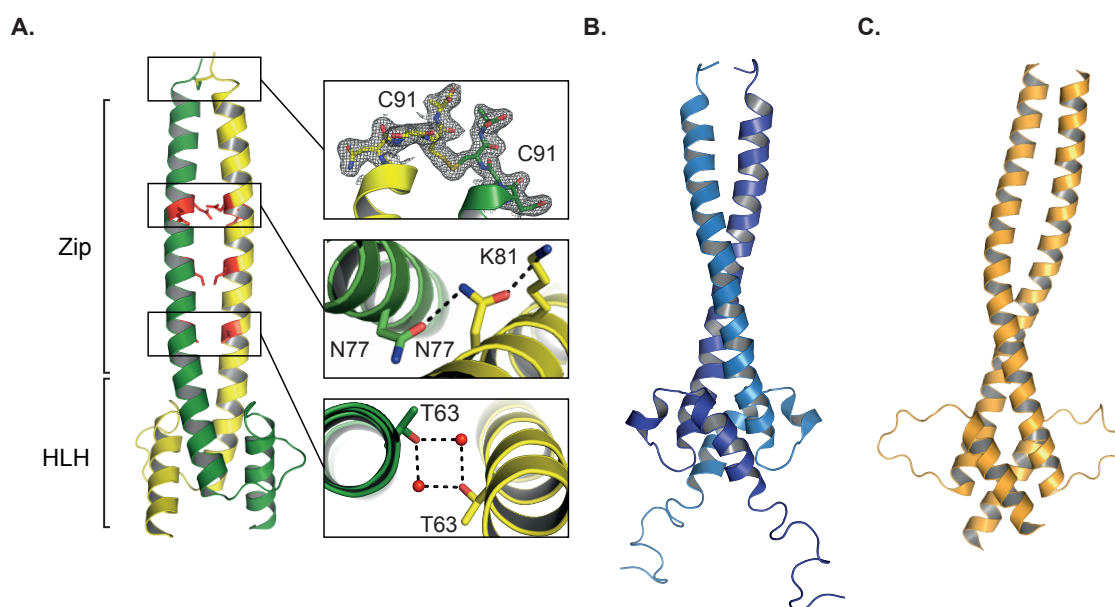

Figure 4.10: OmoMYC forms a tight homodimer and resembles previously published b/HLH/Zip apo structures[1]

(A) Schematic representation of the OmoMYC apo crystal structure. Mutations introduced into OmoMYC are shown in red. Boxes to the right highlight characteristic protein-protein interactions. Enlarged are a C-terminal disulfide bridge with $2F_o-F_c$ electron density contoured as a mesh at 1 σ (top), a hydrogen bond network involving N77 (center), as well as hydrogen bonds bridged by water molecules (red, bottom) at T63 (PDB entry 5I4Z).

(B) Schematic representations of the MAX homodimer apo NMR structure (Sauvé et al., 2004) (PDB entry 1R05).

(C) MITF homodimer crystal structure (Pogenberg et al., 2012) (PDB entry 4ATH).

All images included in this figure were generated using PyMOL.

Even though mutations were only implemented in the leucine zipper domain, the OmoMYC homodimer displayed additional stabilizing interactions throughout the entire protein-protein interface, which cannot be found in the MYC/MAX heterodimer (Figure 4.10 A, Figure

4.11 A). These interactions included salt bridges and hydrophobic interactions in the HLH region and surrounding residues 66, 69 and 80/81. Interestingly, OmoMYC contained a disulfide bridge formed by cysteines 91 (Figure 4.10 A, top panel). This analysis already indicated that the OmoMYC homodimer shows an increased stability of the protein-protein interface. Additionally, the estimated solvation free energy gained upon building the protein-protein interface using the PDBePISA tool (Krissinel and Henrick, 2007), supports the hypothesis that the OmoMYC homodimer is more stable than the MYC/MAX heterodimer (ΔiG total = -41.7 kcal/mol versus -32.8 kcal/mol; Table 7.4).

Molecular modeling of putative heterodimers indicated that OmoMYC/MYC heterodimers would contain significant repulsive interactions and that the OmoMYC/MAX complex would lack important stabilizing interactions making them less stable than the OmoMYC homodimer (Figure 4.11 B and C), thereby suggesting that homodimers would be formed preferentially. In the putative OmoMYC/MAX heterodimer, the hydrogen bond network between T63 and two water molecules in the homodimer would most likely be replaced by a hydrogen bond between T63 in OmoMYC and an asparagine at an equivalent position in MAX (N63, OmoMYC numbering) in the OmoMYC/MAX heterodimer (Figure 4.11 C, left panel). The hydrophobic interactions mediated by T63 in OmoMYC/OmoMYC, could not be modeled at this position in OmoMYC-MAX due to the lack of acceptor residues (L66 and T63) in MAX. In OmoMYC/MYC, glutamates 69 and 70 would presumably be in close contact (Figure 4.11 C, right panel). Additionally, a salt bridge would be present between E69 and R74, similar to that observed in OmoMYC/OmoMYC. However, only in the homodimer would this salt bridge be found on the opposite side as well. Importantly, an extensive hydrophobic core, which is lined by two I70, L66, and T63 residues, each in the homodimer, would not be as elaborate in the putative OmoMYC/MYC heterodimer, due to the presence of hydrophilic residues at equivalent positions of T63 and I70.

Subsequent to the crystallization of OmoMYC in the free state, the DNA-bound OmoMYC homodimer structure was determined to a resolution of 2.7 Å (Figure 4.12). In this complex, the basic region adopted an α-helical fold and the protein bound the major groove of the 22-mer oligonucleotide by forming a scissor-like structure at the E-box sequence (Figure 4.12 A and B). Superposition of the apo and the DNA-bound OmoMYC structure (not considering the basic region and the dsDNA residues) with PyMOL showed no significant rms deviations for the main chain atoms (0.60 Å; Table 7.5 A). Furthermore, a close inspection of the dimer
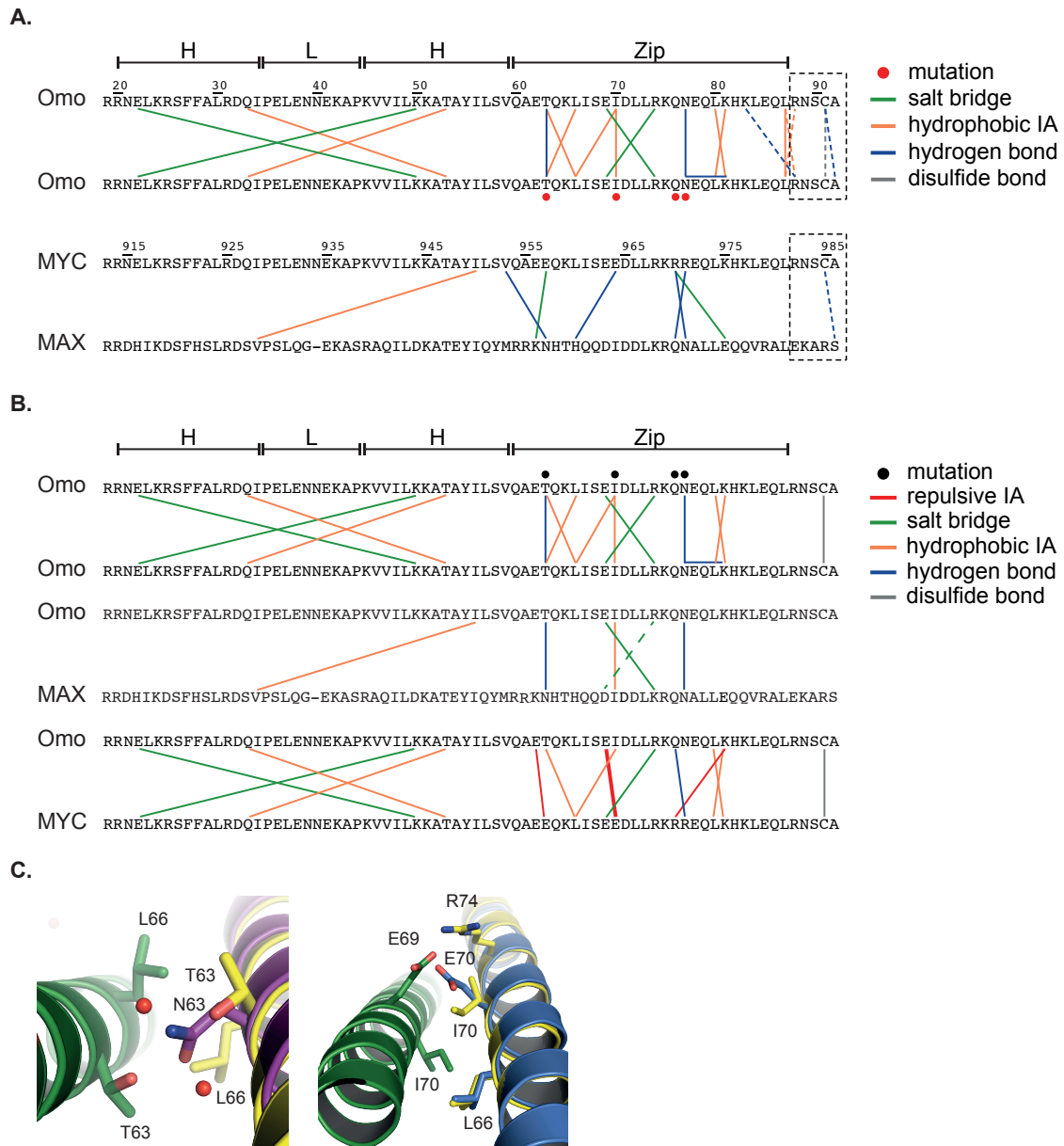
Figure 4.11: OmoMYC homodimers are more stable than various heterodimers[1]

(A) Direct comparison of differing interactions of the OmoMYC homodimer (upper panel) and the MYC/MAX protein-protein interfaces (lower panel) derived from the analysis of the OmoMYC apo (PDB entry 5I4Z) and the published MYC/MAX crystal structure (Nair and Burley, 2003)(PDB entry 1NKP). Red circles indicate mutations of OmoMYC relative to MYC. Each line represents an interaction. Salt bridges are shown in green, hydrophobic interactions (IA) in orange, hydrogen bonds in blue and disulfide bonds in grey. As the MYC/MAX C-terminus was manipulated in the crystal structure, it was omitted from the comparison indicated by dotted lines.

(B) Comparison of putative OmoMYC heterodimer interactions with the homodimer interface (derived from the crystal structure). Modeling of heterodimers was performed with Coot (CCP4 suite) by superimposing the OmoMYC apo structure (PDB entry 5I4Z) with the MYC-MAX-DNA crystal structure (PDB entry 1NKP) and exchanging one chain of OmoMYC against either MYC or MAX. Labeling is according to (A) except repulsive interactions are shown in red, mutations from MYC to OmoMYC in black. As in (A), only diverging interactions are shown. C-terminal interactions outside the leucine zipper other than putative disulfide bridges are not considered.

(C) Left panel: Superposition of the putative OmoMYC-MAX heterodimer with the OmoMYC homodimer (PDB entry 5I4Z). MAX is shown in purple, OmoMYC in green and yellow, water molecules in red. Right panel: Superposition of the putative OmoMYC-MYC heterodimer with the OmoMYC homodimer. MYC is shown in blue, OmoMYC in green and yellow. Images were generated using PyMOL.

86

interface in both structures correspondingly showed that DNA-binding did not alter the protein-protein interface. Additionally, calculations estimating solvation free energies of the protein-protein interface of both structures (using PDBePISA; Table 7.4) yielded nearly identical values. Thus, the analysis of the protein-protein interface deduced from the apo structure could also be adapted to the DNA-bound structure (Figure 4.11).
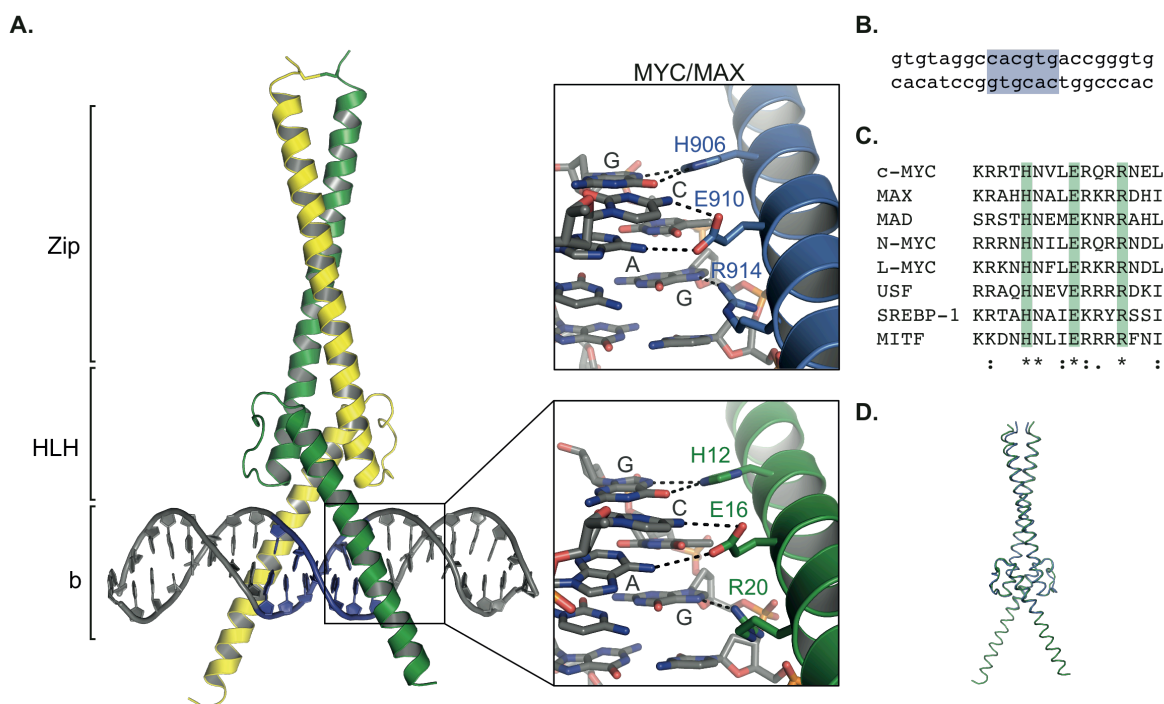

A.

B.

```
gtgtaggccacgtgaccgggtg
cacatccggtgcactggcccac
```

MYC/MAX

G — H906
C — E910
A — R914
G

C.

```
c-MYC     KRRTHNVLERQRRNEL
MAX       KRAHHNALERKRRDHI
MAD       SRSTHNEMEKNRRAHL
N-MYC     RRRNHNILERQRRNDL
L-MYC     KRKNHNFLERKRRNDL
USF       RRAQHNEVERRRRDKI
SREBP-1   KRTAHNAIEKRYRSSI
MITF      KKDNHNLIERRRRFNI
          :  ** :*:. *  :
```

D.

G — H12
C — E16
A — R20
G

Zip

HLH

b

Figure 4.12: Distinct protein-DNA interactions in the basic region allow E-box recognition[1]
(A) Schematic representation of the OmoMYC homodimer (green and yellow) bound to a consensus E-box containing oligonucleotide. The central palindromic CACGTG sequence is depicted in blue. To the lower right, an enlargement of the base-specific interactions of one arm of the OmoMYC basic region (green) with one half of the E-box motif (grey) is shown. The analogous region in the DNA-bound MYC-MAX heterodimer crystal structure (Nair and Burley, 2003) (PDB entry 1NKP) is illustrated (upper left) with DNA contacts of MYC shown in blue. Images were generated using PyMOL.
(B) Sequence of the double-stranded oligonucleotide used for co-crystallization (as used for MAX homodimer crystallization (Ferre-D'Amare et al., 1993)). The consensus E-box sequence is marked in blue.
(C) Partial sequence alignment of the basic region DNA-binding domain of the human c-MYC protein with b/HLH/Zip family proteins. The highly conserved HER triad described in (A) is highlighted in green. An asterisk (*) indicates fully conserved residues, a colon (:) residues of strongly similar properties, and a period (.) conservation between residues of weakly similar properties. Alignments were performed with Clustal Omega.
(D) Superposition of the DNA-bound OmoMYC crystal structure (shown as green ribbons) with the OmoMYC apo crystal structure (shown in blue). This image was generated using PyMOL.

The DNA-bound OmoMYC complex displayed an overall structure that is very similar to the MYC/MAX-DNA complex (Nair and Burley, 2003) (rms deviations for main chain atoms are 0.58 Å; Table 7.5 A; calculated using PyMOL) as well as the MAX homodimer DNA

complex (Ferre-D'Amare et al., 1993) (rmsd: 1.05 Å; Table 7.5 A). Rmsd calculations over the DNA binding regions support this hypothesis (Table 7.5 B).

In both the OmoMYC as well as the MYC/MAX co-crystal structure, the B-DNA adopted a modified conformation with a widened minor groove and a narrowed major groove (Nekludova and Pabo, 1994) characteristic for b/HLH/Zip co-crystal structures. Both base-specific and phosphate-backbone interactions mediate DNA-binding of OmoMYC. A histidine (H12), glutamate (E16), arginine (R20) triad (Figure 4.12 A, lower box) in the basic region of each monomer allowed sequence-specific contacts. This triad is highly conserved in the b/HLH/Zip protein family (Figure 4.12 C). E-box recognition could thus very likely be identical in this OmoMYC structure to the published MYC and MAX structures (Figure 4.12 A, upper box) (Ferre-D'Amare et al., 1993; Nair and Burley, 2003).

4.1.6 OmoMYC forms homodimers *in vivo*

To evince that OmoMYC homodimers are also formed in cells, both hydrogen peroxide (H_2O_2) treatments and co-immunoprecipitations were performed. Oxidation of cysteine residues has been proposed to be used as an H_2O_2-sensing mechanism in response to stress conditions (Delaunay et al., 2000) and disulfide bond formation has been shown to modulate dimer formation, e.g. of b/HLH transcription factors (Danciu and Whitman, 2010; Marinho et al., 2014).

To assess if OmoMYC forms homodimers in a redox-sensitive manner, a human osteosarcoma cell line (U2OS) expressing a doxycycline-inducible allele of MYC (Walz et al., 2014) (hereafter referred to as U2OS[Tet-On]) was lentivirally infected with either a HA-tagged OmoMYC construct or an HA-tagged OmoMYC mutant allele in which the penultimate cysteine residue was mutated to serine (OmoMYC-CS). Mild treatment of the cells with hydrogen peroxide (100 μM H_2O_2, 5 min) resulted in the formation of an OmoMYC complex with the expected size of a covalently-linked homodimer under non-reducing conditions in immunoblots (-DTT; Figure 4.13). This complex disappeared if a reducing agent was added to the sample (+DTT; Figure 4.13), which is indicative of disulfide bond formation. The CS-mutant did not show this behavior, confirming that this residue is involved in dimerization under oxidizing conditions. Notably, oxidation of OmoMYC resulted in protein stabilization.

Importantly, no H_2O_2-dependent formation of a complex of the size of an OmoMYC/MYC heterodimer (molecular weight of approximately 80 kDa) was observed both in immunoblots using α-HA-antibodies (to detect OmoMYC) or α-MYC antibodies. Additionally, overexpression of MYC (via treatment with doxycycline (DOX)) did not cause the formation of heterodimers under oxidizing conditions (Figure 4.13).
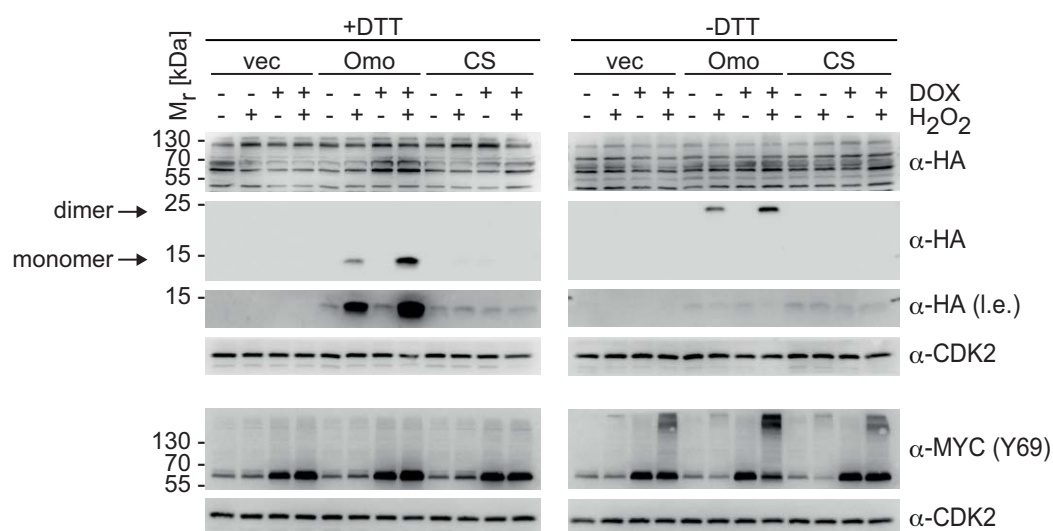

Figure 4.13: Covalently crosslinked OmoMYC homodimers are formed in cells
U2OS[Tet-On] cells stably expressing N-terminally HA-tagged OmoMYC or the CS mutant (C91 in OmoMYC was replaced by a serine) were treated with 100 μM H_2O_2 and/or 1 μg/ml doxycycline (DOX; to induce MYC overexpression) where indicated. SDS-PAGE was performed under reducing or non-reducing conditions (± DTT) and immunoblots probed with α-HA or α-MYC (Y69) antibodies. CDK2 was used as a loading control (n=3; from here on, n indicates the number of independent biological replicates). Vec: empty vector control; Omo: HA-OmoMYC; CS: HA-OmoMYC-CS mutant; l.e.: longer exposure.

To further investigate if OmoMYC homodimers are the most stable species in cells, co-immunoprecipitations were executed by Dr. Anneli Gebhardt. The experiment was performed using both HA- and FLAG-tagged OmoMYC alleles in U2OS[Tet-On] cells, both with and without elevated MYC levels (as an untagged protein (± DOX) or HA-tagged (via lentiviral infection)). Lysates were precipitated using an α-FLAG antibody and probed with α-MYC, α-HA as well as α-MAX antibodies (Figure 4.14). This validated that OmoMYC could both form heterodimers with MYC and MAX, as reported previously (Savino et al., 2011). Yet, in direct comparison, OmoMYC formed homodimers to a larger extent than heterodimers with MYC. Strikingly, the OmoMYC/MAX complex was disrupted at rising levels of MYC while

OmoMYC homodimers were not affected (Figure 4.14). These results paralleled the estimations from the molecular modeling approach (Figure 4.11 B).

This data altogether indicated that OmoMYC forms unexpectedly stable homodimers which are able to bind DNA at the E-box motif. DNA binding of OmoMYC was mediated via the same contacts as for MYC/MAX. In addition, the DNA-binding affinity was very similar, suggesting that OmoMYC could compete with MYC/MAX for E-box binding.
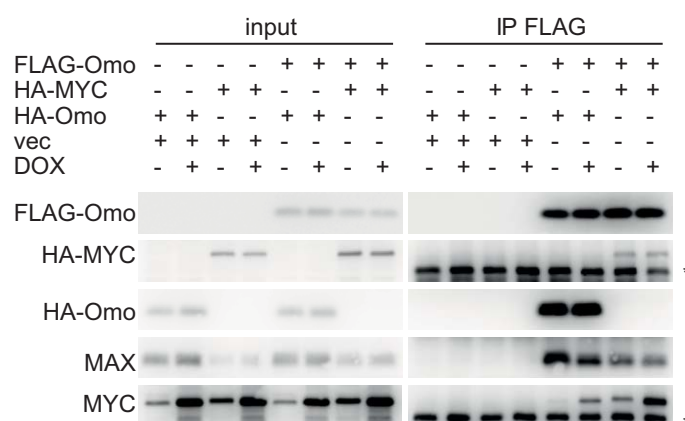

Figure 4.14: OmoMYC homodimers are favored over heterodimers *in vivo*[1]
Co-immunoprecipitations (co-IPs) in U2OS^{Tet-On} cells using α-FLAG antibody were compared to 8 % (α-FLAG and α-MYC immunoblots) or 4 % (α-HA and α-MAX immunoblots) input material (n=3). *: heavy chain, vec: empty vector control. This experiment was performed by Dr. Anneli Gebhardt.

4.2 OmoMYC attenuates promoter invasion by oncogenic MYC

As the *in vitro* data presented in section 4.1 of this study indicated that the mechanism of action of OmoMYC could involve a direct competition with MYC binding to chromatin, it was investigated to see whether OmoMYC binds to chromatin at MYC binding sites and which effect OmoMYC expression has on MYC binding and recruitment. Previously published data already indicated that OmoMYC is able to bind to DNA of reporter plasmids (Savino et al., 2011), but no global analysis of OmoMYC's effects on MYC's ability to bind DNA have been reported so far.

4.2.1 OmoMYC binds to chromatin

To analyze OmoMYC's chromatin binding properties, U2OS$^{\text{Tet-On}}$ cells were stably infected with either N-terminally HA-tagged OmoMYC or an empty vector as a control (Figure 4.15 A), and chromatin immunoprecipitation (ChIP) experiments were performed. OmoMYC binding was strongly enriched over IgG at the transcriptional start site (TSS) of MYC-bound and regulated promoters (Figure 4.15 B). Only neglectable binding to an intergenic control region on chromosome 11 could be detected, which served as a control. The specificity of the HA-antibody was verified, as there was no specific enrichment in empty vector infected cells.

To generate genome-wide OmoMYC and MYC binding profiles, chromatin immunoprecipitations followed by high-throughput sequencing (ChIP-sequencing) experiments were performed (Figure 4.15 C and D). Dr. Susanne Walz carried out the bioinformatic analysis of ChIP-sequencing data shown in this and the following sections. Inspection of both promoter-close and intergenic regions containing MYC binding sites showed that OmoMYC's chromatin binding sites highly overlapped with those of MYC (Figure 4.15 C). Consistently, *de novo* motif analysis identified both consensus (CACGTG) and non-consensus (CANNTG; N represents any nucleic acid) E-box motifs within the center of the OmoMYC peak (Figure 4.15 D).

4.2.2 OmoMYC blunts promoter invasion of MYC

Despite being a tumor cell line, endogenous MYC levels in U2OS$^{\text{Tet-On}}$ cells are relatively low and comparable to those found in non-transformed cell lines (IMEC, HMLE, MCF10A). As the cell line was engineered to express a doxycycline-inducible allele of MYC, MYC levels can be increased to reach those of other tumor cell lines (HeLa, HCT116) (Lorenzin et al., 2016). At these "oncogenic levels", MYC is recruited to promoters, which are only weakly occupied by lower protein levels. This concept has been termed "promoter invasion" (Fernandez et al., 2003; Guccione et al., 2006). It was expanded demonstrating that MYC-invaded genes are regulated and therefore relevant targets (Nie et al., 2012; Walz et al., 2014). Further in-depth analysis identified that promoter affinities (EC$_{50}$ values) for MYC binding strongly vary (Lorenzin et al., 2016).
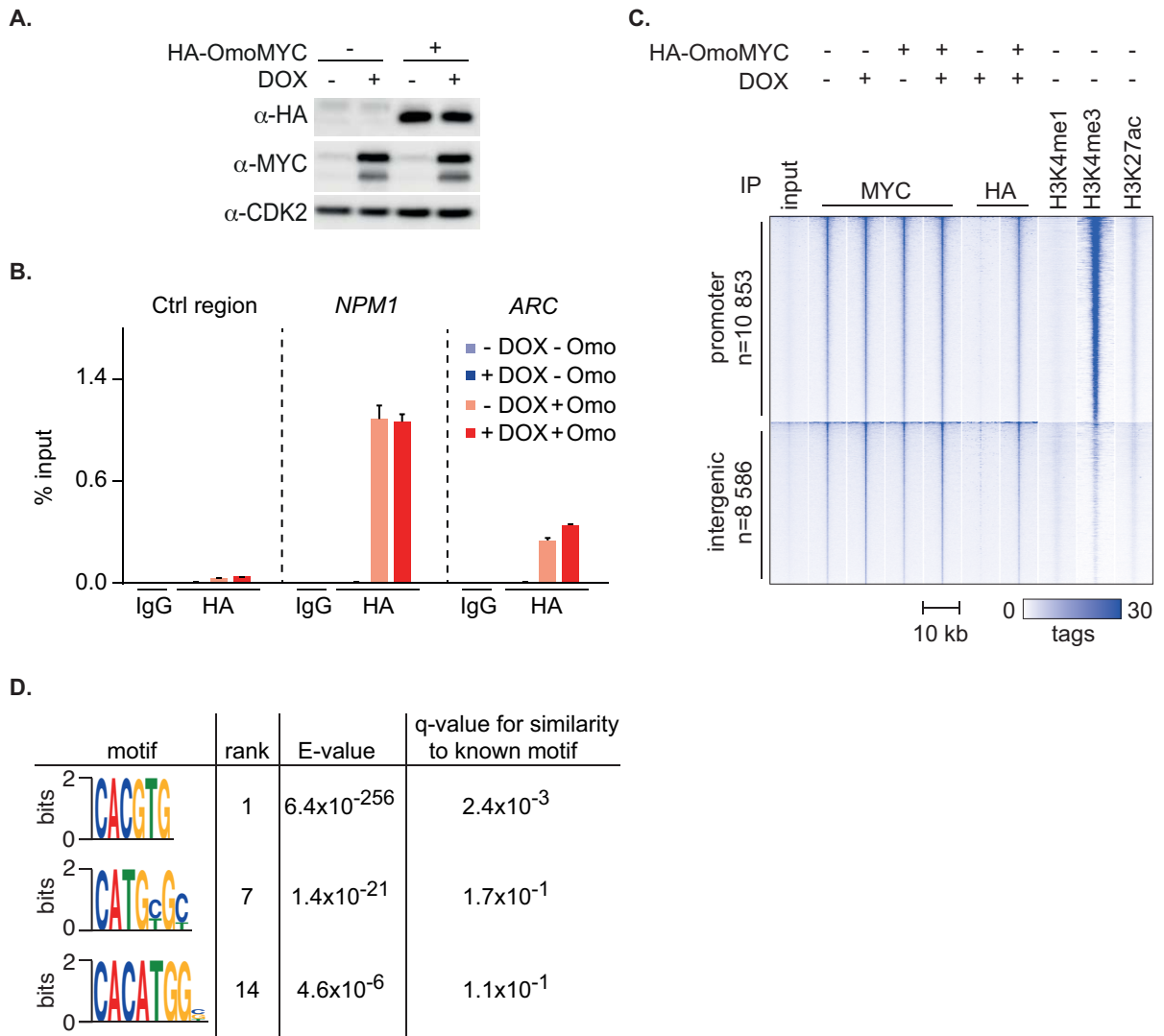
Figure 4.15: OmoMYC binds to chromatin[1]
(A)   Immunoblot of empty vector (-) or HA-OmoMYC (+) infected U2OS[Tet-On] cells. MYC overexpression was induced via DOX treatment (1 μg/ml; 8 h). Lysates were probed with α-MYC, α-HA and α-CDK2 antibodies (n=3).
(B)   ChIP-qPCR analysis of HA-OmoMYC-expressing U2OS[Tet-On] cells. Immunoprecipitations were performed with an HA antibody or an unspecific IgG as a control. DNA was analyzed by qPCR with primers directed against the transcriptional start site (TSS) of the indicated genes or an intergenic control region (Ctrl region). Error bars indicate SD of technical triplicates (n=2).
(C)   Comparison of genome-wide MYC and OmoMYC binding to chromatin. Heat maps of ChIP-sequencing data (ChIP-seq) documenting binding of MYC and OmoMYC to promoters (defined by having a MYC peak in +/-1 kb around annotated TSS) and intergenic regions. Peaks are sorted based on MYC occupancy and the heat map is centered to the MYC peak summit in a window of ±5 kb at a resolution of 50 bp. ChIP-seq was performed from U2OS[Tet-On] cells described in (A) using an α-HA-antibody to IP OmoMYC as well as a α-MYC antibody (N262) directed against the N-terminus of the protein, which would not recognize OmoMYC. Histone modification ChIP-seq data was taken from (Walz et al., 2014). Input and HA-IP without HA-OmoMYC expression are shown as controls.
(D)   *De novo* motif analysis using the DREME algorithm included in the MEME Suite. Well-characterized binding motifs such as consensus and non-consensus E-boxes were identified in OmoMYC peaks located in promoters.
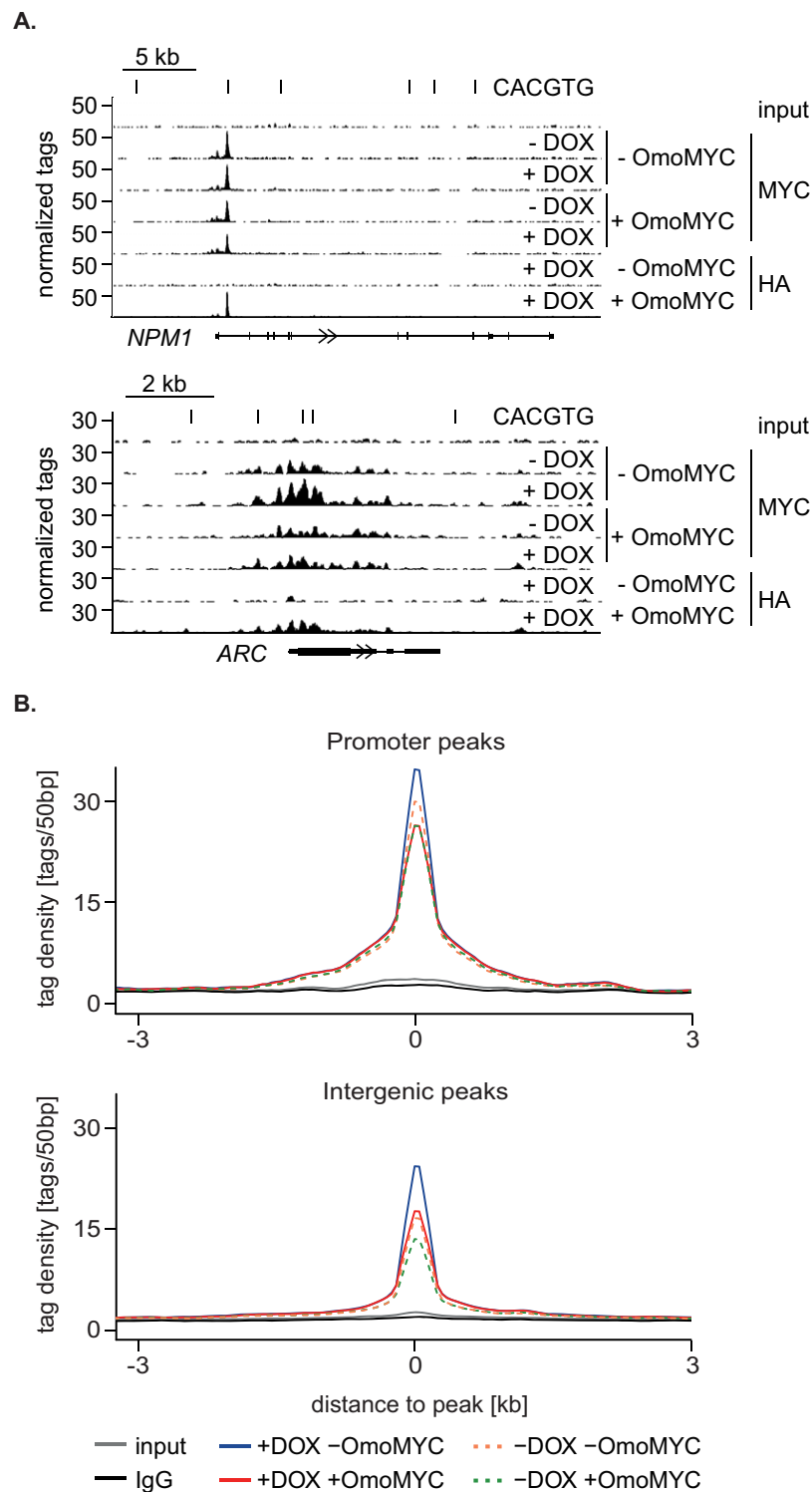
Figure 4.16: OmoMYC reduces MYC's chromatin occupancy[1]

(A) Representative ChIP-sequencing traces of one high-affinity (*NPM1*) and one low-affinity gene (*ARC*) for MYC binding. The location of a consensus E-box (CACGTG) is indicated by a line. ChIP-sequencing was performed as described in Figure 4.15 C.

(B) Tag density plots illustrating MYC binding in the presence and absence of OmoMYC at binding sites containing a consensus E-box. Endogenous MYC binding (-DOX; dashed lines) and MYC binding after overexpression (+DOX; solid lines) is shown. The upper panel includes binding sites at core promoters (n=1,868), the lower panel non-promoter binding sites (n=2,543). Input and IgG-ChIPs serve as controls.

Having established that the OmoMYC protein itself is able to bind DNA *in vivo*, it was analyzed if and how OmoMYC expression affects chromatin association of MYC. To this end, ChIP-sequencing data of MYC was further analyzed in the presence and absence of OmoMYC and in the context of both endogenous and elevated MYC levels.

Inspection of individual genes with promoter-close binding sites displayed a range of affinities for MYC binding (representative ChIP-sequencing tracks demonstrating high- and low-affinity binding are shown in Figure 4.16 A) as seen by (Lorenzin et al., 2016). In the presence of OmoMYC, a decrease in MYC binding was observed. Low-affinity sites showed an especially strong decrease in MYC binding (Figure 4.16 A). To analyze this effect on a genome-wide level, tags were counted within a distance of 3 kb around the MYC peak in both intergenic and promoter-proximal regions (Figure 4.16 B). A reduction in MYC occupancy was obvious in both regions. Interestingly, areas containing consensus E-box motifs (as shown in Figure 4.16 B) showed a stronger decrease in MYC binding than areas with a non-consensus or no E-box motif (Jung et al., 2016).
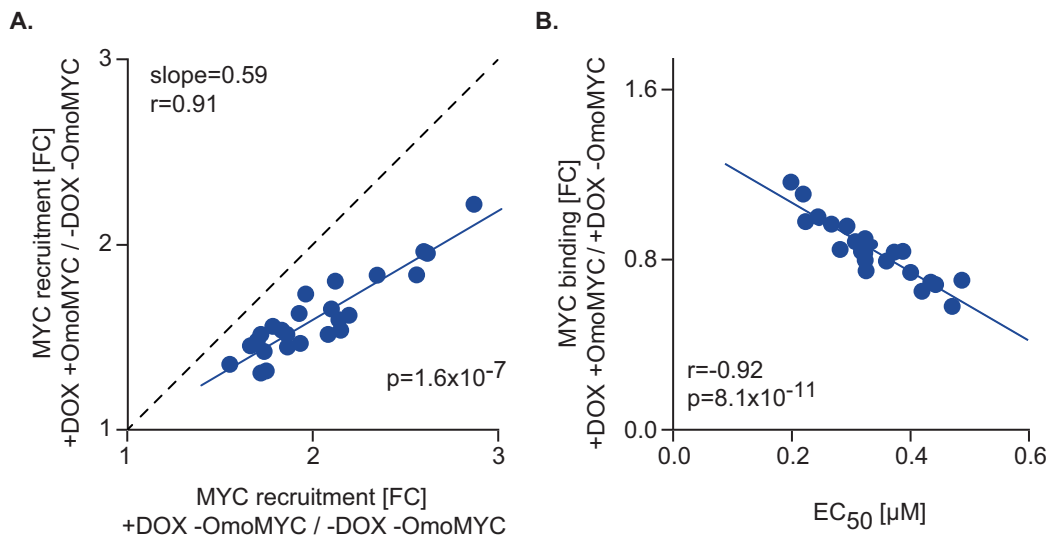

Figure 4.17: OmoMYC blunts promoter invasion of MYC[1]
(A) Diagram demonstrating the effect of OmoMYC expression on the recruitment of MYC to its binding sites. Directly MYC-bound promoters (n=7,379) were sorted according to their MYC recruitment in an independent experiment (Walz et al., 2014) and grouped into 25 bins. MYC recruitment was plotted in the absence (x-axis) or the presence of OmoMYC (y-axis). Calculation of the p-value (p) was performed with a linear model and a t-test with an offset of 1. r: Pearson's correlation coefficient.
(B) Correlation of the change in MYC binding upon OmoMYC expression with the EC_{50} value for MYC binding of the respective gene. Binding affinity (EC_{50}) data was taken from (Lorenzin et al., 2016). Binding data for MYC in the presence or absence of OmoMYC were sorted according to MYC recruitment and grouped into equally sized 25 bins. The mean of each bin was plotted; the line reflects a linear fitting model. The p-value (p) was calculated using a two-tailed t-test. r: Pearson's correlation coefficient.

To discover further differences in MYC occupancy upon OmoMYC expression, MYC recruitment (i.e., the ratio of MYC occupancy upon doxycycline treatment vs. MYC occupancy at endogenous levels) to promoter-proximal regions in the presence and absence of OmoMYC was plotted (Figure 4.17 A). Surprisingly, the decrease in MYC recruitment upon OmoMYC expression was not uniform. At highly MYC-occupied promoters that displayed little additional MYC recruitment upon overexpression (i.e., high-affinity promoters), OmoMYC had little impact on MYC recruitment. Whereas at sites with a low binding affinity for MYC, which are characterized by the ability to recruit additional MYC protein (Lorenzin et al., 2016), OmoMYC decreased the recruitment of MYC upon overexpression (Figure 4.17 A). The decrease in MYC binding upon OmoMYC expression (MYC displacement) correlated with the EC_{50} value determined for the respective gene (EC_{50} calculation was performed in (Lorenzin et al., 2016)) (Figure 4.17 B).

Taken together, the ChIP-sequencing analysis revealed that OmoMYC bound chromatin at MYC binding sites. The protein was able to reduce the recruitment of MYC, especially to low-affinity sites, and thereby suppress the promoter invasion of high levels of MYC.

4.3 OmoMYC attenuates gene regulation by oncogenic MYC

4.3.1 MYC-dependent transcriptional activation and repression are buffered by OmoMYC

The ChIP-sequencing results suggested that OmoMYC expression had a marked effect on MYC binding; thus it was analyzed to discover whether this competition with DNA binding resulted in changes on the MYC-dependent transcriptome. Previous studies already established that OmoMYC is able to affect gene regulation by MYC (Savino et al., 2011; Sodir et al., 2011; Soucek et al., 1998; Soucek et al., 2002). In the U2OS[Tet-On] system (as described in section 4.2.1), qPCR experiments revealed that OmoMYC abrogated the induction of one of the most strongly regulated MYC target genes (Figure 4.18 A).

To analyze whether cells expressing OmoMYC were generally compromised in MYC-dependent transcriptional regulation, global gene expression profiles of cells with and without OmoMYC expression exhibiting either low (–DOX) or high MYC levels (+DOX) were
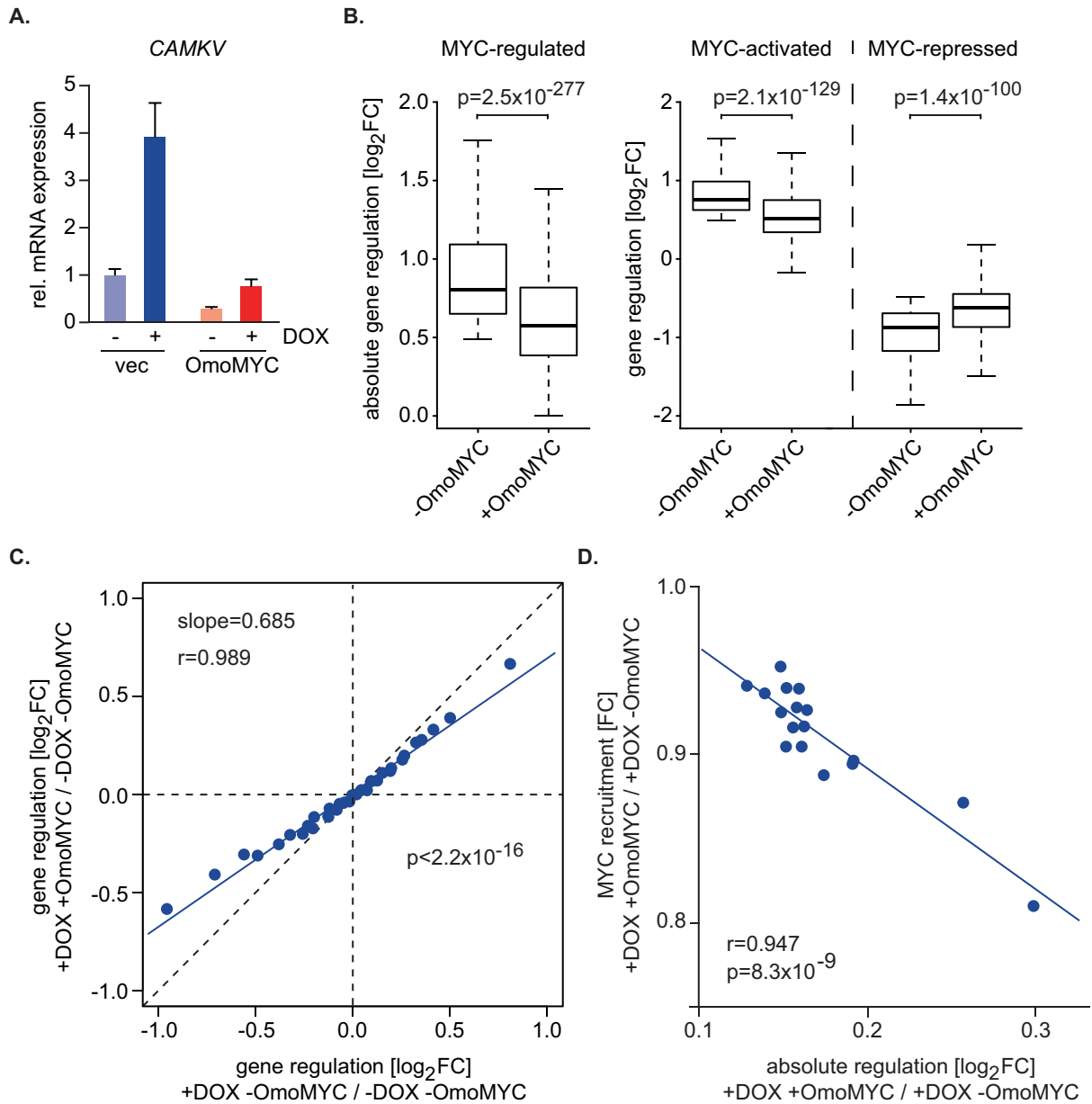
Figure 4.18: OmoMYC attenuates gene regulation by oncogenic MYC[1]

(A) qPCR analysis of *CAMKV* expression in U2OS[Tet-On] cells infected with either an HA-tagged OmoMYC construct or an empty vector (vec). MYC expression was induced with doxycycline (DOX) for 8 h (1 μg/ml). Error bars indicate SD of technical triplicates (n=2).

(B) Box plots showing global changes (log$_2$ fold change=log$_2$FC; +DOX vs. -DOX) in MYC-dependent gene expression in the context of OmoMYC expression. MYC expression was induced for 30 h with 1 μg/ml DOX. The left panel shows absolute values for differential gene expression of significantly MYC-regulated genes (q-value<0.05). The right plot distinguishes between significantly MYC-activated (883 genes; log$_2$FC>0) and MYC-repressed (785 genes; log$_2$FC<0) genes. Note that outliers are not shown.

(C) Correlation of changes in MYC-dependent gene regulation (30 h, 1 μg/ml DOX) in the presence (y-axis) or absence (x-axis) of OmoMYC expression. Expressed genes were sorted according to MYC-regulation using an independent dataset and binned (38 bins, 490 genes per bin). Regression was calculated using a linear model. r: Pearson's correlation coefficient.

(D) Correlation of OmoMYC-dependent changes in gene expression (x-axis) with MYC promoter recruitment (changes in promoter occupancy of MYC; y-axis). MYC-bound promoters were grouped into bins (17 bins, 400 genes per bin) and sorted for changes in gene expression upon MYC-induction. The p-value (p) was calculated using a two-tailed Student's t-test. r: Pearson's correlation coefficient.

compared by RNA-sequencing (RNA-seq). To reliably evaluate effects on transcriptional repression, ectopic MYC expression was induced for an extended period (30 hours). Dr. Carsten Ade and Dr. Susanne Walz carried out the bioinformatic analysis of RNA-sequencing data shown in this and the following sections. Log$_2$ fold changes (log$_2$FC) in gene expression of significantly MYC-regulated genes (+DOX vs. –DOX; q<0.05) were visualized as box plots. The analysis confirmed that OmoMYC globally attenuated gene regulation by MYC (Figure 4.18 B, left panel). In contrast to observations published in previous studies (mentioned above), both transcriptional activation and repression by MYC were inhibited (Figure 4.18 B, right panel). As shown for OmoMYC's effects on DNA binding (Figure 4.17), the global changes in gene expression were also not homogeneous (Figure 4.18 C). Gene regulation by MYC was most evidently buffered at genes that responded strongly to an increase in MYC levels.

Previous studies of U2OS^{Tet-On} cells demonstrated that the magnitude of response of a certain gene to the induction of ectopic MYC expression correlated with the change in its promoter occupancy by MYC (Lorenzin et al., 2016; Walz et al., 2014). Genes with a low-affinity (high EC$_{50}$ values) for MYC binding were shown to be able to recruit additional MYC to promoter sites (i.e., exhibit "promoter invasion"); they also displayed the strongest changes in gene expression. To directly link the effect of OmoMYC expression on MYC's DNA binding ability to the reduction in transcriptional response, OmoMYC-dependent changes in gene expression were plotted over changes in MYC promoter occupancy (Figure 4.18 D). Genes that responded most strongly to OmoMYC expression displayed the strongest reduction in MYC binding. This is consistent with the observation that low-affinity sites showed the strongest displacement of MYC (Figure 4.17) while exhibiting the strongest reduction in gene expression (Figure 4.18 C) in the presence of OmoMYC.

The RNA-sequencing data was further analyzed by gene set enrichment analysis (GSEA), which compares the generated gene expression profiles with e.g. published gene sets (Subramanian et al., 2005). It calculates an enrichment score (ES) that reflects how strongly a gene set is overrepresented at the top (positive ES) or bottom (negative ES) of a ranked list of genes (i.e., expression data). Both MYC-regulated and OmoMYC-regulated expression profiles were compared with gene sets deposited in the Molecular Signature Database (MSigDB). Selected results from several characteristic MYC target gene signatures from the C2 collection (curated gene sets) including different biological systems (i.a., B lymphocytes,

small cell lung carcinoma and monoblastic leukemia cell lines) are shown in Figure 4.19. Both MYC-up- and downregulated genes were strongly similar to previously identified target gene signatures, while in the presence of OmoMYC, the regulation of these signatures was reverted.

	MYC(DOX)-regulated		OmoMYC-regulated	
	NES	q-value	NES	q-value
Ben-Porath: MYC targets with E-box	1.7	6.9e-2	-1.8	4.0e-2
Dang: Regulated by MYC up	1.8	4.1e-2	-1.5	2.0e-1
Kim: MYC amplification targets down	-1.9	5.2e-3	1.8	6.8e-2
Kim: MYCN amplification targets down	-2.0	1.4e-3	2.0	6.2e-3

Figure 4.19: OmoMYC reverts MYC-dependent gene expression programs[1]
Gene set enrichment analysis (GSEA) of MYC-regulated genes (left; upon MYC induction via doxycycline treatment; 30 h, 1 μg/ml) and of OmoMYC-regulated genes (right) in U2OS[Tet-On] cells (Ben-Porath et al., 2008; Kim et al., 2006; Zeller et al., 2003). Normalized enrichment scores (NES) and q-values of selected well-characterized MYC-dependent gene sets are listed. GSE analyses were performed using the C2 gene set collection of the MSigDB (Subramanian et al., 2005).

4.3.2 Basic region mutants of OmoMYC are compromised in inhibiting MYC-dependent transcription

To further support the model that OmoMYC's transcriptional effects are dependent on specific DNA binding of the OmoMYC protein itself, two mutant OmoMYC alleles were designed based on the information obtained by the DNA-bound crystal structure (Figure 4.12). In the first mutant, OmoMYC(HER), all three residues of the E-box recognition triad (H12, E16, R20) in the basic region were mutated to alanine. The second mutant, OmoMYC(HE) carried only mutations in the first two residues as the arginine moiety was also involved in unspecific DNA-binding via phosphate backbone interactions. Thus, mutation of R20 was hypothesized to result in an overall decrease in DNA-binding affinity of the protein.

Using lentiviral transduction, both HA-tagged OmoMYC mutants were stably expressed in U2OS[Tet-On] cells. All three proteins localized to the nucleus (Jung et al., 2016). OmoMYC(HE) was expressed at similar levels as "wild type" OmoMYC, while OmoMYC(HER) expression levels were slightly lower than those of the other two OmoMYC
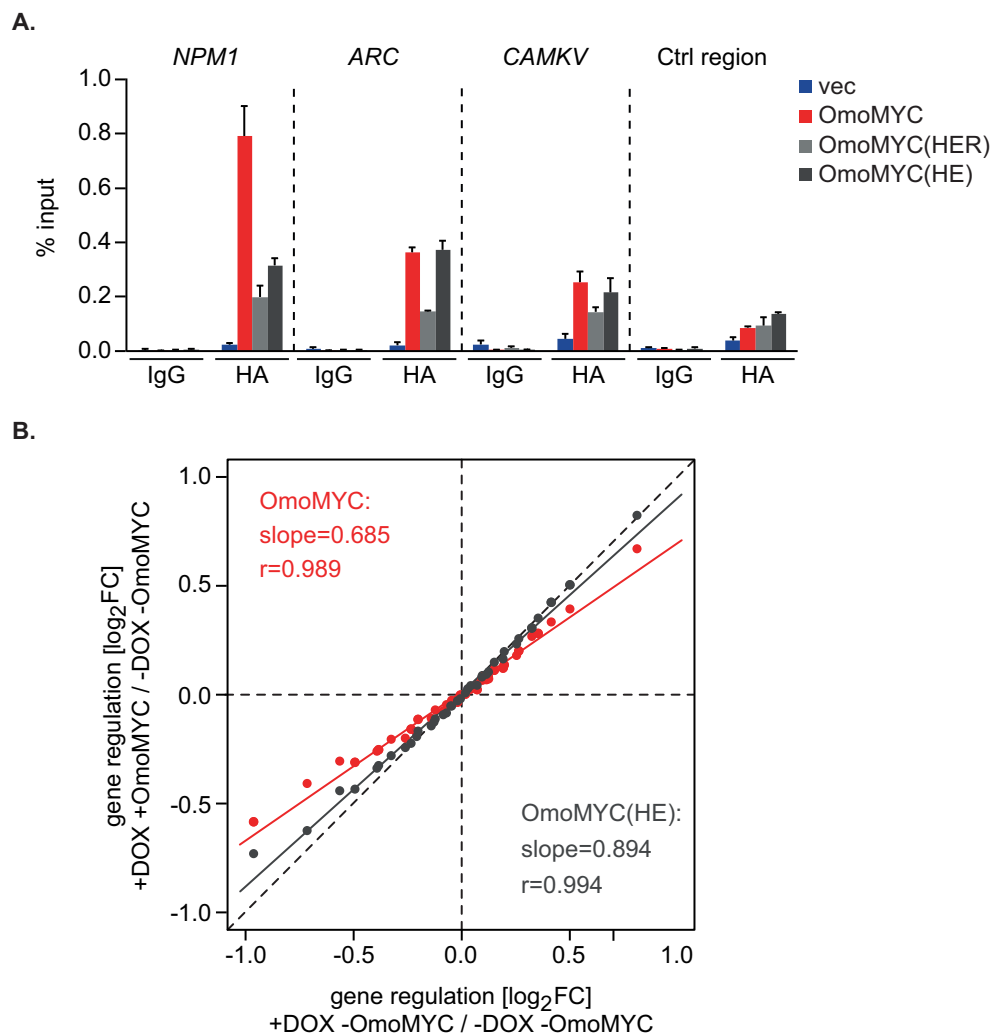
A.

B.

Figure 4.20: OmoMYC basic region mutants show a reduced ability to inhibit MYC-dependent gene expression[1]

(A) ChIP-qPCR experiments of U2OS[Tet-On] cells expressing either HA-OmoMYC, a mutant OmoMYC allele (OmoMYC(HER) or OmoMYC(HE)) or an empty vector. ChIPs were performed with an HA antibody or an unspecific IgG as a control. qPCR analysis was undertaken with primers directed against the transcriptional start site (TSS) of the indicated genes or an intergenic control region (Ctrl region). Error bars indicate SD of technical triplicates.

(B) Correlation of changes in MYC-dependent gene regulation (30 h, 1 μg/ml DOX) in the presence (y-axis) or absence (x-axis) of OmoMYC (red) or OmoMYC(HE) (grey) expression. Binning was performed as described in Figure 4.18 C. Regression was calculated using a linear model. r: Pearson's correlation coefficient.

alleles (Jung et al., 2016). ChIP-qPCR experiments confirmed that binding of both mutants to MYC target gene promoters was weaker than "wild type" OmoMYC. Consistent with their design, DNA-binding of the mutants relative to the wild type allele appeared to have decreased with the amount of canonical E-boxes (*NPM1* displays several CACGTG sites in the promoter, whereas no E-boxes are located in the control region). RNA-sequencing

experiments were conducted; they revealed that both mutants were severely compromised in repressing MYC-dependent transcription (Figure 4.20 and (Jung et al., 2016)).

In summary, OmoMYC globally buffers gene regulation of MYC target genes. It affects both MYC-dependent gene activation and repression and reverts characteristic MYC target gene signatures. These effects are largely dependent on DNA binding of the OmoMYC protein and thus on the competition with MYC/MAX heterodimers on chromatin.

4.4 OmoMYC-regulated genes identify multiple MYC-driven tumors and comprise key targets that interfere with tumor cell growth

4.4.1 OmoMYC-regulated gene signatures stratify numerous MYC-driven tumors

Initial analysis of RNA-sequencing data clearly suggested that OmoMYC is able to revert MYC-dependent gene expression programs (see section 4.3.1). MYC overexpression and deregulation can be found in various human tumors and it is often associated with high aggressiveness and poor prognosis (Albihn et al., 2010; Oster et al., 2002) and could thus serve as a diagnostic marker for specific diseases (Kraehn et al., 2001; Obara et al., 2001). Several mouse models demonstrated that OmoMYC expression caused the regression of lung adenocarcinomas, glioblastomas and pancreatic tumors while showing mild and reversible side effects (Annibali et al., 2014; Sodir et al., 2011; Soucek et al., 2008; Soucek et al., 2013) suggesting that OmoMYC is able to discriminate "oncogenic" from "physiological" MYC functions. This led to the question of whether one could use OmoMYC-dependent gene expression data generated in U2OS^{Tet-On} cells to identify tumors displaying high MYC levels.

As described above for well-known MYC target gene signatures (see section 4.3.1), gene set enrichment analyses were executed using gene expression signatures from patient samples. This method can identify whether a group of genes is related to a dataset and can thus be used for phenotypic class distinction. Data from neuroblastoma, multiple myeloma, medulloblastoma, colorectal carcinoma and Burkitt lymphoma patients was downloaded from the Gene Expression Omnibus (GEO) database (Edgar et al., 2002). GSE analysis was able to stratify stage 4 from stages 1-3 neuroblastoma (Figure 4.21 A) as well as several other tumor
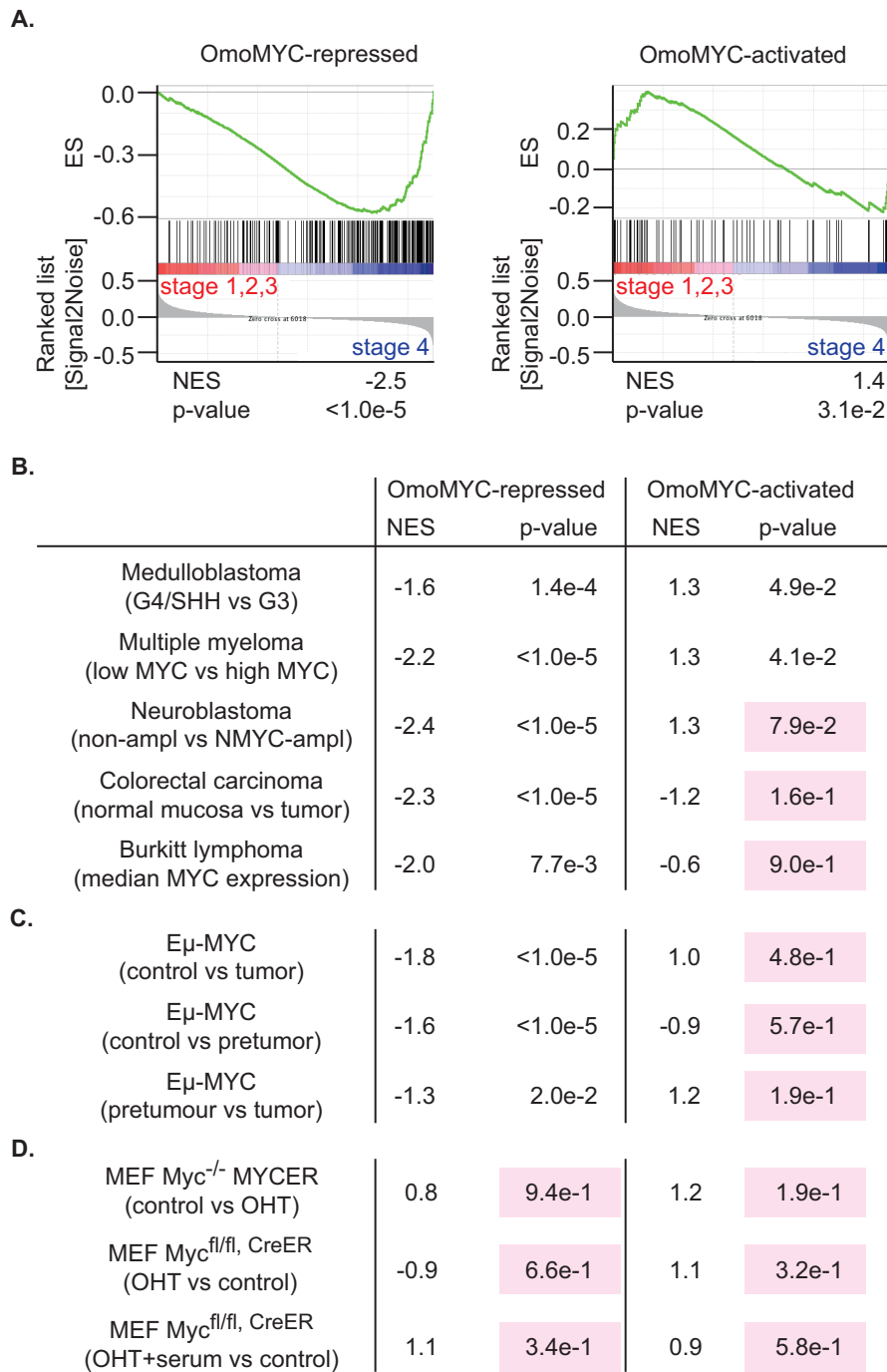
A.

B.

	OmoMYC-repressed		OmoMYC-activated	
	NES	p-value	NES	p-value
Medulloblastoma (G4/SHH vs G3)	-1.6	1.4e-4	1.3	4.9e-2
Multiple myeloma (low MYC vs high MYC)	-2.2	<1.0e-5	1.3	4.1e-2
Neuroblastoma (non-ampl vs NMYC-ampl)	-2.4	<1.0e-5	1.3	7.9e-2
Colorectal carcinoma (normal mucosa vs tumor)	-2.3	<1.0e-5	-1.2	1.6e-1
Burkitt lymphoma (median MYC expression)	-2.0	7.7e-3	-0.6	9.0e-1

C.

Eμ-MYC (control vs tumor)	-1.8	<1.0e-5	1.0	4.8e-1
Eμ-MYC (control vs pretumor)	-1.6	<1.0e-5	-0.9	5.7e-1
Eμ-MYC (pretumour vs tumor)	-1.3	2.0e-2	1.2	1.9e-1

D.

MEF Myc^{-/-} MYCER (control vs OHT)	0.8	9.4e-1	1.2	1.9e-1
MEF Myc^{fl/fl}, CreER (OHT vs control)	-0.9	6.6e-1	1.1	3.2e-1
MEF Myc^{fl/fl}, CreER (OHT+serum vs control)	1.1	3.4e-1	0.9	5.8e-1

Figure 4.21: OmoMYC target genes stratify MYC-dependent tumors[1]

(A) Enrichment plots of significantly (q-value<0.05) OmoMYC-repressed ($\log_2$FC<0; n=383) and -activated ($\log_2$FC>0; n=137) genes generated by GSE analysis comparing stage 4 vs. stage 1-3 neuroblastomas (GEO accession: GSE16476). ES: enrichment score; NES: normalized enrichment score; ampl: amplified.

(B) GSE analysis of OmoMYC-activated or -repressed genes in comparison to expression changes in human tumor profiles showing high MYC or N-MYC expression. Data sets GSE16476, GSE37382, GSE4475, GSE26760, and GSE39582 were taken from the GEO database. NES: normalized enrichment score.

(C) GSEA now comparing different stages of B cell lymphomagenesis using the Eμ-MYC model in mice (GEO accession: GSE51008) (Sabò et al., 2014).

(D) GSEA using expression data from non-transformed murine embryonic fibroblasts (MEFs). OHT (4-hydroxytamoxifen) treatment either induced MYC activation (via MYC-ER; top row) (Sabò et al., 2014) or MYC-knockout (via Cre-ER; rows below) (Perna et al., 2012).

entities displaying high levels of MYC protein (Figure 4.21 B). Genes that were repressed by OmoMYC (and hence majorly activated by MYC) uniformly overlapped with high MYC expressing subtypes, while OmoMYC activated (representing mainly MYC repressed genes) could not discriminate all tumor types analyzed. This might be due to the assumption that MYC-mediated repression is not the key transcriptional mechanism in these subtypes.

Additionally, expression data from a well-characterized murine tumor model (Sabò et al., 2014), in which MYC drives B cell lymphomagenesis, was analyzed. This system, where MYC is fused to an immunoglobulin enhancer (Eµ), highly recapitulates human lymphomas (Adams et al., 1985). Consistent with the results generated from patient data (Figure 4.21 B), OmoMYC-repressed genes stratified lymphomas from control cells and from a pre-lymphomagenic stage (Figure 4.21 C). Importantly, also late-stage lymphomas could be separated from pre-tumoral stages using the OmoMYC repressed gene signature (Figure 4.21 C). Again, OmoMYC-activated genes failed to do this. As a control, OmoMYC expression data was also tested to determine if it could identify gene sets generated by serum-stimulation of fibroblasts, which feature gene regulation by endogenous MYC, or a gene set generated by overexpression of MYC in murine fibroblasts (Figure 4.21 D). As expected, the results were non-significant.

4.4.2 Identification of crucial OmoMYC target genes important for tumor cell growth

After knowing that the set of OmoMYC-regulated genes can be used to specifically identify tumors with high levels of MYC in patient data, the aim was to pinpoint crucial OmoMYC target genes that were able to drive tumor growth. To this end, a targeted shRNA screen was performed using candidate genes that were both significantly (p-value <0.05) repressed by OmoMYC while significantly activated by MYC induction and druggable.

Relative mRNA expression levels of OmoMYC decreased by at least 40 % within 14 days of culturing (after infection and puromycin selection) in U2OS^{Tet-On} cells. This rapid counterselection impeded long-term studies in this cell system. Therefore, a cell line derived from KRAS-driven pancreatic tumors (KRAS/p53^{mut} cells: KPC) was chosen. Doxycycline-inducible expression of OmoMYC in this cell line reduced both anchorage-independent and

adherent growth. RNA-sequencing showed that OmoMYC-dependent expression profiles were highly similar in U2OS[Tet-On] cells and KPCs (Jung et al., 2016).
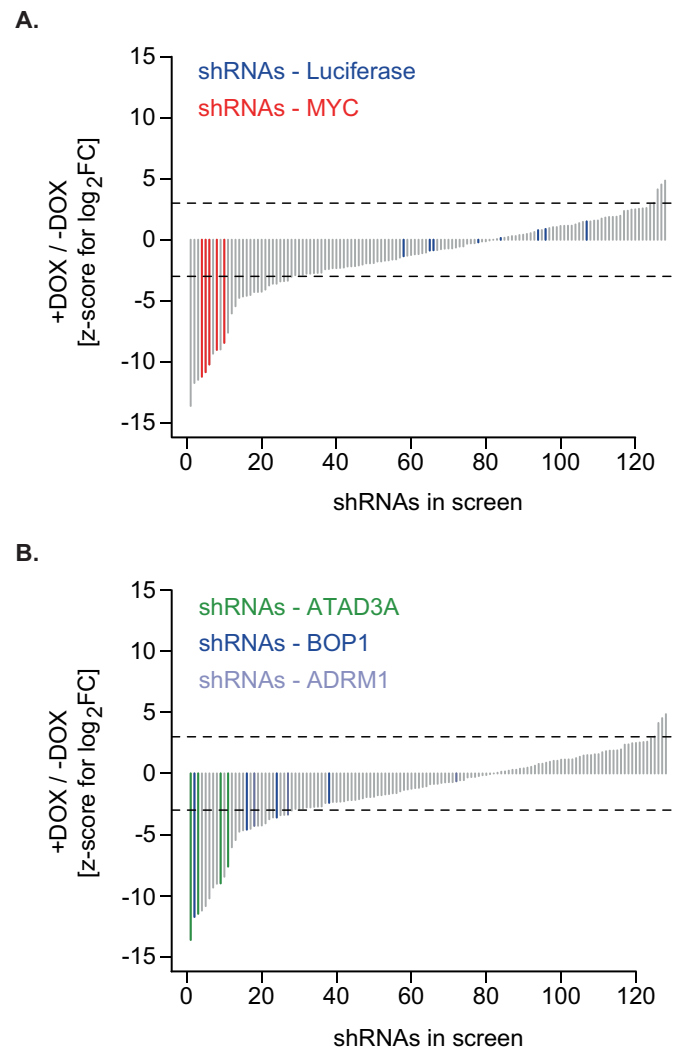
A.

B.

Figure 4.22: Identification of critical OmoMYC target genes using a focused RNAi screen[1]
(A) Waterfall plots for z-scores demonstrating the results of the polled negative shRNA screen. Z-scores for log_2FC in shRNA representation between DOX-treated (activation of shRNA expression) and untreated KPC cells are shown. Dotted lines indicate z-scores $\pm$ 3. Positive controls (shRNAs targeting MYC) and negative controls (shRNA targeting *Renilla* luciferase) are highlighted in blue and red, respectively.
(B) Waterfall plots as shown in (A). shRNAs targeting ATAD3A (green), BOP1 (blue) and ADRM1 (light blue) are highlighted.

A custom-designed doxycycline-inducible shRNA library was built that included 27 OmoMYC target genes covered by five shRNAs each by Dr. Carsten Ade. As selection criteria, both significant regulation (repression by OmoMYC and activation by MYC induction) and druggability of the target gene/protein itself, an interacting protein or upstream pathway were considered. Changes in shRNA representation were monitored in KPCs after

four days of shRNA induction using deep sequencing of shRNA guide strands amplified from genomic DNA. Bioinformatic analysis of screening results was performed by Dr. Carsten Ade. Using the scoring criterion of a z-score of more than -3, all 5 positive control shRNAs targeting MYC were identified (Figure 4.22 A; shown in red), while negative control shRNAs did not score at all (shown in blue). Genes for which at least 50 % of all recovered shRNAs scored were considered as hits. Three hits emerged from this analysis, BOP1, a protein important for maturation of ribosomal RNAs (Rohrmoser et al., 2007), ADRM1 (also known as RPN13), an ubiquitin receptor on the proteasome (Husnjak et al., 2008), and ATAD3A, protein that promotes mitochondrial fusion (Fang et al., 2010) (Figure 4.22 B).
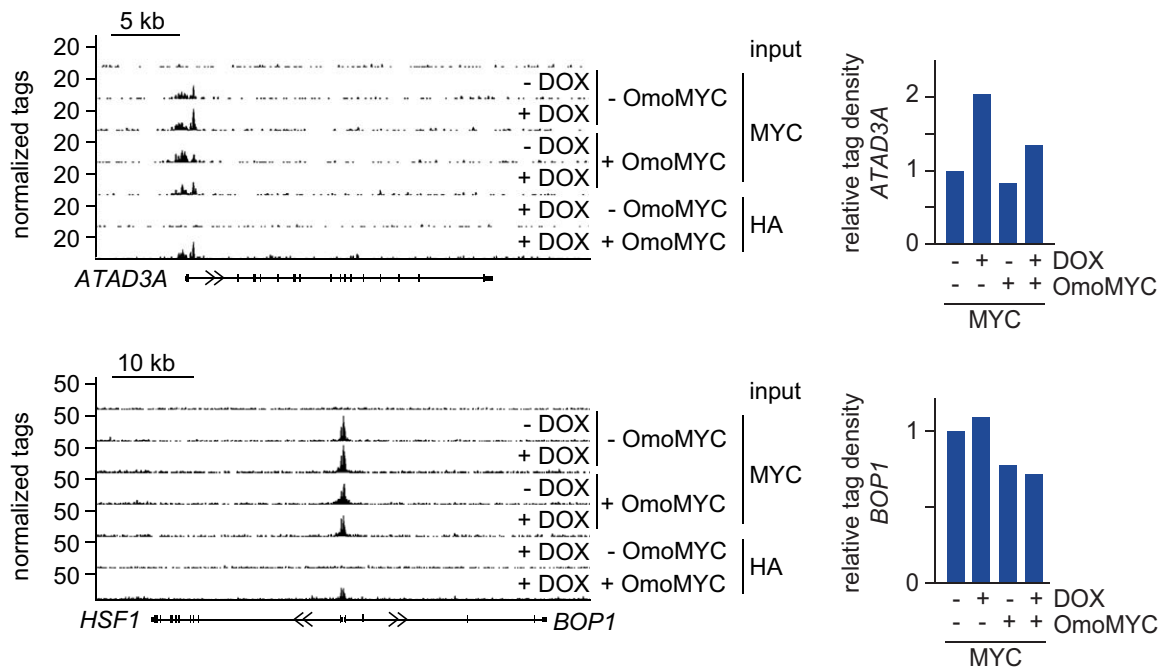

Figure 4.23: ATAD3A and BOP1 are direct targets of MYC and OmoMYC[1]
ChIP-sequencing tracks at the ATAD3A (upper panel) and BOP1 (lower panel) locus. ChIP-sequencing was performed as described in Figure 4.15 C. Tag densities 100 bp around the summit of the MYC peaks were calculated using the density array method with SeqMiner (right panels) by Dr. Carsten Ade.

Both ATAD3A and BOP1 were shown to be direct targets of both OmoMYC and MYC (Figure 4.23; left panels). OmoMYC expression reduced MYC binding at their promoters (Figure 4.23; right panels). The three hits were subjected to further validation using either small molecule inhibitors or individual shRNAs. Inhibitors of ribosome biogenesis (via the RNA Polymerase I inhibitor CX-5461) and ADRM1 (RA 190) repressed growth of KPCs (Figure 4.24 A).
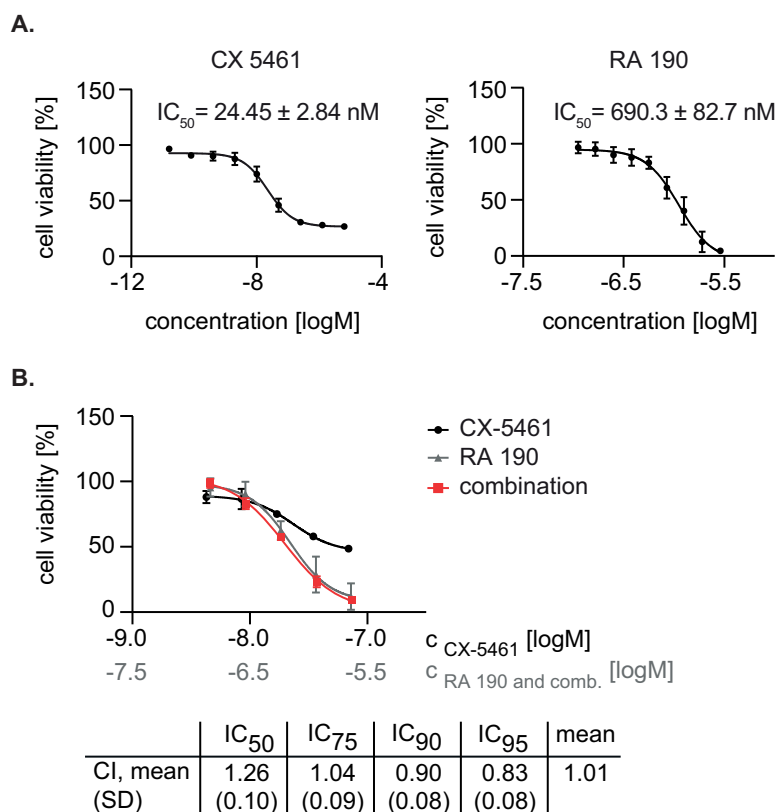
Figure 4.24: Inhibitors of ribosome biogenesis and a proteasomal ubiquitin receptor inhibit cancer cell growth[1]

(A) Dose response curves demonstrating the effect of RNA Polymerase I (left panel; CX-5461) and ADRM1 (right panel; RA 190) inhibition. KPCs were treated with the indicated compounds for 48 h. Cell viability was measured using MTT assays. Error bars indicate standard deviation of 6 technical replicates. IC_{50} values (indicating the concentration of an inhibitor where the response is reduced by half) are given as mean ± standard deviation (n=3).

(B) Combinatory treatment of inhibitors shown in (A). Dose response curves were generated as described in (A). Shown is the result of one representative experiment, in which error bars represent SD of at least 4 technical replicates. The table below shows combinatory indices (CI) calculated for different inhibitor concentrations (at IC_{50}-IC_{95}). Means of CI values are shown, SD are given in parentheses (n=3). CI scores below 0.75 were considered as synergistic, scores between 0.75 and 1.5 as additive, and scores above 1.5 as antagonistic.

To explore the possibility that a combination of both inhibitors might be beneficial for cancer treatment, drug-induced inhibition of cancer cell proliferation was determined to reveal additive, antagonistic or synergistic effects using fixed-ratio combinations according to the Chou-Talalay method (Chou and Talalay, 1984). No synergistic effects were noticed, but an additive effect of a combination of both inhibitors was observed over a range of different dose levels.

For ATAD3A, no small molecule inhibitor is commercially available so far. Therefore, shRNA-mediated depletion of the protein was investigated to see whether it is sufficient to reduce cell growth in the pancreatic tumor cell line KPC (experiment was performed by Dr. Anneli Gebhardt). Indeed, the cells responded to a reduction in ATAD3A protein levels with a decrease in anchorage-dependent growth (Figure 4.25 A and B).
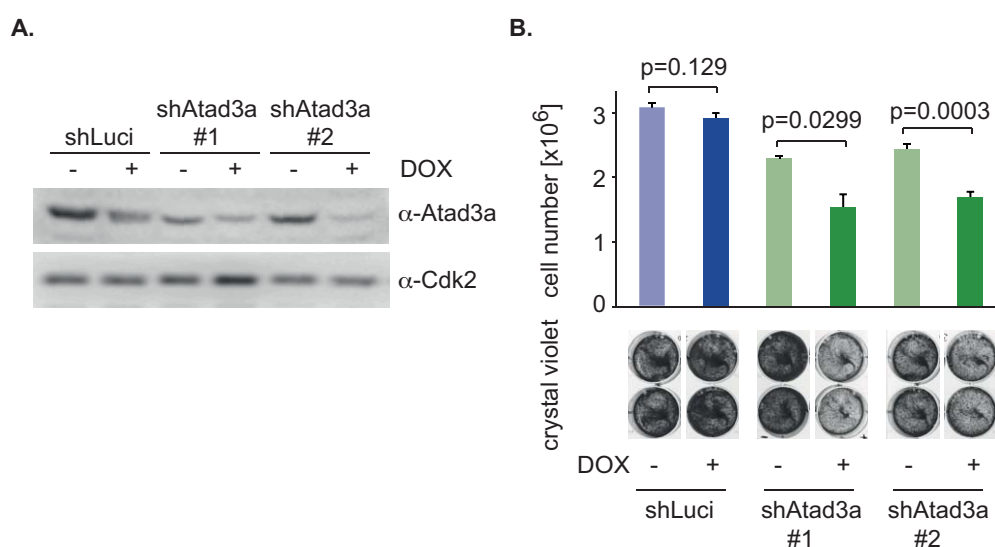

Figure 4.25: shRNA-mediated depletion of ATAD3A reduces cancer cell growth[1]
(A) Immunoblot of KPC cells expressing doxycycline-inducible shRNAs directed against Atad3a or an shRNA targeting *Renilla* luciferase as a control. Cells were treated with DOX for 48 h where indicated. Immunoblots were probed with α-Atad3a or α-CDK2 antibodies. CDK2 was used as a loading control. This experiment was performed by Dr. Anneli Gebhardt.
(B) Cell proliferation assay of KPCs expressing shRNAs as described in (B). Cells were either counted after three days of growth (cell numbers shown in upper bar graph) or stained with crystal violet after four days (lower pictures). Data is represented as mean ± SD and p-values were calculated using a paired two-tailed Student's t-test (n=3). This experiment was performed by Dr. Anneli Gebhardt.

Taken together, these results suggest that especially OmoMYC-repressed target genes are characteristic for tumor subtypes displaying high MYC expression levels in multiple entities and could thus serve as diagnostic markers. Gene expression profiles of normal proliferating cells could not be shown to overlap with OmoMYC-dependent changes in gene expression, thereby indicating a cause for the wide therapeutic window *in vivo*. A focused RNAi screen revealed that OmoMYC target genes include several candidate genes, e.g. BOP1, ADRM1 and ATAD3A, each of which could be further exploited for tumor therapy as they inhibited cancer cell growth.

5   Discussion

Expression of the MYC mutant OmoMYC causes long-term regression of several tumor entities with tolerable and reversible side effects in mouse models. It thus demonstrates that strategies inhibiting the oncogene MYC could have significant therapeutic benefits. Current concepts of MYC-targeting show either low *in vivo* efficacy or they can only be applied to a subset of tumors harboring, for example, super-enhancer-driven MYC expression (see section 1.2.4). Therefore, comprehensively understanding and subsequently mimicking OmoMYC's mode of action could translate into new strategies targeting MYC. Up to now, the biochemical features of OmoMYC remained obscure. Consequently, the aim of this thesis was to elucidate OmoMYC's structural and biochemical properties to highlight essential oncogenic features of deregulated MYC.

5.1   The OmoMYC homodimer binds E-box containing DNA with high affinity *in vitro*

Recombinant expression and native purification of OmoMYC, MAX and the b/HLH/Zip domain of MYC (see 4.1.1- 4.1.3) made it possible to perform band shift assays to compare DNA-binding affinities of the three proteins (see 4.1.4). Previous reports by Soucek and colleagues concluded that recombinant GST-tagged OmoMYC is capable of binding to E-box-containing DNA only at very high protein concentrations, but did not determine dissociation constants (K_d) (Soucek et al., 1998). In the study at hand, K_d values for the protein-DNA interaction were determined for MAX and OmoMYC homodimers as well as for MYC/MAX and OmoMYC/MYC heterodimers (Figure 4.6 - Figure 4.8). This showed that OmoMYC homodimers have the highest DNA-binding affinities; OmoMYC/MYC heterodimers bound DNA with intermediate affinities, and MAX homodimers showed the lowest affinities. Yet, even though differences between K_d values of the various dimers are statistically significant, they did not differ more than three fold, suggesting that all affinities lie within a similar nanomolar range. However, these results did not match the observation by Soucek et al., which might have been due to incomplete protein purification (Soucek et al., 1998). Bacterial DNA contaminations had to be removed by IEC during protein purification, especially with respect to MYC and OmoMYC. This purification step was not included by

Soucek et al. and could explain why the binding affinities for OmoMYC to DNA presented in this study were higher and therefore similar to MYC/MAX. Multiple other groups have reported DNA-binding affinities for MYC/MAX heterodimers and MAX homodimers generated by EMSAs or fluorescence anisotropy assays ranging from 0.01 to around 150 nM, hence differing more than 10,000 fold (Fieber et al., 2001; Guo et al., 2014a; Hu et al., 2005; Park et al., 2004). This extreme heterogeneity could be due to differences in the experimental setups, in the protein purification protocols as many laboratories use protein refolding strategies from inclusion bodies, in the amino acid sequence as full length MYC may contain N-terminal residues stabilizing the association with DNA, and the DNA sequence flanking the central E-box. The results presented in this study are comparable to the previously reported values as they largely overlap with data published by the Yang and Gross labs (Hu et al., 2005; Park et al., 2004).

The formation of OmoMYC/MAX heterodimers *in vitro* could not be conclusively determined in this study. EMSAs using combinations of OmoMYC and MAX proteins at different concentrations showed several DNA-bound entities. Even though supershift assays were performed (using antibodies recognizing OmoMYC, the OmoMYC His-tag, or MAX, respectively), it could not be ascertained which band belonged to which DNA-bound protein complex. The same difficulties were reported by Soucek and colleagues (Soucek et al., 1998). Although experimental data are lacking, it is yet likely that OmoMYC/MAX heterodimers bind DNA, given that MYC/MAX complexes associate with DNA and the DNA-binding domain was not manipulated when designing OmoMYC.

5.2 OmoMYC homodimers are highly stable and bind E-boxes in a sequence-specific manner

The purified OmoMYC protein was used for high-throughput sparse-matrix crystallization screens. Two crystal structures were obtained: one, which showed the OmoMYC homodimer in its free state (Figure 4.10), while the other one presented the protein co-crystallized with DNA (Figure 4.12). To compare these structures to one another and to previously published b/HLH/Zip structures, protein-protein interfaces of both complexes were analyzed visually (Figure 4.11; Table 7.3) and root-mean-square deviations between the main chain atoms of the superimposed structures as well as solvation free energies estimating stabilities were

calculated (Table 7.4, Table 7.5). This revealed that both OmoMYC homodimer structures display no significant differences and protein-protein interactions within the leucine zippers can be regarded as identical. Comparison of the OmoMYC structures with published b/HLH/Zip structures of MAX and MITF homodimers disclosed that all three proteins are capable of dimerization in the absence of DNA and that the basic region adopts an α-helical fold upon DNA-binding (Pogenberg et al., 2012; Sauvé et al., 2004) (Figure 4.10).

Three out of four mutations introduced into OmoMYC resulted in new interactions, as a careful analysis of all protein-protein interactions between the two OmoMYC molecules revealed. This, in combination with an unexpected strengthening of the hydrophobic core, might lead to a stabilization of the homodimer interface. Modeled OmoMYC heterodimers with MAX lacked both hydrophobic and other non-covalent interactions. Modeled OmoMYC/MYC heterodimers showed repulsive interactions in the hotspot region involving residues 76 and 77 in OmoMYC (Figure 4.10). It is therefore likely that the OmoMYC homodimer is the most stable species among various dimers.

Interestingly, a C-terminal disulfide bridge could be observed in both crystal structures. Rmsd calculations and calculations estimating solvation free energies upon binding implicated that the disulfide bridge might not deform the helical fold of the leucine zipper nor hinder assembly on DNA (Table 7.4, Table 7.5). The C-terminal cysteine, which forms the disulfide bridge, is found in c-MYC and N-MYC and most higher vertebrates down to squirrels, while neither rodents (like mice, rats or hamsters) nor fruit flies share this residue (sequence alignments were performed with Clustal Omega, data not shown). This might indicate that redox-sensitive dimerization of MYC is not required for basic cellular functions or protein stability.

A highly conserved histidine-glutamate-arginine triad in the basic region of MAX homodimers as well as MYC/MAX heterodimers mediates base-specific interactions with DNA (Ferre-D'Amare et al., 1993; Nair and Burley, 2003). This triad was not mutated when generating OmoMYC. As expected, the exact same residues mediate E-box recognition of the OmoMYC molecule (Figure 4.12).

5.3   OmoMYC homodimers are predominantly found in cells

Co-immunoprecipitations were performed with U2OS cells carrying a doxycycline-inducible MYC allele (U2OS[Tet-On]) and stably expressing HA- and FLAG-tagged OmoMYC alleles together with an HA-tagged MYC construct (see 4.1.6). They demonstrated that OmoMYC forms homodimers and heterodimers with MYC and MAX, as shown previously by the Nasi laboratory and by another study published in parallel to this work (Fiorentino et al., 2016; Savino et al., 2011).

By manipulating MYC levels in the cells and using oxidative stress, the present study was able to extend these findings. Induction of HA-MYC expression displaced MAX from binding to OmoMYC while it did not impede OmoMYC homodimerization. In addition, oxidative stimulation of U2OS[Tet-On] cells expressing the OmoMYC transgene resulted in the formation of covalently-linked OmoMYC homodimers. Disulfide-linked OmoMYC/MYC heterodimers were not detected. In addition, a stabilization of the OmoMYC protein was observed (Figure 4.13). Together with modeling studies using the OmoMYC crystal structure (see 4.1.5), the data argue that the OmoMYC homodimer is the prevalent OmoMYC complex in cells, while heterodimers are less stable.

How could oxidation of cysteine residues aid towards homodimer stability? Two mechanisms are plausible: Firstly, OmoMYC binds to DNA in a similar manner as MYC/MAX, forming a scissor- or fork-like structure (O'Neil et al., 1990; Vinson et al., 1989). The addition of a covalent interaction at the C-terminal end might freeze the structure, disabling further movement (i.e., sliding) on DNA and locking the protein at the promoter. This could impair transcriptional regulation, especially since it was shown that turnover of MYC is important for transcriptional elongation (Jaenicke et al., 2016). A "disulfide-sealed" OmoMYC protein could thereby also compete with MYC binding to DNA more effectively. Secondly, stabilization of the C-terminal end of the leucine zipper could impair protein degradation, especially when tethered at the promoter, e.g., by inhibiting the binding of ubiquitin ligases or the transport to the proteasome.

Previous studies showed that the interaction between MYC and MIZ1 is largely dependent on amino acid residues in MYC's HLH domain (Herold et al., 2002; Peukert et al., 1997). Mutation of valine 394 to aspartate strongly reduced the formation of a MYC/MIZ1 complex. In the study at hand, complex formation between OmoMYC and MIZ1 was not evaluated by

immunoprecipitations, as it was known that OmoMYC binds MIZ1 from a previous publication (Savino et al., 2011). In both OmoMYC homodimer crystal structures, V394 retained its position and was solvent-exposed. This residue should thus be available for interaction with MIZ1 in the same manner as for MYC/MAX. How complex formation with MIZ1 is manipulated if two valine residues are available in an OmoMYC homodimer or OmoMYC/MYC heterodimer remains to be determined. One could speculate that a tetrameric MIZ1/OmoMYC/(Omo)MYC/MIZ1 complex is sterically unfavorable, but the data presented by the Nasi group argued against this hypothesis (Savino et al., 2011).

5.4 Promoter invasion by elevated MYC levels is abrogated by OmoMYC expression

The *in vitro* results discussed above clearly pointed to a mode of action in which DNA-binding of OmoMYC plays a crucial role. To elucidate whether OmoMYC can bind to chromatin in cells and how OmoMYC expression affects DNA binding of MYC, global DNA binding profiles of MYC and OmoMYC were generated using ChIP-sequencing.

U2OS^{Tet-On} cells were chosen as the experimental system. These cells harbor low levels of MYC despite being tumor cells. MYC's effects on transcriptional regulation and DNA association upon doxycycline-mediated expression to supra-physiological levels have been intensely characterized in this cell line (Lorenzin et al., 2016; Walz et al., 2014). Enhanced MYC expression induces transcription programs characteristic for tumor cells by regulating a specific set of target genes. These genes are weakly bound by low, endogenous levels of the transcription factor but recruit MYC protein to their promoters when levels rise. Target genes implicated in transcription programs driving physiological growth and cell division (i.e., ribosomal protein biosynthesis) do not respond to an increase in MYC levels as promoter-close binding sites for MYC are already fully occupied (saturated). At these high-affinity sites, MYC is stabilized by protein-protein interactions, i.e., with WDR5. Promoter affinity for MYC thus confers specificity to gene regulation stratifying tumor-specific from physiological processes (Lorenzin et al., 2016; Thomas et al., 2015; Walz et al., 2014). This cellular system was therefore considered as most suitable for characterizing OmoMYC, since both tumor-specific effects and effects on normal proliferation could be studied side by side by tuning MYC levels using doxycycline.

OmoMYC was found to bind to chromatin in a similar pattern as MYC, showing a slight preference for promoters containing consensus E-boxes (Figure 4.15, (Jung et al., 2016)). This was quite unexpected since homodimers or heterodimers with MAX were predicted to be tethered to consensus E-boxes to a higher degree than MYC/MAX dimers. MYC/MAX complexes were previously shown to be guided to DNA binding sites by sequence-specific DNA interaction with E-box motifs but also by N-terminal protein-protein interactions with promoter-bound factors (see below) (Wolf et al., 2014). The equal distribution of MYC and OmoMYC binding shown in this thesis is unlikely to be due to the formation of an excessive amount of OmoMYC/MYC heterodimers, since co-IPs showed that these heterocomplexes were less stable and less abundant than homodimers in cells (Figure 4.14). One way to rationalize these findings is the suggestion that the C-terminal b/HLH/Zip domain also mediates important protein-protein interactions guiding general promoter binding of MYC. MIZ1 and p300/CBP have been shown to use this interaction surface (Herold et al., 2002; Peukert et al., 1997; Vervoorts et al., 2003). It is therefore possible that the binding of these known factors is not affected by the mutations introduced into OmoMYC. Further studies using for example mass spectrometry could clarify the impact of protein-protein interactions mediated by the C-terminal and/or other domains of MYC on chromatin association.

The present study showed that OmoMYC expression distinctively reduced MYC recruitment to low-affinity sites. These promoters were invaded when MYC protein concentrations reach supra-physiological levels (Figure 4.16 and Figure 4.17). MYC binding to high-affinity sites was – if at all – mildly affected by OmoMYC (Figure 4.16 and Figure 4.17). These results fit the results published by Lorenzin et al. as one could envision that competition of an OmoMYC dimer would be easier at binding sites, which do not harbor proteins that associate with the MYC N-terminus (Lorenzin et al., 2016). Several promoter-bound factors have recently been identified to associate with MYC boxes such as WDR5, transcriptional co-activators such as TRAPP, or pause release and elongation factors such as p-TEFb or PAF1C (see 1.2.1.1 and Figure 1.1) (Bouchard et al., 2001; Eberhardy and Farnham, 2002; Jaenicke et al., 2016; McMahon et al., 1998; Thomas et al., 2015). These, and possibly numerous other MYC-interacting promoter-bound proteins, tie MYC to high-affinity binding sites. Since OmoMYC does not encompass the MYC N-terminus, these interactions should not be possible with OmoMYC homodimers or heterodimers with MAX at high-affinity binding sites precluding effective competition. As a result, competition by OmoMYC is not uniform and more effective on low-affinity promoters. This specific targeting of MYC DNA-binding

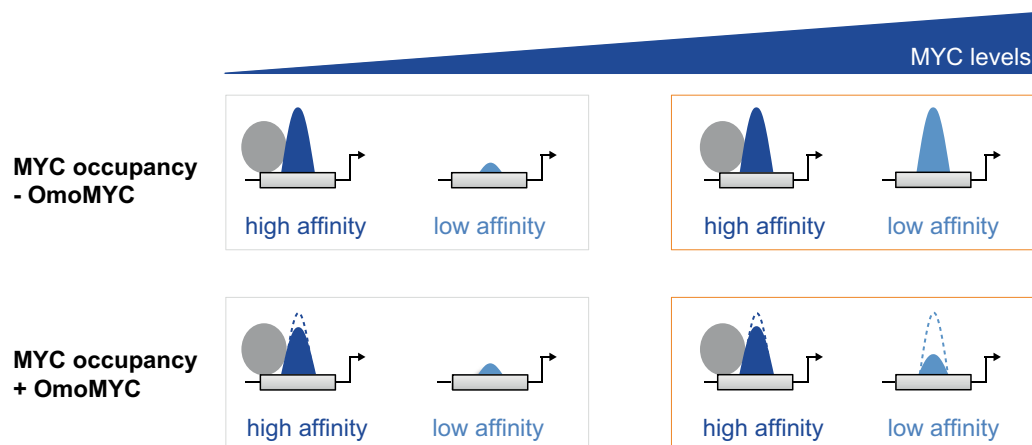could explain the selective effects on oncogenic and physiological MYC functions *in vivo* (Figure 5.1).

Figure 5.1: Proposed model showing non-uniform competition of OmoMYC with MYC binding to promoters[1]
MYC occupancy is shown as blue peaks at promoter binding sites. Two representative situations are depicted in boxes: The left set indicates a situation with low levels of MYC, while boxes to the right highlight the effects on MYC binding at elevated MYC levels without (upper panels) and with OmoMYC expression (lower panels). Grey circles represent proteins stabilizing MYC at high-affinity promoters.

5.5 OmoMYC diminishes gene regulation by oncogenic MYC enabling the identification of tumors with elevated MYC levels

Next, OmoMYC's effects on MYC-dependent transcription were characterized using RNA-sequencing. OmoMYC attenuated both activation and repression of MYC-induced target genes (Figure 4.18). Effects were again strongest on low-affinity genes (having high EC_{50} values for MYC binding), which react upon elevation of MYC levels in $U2OS^{Tet-On}$ cells. Consequently, the degree of displacement of MYC from promoters by OmoMYC correlated with the change in regulation of the respective gene (Figure 4.18). GSEA analysis underlined the dependency of OmoMYC's effects on MYC, demonstrating that known MYC-regulated gene sets were inversely regulated by OmoMYC (Figure 4.19).

From a dominant-negative protein, equal effects on activation and repression of target genes would indeed have been expected. Yet, previous publications reported that OmoMYC expression has a differential effect on MYC-dependent gene regulation, reducing activation but enhancing gene repression by MYC (Savino et al., 2011; Sodir et al., 2011; Soucek et al.,

1998; Soucek et al., 2002). This differential effect was unexpected and difficult to explain. Importantly, the studies mentioned above performed reporter assays or qPCRs on single MYC targets. Thus, they might have selected target genes that could be highly dependent on, e.g., MIZ1 binding, and could therefore show an untypical behavior. A broader analysis was performed using a microarray experiment of serum-stimulated fibroblasts; it showed that OmoMYC could both activate and repress transcription (Savino et al., 2011). Importantly, more recent studies on single target genes support the data presented in the current investigation, showing that repression was also dampened by OmoMYC (Fiorentino et al., 2016; Dan Lu, personal communication).

To strengthen the point that direct binding of OmoMYC, and thereby direct competition with MYC/MAX, is the prerequisite for the observed effects on MYC-dependent gene regulation, OmoMYC mutants were used, which harbor mutations in the amino acid residues conferring base-specific E-box recognition (OmoMYC-HE and -HER; Figure 4.20). This clearly showed that a mutated OmoMYC allele, which does not recognize E-boxes, is hampered in inhibiting MYC-dependent gene regulation. The OmoMYC mutants did not completely rescue the effect of OmoMYC, since they retained some residual non-sequence-specific DNA binding (Figure 4.20). Thus, additional studies deleting the entire basic region could be done to show that fully abrogating DNA binding would lead to a complete rescue. Regardless, global DNA-binding patterns of MYC mutants harboring the same mutations in the HER triad could be examined to discriminate sequence-specific from protein-interaction-dependent chromatin binding effects of MYC.

RNA-sequencing data generated from cultured cell lines was subsequently used to identify similarities in gene regulation in expression profiles generated from tumor patient samples (Figure 4.21; (Jung et al., 2016)). Surprisingly, the OmoMYC-dependent data set obtained in an osteosarcoma cell line recognized subgroups in several tumor entities expressing particularly high MYC or N-MYC levels. This was not a trivial result since gene expression profiles from an *in vivo* situation should include genes regulated in a non-autonomous manner including immune modulatory effects, which should not be visible in cell culture. So even without these *in vivo*-specific effects, OmoMYC regulated genes were able to stratify MYC-dependent tumor profiles.

5.6   The role of homodimers in OmoMYC's mode of action

The present study showed that OmoMYC forms stable homodimers and to a lesser extent heterodimers with MYC and MAX (see 4.1). These dimeric complexes are capable of E-box recognition and DNA binding (note that experimental data is lacking for OmoMYC/MAX). OmoMYC expression buffers transcriptional activation and repression of MYC target genes by displacing MYC/MAX and supposedly also MAX/MAX dimers from DNA.
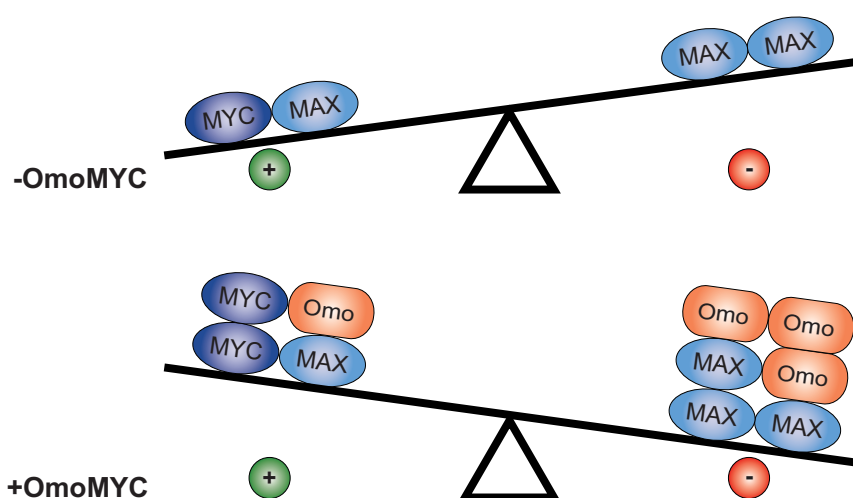

Figure 5.2: Proposed model for a shift in balance between positive and negative driving forces of transcriptional regulation upon OmoMYC expression
MYC/MAX complexes are able to stimulate transcription (+). MAX homodimers are thought to be neutral to dominant-negative regarding this effect, thus the balance in this system shifts to effects inciting transcriptional regulation (upper panel). When OmoMYC molecules (Omo) are present, various DNA-binding homo- and heterodimers are formed, shifting the balance to dampening effects (-) on transcription. Note that the relative abundance (OmoMYC/MYC heterocomplexes are not formed to the same extent as OmoMYC homodimers in cells) of the dimers is not considered in this model.

OmoMYC and MAX proteins lack a TAD. As a result, only MYC-containing complexes should be able to actively drive transcriptional regulation similar to MYC/MAX (Figure 5.2). MAX homodimers, when overexpressed, repress MYC-dependent transcription (Cogliati et al., 1993; Kretzner et al., 1992b; Lindeman et al., 1995; Montagne et al., 2012). Thus, upon OmoMYC expression, both complexes positively (OmoMYC/MYC) and negatively (OmoMYC/OmoMYC, OmoMYC/MAX) manipulating the balance are formed. As a result, MYC-dependent transcriptional regulation is buffered.

Following this model, the biological effects of OmoMYC are attenuated by the formation of OmoMYC/MYC heterodimers, which could be competent in regulating transcription in the

same manner as MYC/MAX heterodimers, assuming that MAX has the sole purpose to be a dimerization partner for MYC, enabling folding and assembly on DNA (as described by (Kretzner et al., 1992a)). This implies that the design of more potent OmoMYC alleles is possible. Improved OmoMYC proteins would be more efficient in forming homodimers. This would be conceivable by introducing four additional mutations in the leucine zipper of OmoMYC: T63I, Q76E, K81R, K83E (Figure 5.3). In this new OmoMYC variant (OmoMYC-4), the homodimer interface could be further stabilized as molecular modeling approaches would suggest that these mutations could lead to the formation of a hydrophobic interaction (at position 63), as well as several salt bridges spanning both sides of the leucine zipper. Follow up studies using OmoMYC as a transgene or therapeutic approaches exploiting the possibility of using OmoMYC as a cell penetrating peptides could especially benefit from this improved OmoMYC allele.
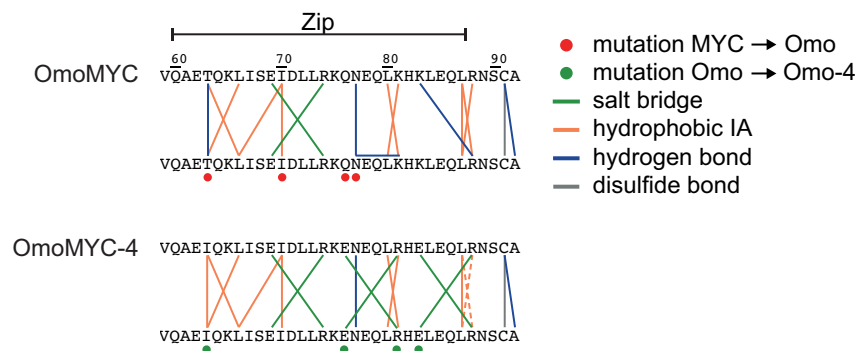
Figure 5.3: Design of a more potent OmoMYC allele (OmoMYC-4)
Direct comparison of differing interactions in the leucine zipper (Zip) of the OmoMYC homodimer (upper panel; derived from the analysis of the OmoMYC apo structure (PDB entry 5I4Z)) and the proposed new OmoMYC mutant (lower panel; OmoMYC-4). Red circles indicate mutations of OmoMYC relative to MYC; green circles represent mutations from OmoMYC to OmoMYC-4 (Omo-4). Each line represents an interaction. Salt bridges are shown in green, hydrophobic interactions (IA) in orange, hydrogen bonds in blue and disulfide bonds in grey.

5.7 Individual OmoMYC target genes drive tumor cell growth

Gene set enrichment analysis did not recognize a certain cellular process that was specifically affected by OmoMYC treatment and thus particularly dependent on deregulated MYC expression. We therefore aimed to identify druggable OmoMYC-regulated proteins that influence tumor growth in MYC-driven tumors using a targeted shRNA screen. A KRAS-driven pancreatic adenocarcinoma cell line (KPC) was selected that strongly responded to

OmoMYC expression with a reduction in proliferation (Jung et al., 2016). Pancreatic cancers currently show a 5-year survival rate of only 7 % and therefore represent a tumor subtype that is particularly challenging to treat (Siegel et al., 2015). Interestingly, these cells do not undergo apoptosis upon OmoMYC induction, but instead show reduced BrdU incorporation, which is indicative of decelerated cell cycle progression (Anneli Gebhardt, personal communication).

The screen was initially designed to identify synergistic effects of shRNA-mediated knockdown together with partial small molecule-mediated inhibition (inhibitor concentration at IC_{20}) of four different OmoMYC target genes. These inhibitors were directed against amino acid transporters (SLC1A5 and SLC7A5); POLRMT, a rate-limiting RNA polymerase enzyme controlling mitochondrial translation; and polyamine metabolism (D'Andrea et al., 2016; Falkenberg et al., 2002; Nicklin et al., 2009; Nilsson et al., 2005). Unfortunately, no significant combinatory effect on cell growth was observed (data not shown). Nutrient- and oxygen-rich tissue culture conditions might explain why these metabolic perturbations did not score in the screen even though they represented valid therapeutic targets for MYC-driven cancer therapy (Dang, 2011).

This work thus focused on effects of single shRNAs in the targeted screen and identified three significant hits (Figure 4.22). BOP1, a known MYC target important for ribosomal biogenesis coordinating cell growth and division, ADRM1 (also referred to as RPN13), a proteasomal ubiquitin receptor, and ATAD3A, a protein controlling mitochondrial dynamics and its connection to the endoplasmic reticulum (ER), were identified in the screen (Chiang et al., 2012; Gilquin et al., 2010; Holzel et al., 2005; Husnjak et al., 2008; Rohrmoser et al., 2007; Schlosser et al., 2003).

Even though mitochondrial transport and metabolism, protein biosynthesis and turnover represent essential functions for non-transformed cell growth and proliferation, a dependence of MYC-driven tumors on these processes was seen (Barna et al., 2008; Ruggero, 2013). A proof of principle that key proteins of essential MYC-driven processes display exploitable therapeutic windows came from studies of PRPS2 (phosphoribosyl-pyrophosphate synthetase 2), a rate-limiting enzyme for nucleotide biosynthesis (Cunningham et al., 2014). MYC is known to globally regulate purine and pyrimidine biosynthesis, yet deregulation of PRPS2 alone can promote enhanced nucleotide biosynthesis (Cunningham et al., 2014; Liu et al.,

2008). This evinces the possibility to locate these rate-limiting proteins and subsequently exploit these vulnerabilities for therapeutic approaches.

Therapeutic targeting of ribosomal synthesis and assembly, using RNA Polymerase I inhibitors, as well as ADRM1, using the small molecule inhibitor RA 190, are indeed currently investigated for cancer treatment (see 1.2.4) (Anchoori et al., 2013; Bywater et al., 2012). Importantly, gene expression of all three hits is enhanced in various tumor entities and correlates with MYC expression and poor clinical prognosis (Chung et al., 2011; Fang et al., 2010; Jung et al., 2016; Killian et al., 2006; You et al., 2013). Therefore, this study focused on finding tumor cell-specific dependencies on ATAD3A, which has been studied to a lesser extent.

ATAD3A, the most significant hit emerging from the RNAi screen, has not been in the focus of cancer drug development so far. It is a nuclear-encoded mitochondrial protein connecting the mitochondrial inner and outer membrane. It regulates mitochondrial fusion and fission, and functions in the network between mitochondria and ER (Gilquin et al., 2010; Hoffmann et al., 2009). ATAD3A is amplified in various cancer entities (Chen et al., 2011; Fang et al., 2010; You et al., 2013). Interestingly, several recent publications identified the ER-mitochondria calcium flux as a new hallmark of cancer, and ATAD3A is newly emerging as a cancer-specific regulatory protein (Cardenas et al., 2016; Raturi et al., 2016; Teng et al., 2016). A study published in parallel to the study at hand also indicates that OmoMYC has a role in regulating mitochondrial morphology especially after hypoxic stimulation (Mongiardi et al., 2016). The present study, and the related publication, demonstrated for the first time that cells with elevated MYC levels show an enhanced dependence on ATAD3A (Jung et al., 2016). This suggests that inhibiting ATAD3A will represent a novel strategy to target MYC-driven cancers.

5.8 Translating knowledge about OmoMYC's mode of action into therapeutic concepts

In this thesis, the mode of action of the MYC mutant OmoMYC was deciphered on a structural and molecular basis and critical druggable targets influencing tumor cell growth were identified. How can we translate this knowledge into new therapeutic concepts targeting the oncoprotein MYC? I propose two distinct approaches to mimic OmoMYC's functions:

first, to target DNA binding of MYC, and second to explore combinatory inhibition of OmoMYC target genes.

The crystallographic, RNA-sequencing and ChIP-sequencing results presented in this work clearly highlighted that OmoMYC's molecular mechanism involves direct competition with MYC/MAX complexes on chromatin. Thus, inhibiting DNA binding of the MYC/MAX complex should be possible using different tools. The simplest approach to proceed into clinical application would be the use of the OmoMYC protein itself. The Soucek laboratory is currently testing cell-penetrating peptides (CPP) encompassing the entire OmoMYC amino acid sequence without addition of further tags *in vivo* (Laura Soucek, personal communication). Another suggestion could be to study CPPs spanning only the b/HLH domain of OmoMYC, as this region would be sufficient for DNA-binding. Several challenges in developing such therapeutic biologics have been described: poor stability in the blood, low bioavailability due to enzymatic degradation, nonspecific delivery to normal tissue, and poor cell permeability are just a few examples (Raucher and Ryu, 2015). This implies that further improvements are needed to bring strategies involving CPP closer to the clinic.

The Fletcher laboratory reported the design of a small molecule compound that abrogates DNA association of the MYC/MAX dimer. This study was published in parallel to the instant study. An α-helix mimetic, termed 4da, was designed to bind to the folded coiled-coil structure of the b/HLH domain and thus prohibits DNA binding (Jung et al., 2015). In contrast, the previously published 10058-F4 compound bound to the unfolded MYC protein and prevented MYC/MYC dimerization (Fletcher and Prochownik, 2015). 4da was also tested in cell-based assays. It inhibited MYC-dependent activation of a luciferase reporter and reduces cell growth promoting cell cycle arrest with a low-micromolar IC_{50}. Importantly, no selectivity for MYC-overexpressing cells was observed. It is tempting to hypothesize that this might be due to a general targeting of MYC's DNA-binding ability both at low-affinity and high-affinity binding sites. New approaches should therefore focus on finding characteristics of low-affinity target genes both regarding the DNA binding motif at this site and site-specific interacting proteins of MYC/MAX and use this information to generate low-affinity site specific inhibitors for MYC/MAX.

Importantly, this study also implied that further improvement of direct MYC/MAX inhibitors may not lead to clinical success, since a general inhibition of the association between MYC

and MAX proteins will both affect tumor-specific processes and cause dramatic side-effects on normal tissue.

The study at hand identified several rate-limiting proteins of essential processes dependent on elevated MYC levels. Clearly, OmoMYC-regulated genes harbor new therapeutic targets for MYC-driven tumors. Yet, in this study, *in vitro*-OmoMYC-regulated genes were selected for the focused RNAi screen. To explore dependencies on *in vivo*-regulated genes, the shRNA screen will need to be repeated after having identified druggable targets of OmoMYC in tumor mouse models expressing the transgene. Alternatively to a second screen using shRNAs or the CRISPR-Cas9 system, one could directly take a limited set of OmoMYC target genes and perform high-throughput combinatorial screens using clinically validated small molecule inhibitors. This could firstly open the possibility to directly screen for effects on MYC-driven or N-MYC amplified tumor cell lines vs. non-amplified or untransformed cells. Secondly, this could give the opportunity to directly find synergistically acting inhibitors minimizing the emergence of resistances, adverse events and toxicities, thus maximizing efficacy of the targeted therapy in the clinic (Sun et al., 2013). Especially the combination of genetic and pharmacological with computational approaches has proven successful for the identification of novel synergistic combinations for cancer therapy (Baranello et al., 2016; Floc'h et al., 2012; Kwong et al., 2012).

Collectively, the data suggest that OmoMYC inhibits cellular processes dependent on oncogenic MYC levels using a DNA-competitive mechanism. OmoMYC is an excellent tool to identify rate-limiting proteins promoting tumor cell growth in a MYC-dependent manner that can be targeted for tumor therapy.

6 Bibliography

Adams, J.M., Harris, A.W., Pinkert, C.A., Corcoran, L.M., Alexander, W.S., Cory, S., Palmiter, R.D., and Brinster, R.L. (1985). The c-myc oncogene driven by immunoglobulin enhancers induces lymphoid malignancy in transgenic mice. Nature *318*, 533-538.

Adams, P.D., Afonine, P.V., Bunkoczi, G., Chen, V.B., Davis, I.W., Echols, N., Headd, J.J., Hung, L.W., Kapral, G.J., Grosse-Kunstleve, R.W.*, et al.* (2010). PHENIX: a comprehensive Python-based system for macromolecular structure solution. Acta crystallographica Section D, Biological crystallography *66*, 213-221.

Albihn, A., Johnsen, J.I., and Henriksson, M.A. (2010). MYC in Oncogenesis and as a Target for Cancer Therapies. Advances in Cancer Research, Vol 107 *107*, 163-224.

Amati, B., Brooks, M.W., Levy, N., Littlewood, T.D., Evan, G.I., and Land, H. (1993). Oncogenic activity of the c-Myc protein requires dimerization with Max. Cell *72*, 233-245.

Amati, B., Dalton, S., Brooks, M.W., Littlewood, T.D., Evan, G.I., and Land, H. (1992). Transcriptional activation by the human c-Myc oncoprotein in yeast requires interaction with Max. Nature *359*, 423-426.

Anchoori, R.K., Karanam, B., Peng, S., Wang, J.W., Jiang, R., Tanno, T., Orlowski, R.Z., Matsui, W., Zhao, M., Rudek, M.A.*, et al.* (2013). A bis-Benzylidine Piperidone Targeting Proteasome Ubiquitin Receptor RPN13/ADRM1 as a Therapy for Cancer. Cancer Cell *24*, 791-805.

Angela, N., Carafa, V., Conte, M., Tambaro, F.P., Abbondanza, C., Martens, J.H., Nees, M., Benedetti, R., Pallavicini, I., Minucci, S.*, et al.* (2016). c-Myc modulation & acetylation is a key HDAC inhibitor target in cancer. Clin Cancer Res.

Annibali, D., Whitfield, J.R., Favuzzi, E., Jauset, T., Serrano, E., Cuartas, I., Redondo-Campos, S., Folch, G., Gonzàlez-Juncà, A., Sodir, N.M.*, et al.* (2014). Myc inhibition is effective against glioma and reveals a role for Myc in proficient mitosis. Nature Communications *5*, 4632.

Arabi, A., Wu, S., Ridderstrale, K., Bierhoff, H., Shiue, C., Fatyol, K., Fahlen, S., Hydbring, P., Soderberg, O., Grummt, I.*, et al.* (2005). c-Myc associates with ribosomal DNA and activates RNA polymerase I transcription. Nat Cell Biol *7*, 303-310.

Arkin, M.R., Tang, Y., and Wells, J.A. (2014). Small-molecule inhibitors of protein-protein interactions: progressing toward the reality. Chem Biol *21*, 1102-1114.

Bailey, T.L., Boden, M., Buske, F.A., Frith, M., Grant, C.E., Clementi, L., Ren, J., Li, W.W., and Noble, W.S. (2009). MEME SUITE: tools for motif discovery and searching. Nucleic acids research *37*, W202-208.

Baranello, L., Wojtowicz, D., Cui, K., Devaiah, B.N., Chung, H.J., Chan-Salis, K.Y., Guha, R., Wilson, K., Zhang, X., Zhang, H.*, et al.* (2016). RNA Polymerase II Regulates Topoisomerase 1 Activity to Favor Efficient Transcription. Cell *165*, 357-371.

Barna, M., Pusic, A., Zollo, O., Costa, M., Kondrashov, N., Rego, E., Rao, P.H., and Ruggero, D. (2008). Suppression of Myc oncogenic activity by ribosomal protein haploinsufficiency. Nature *456*, 971-975.

Beltran, H. (2014). The N-myc Oncogene: Maximizing its Targets, Regulation, and Therapeutic Potential. Mol Cancer Res *12*, 815-822.

Beltran, H., Rickman, D.S., Park, K., Chae, S.S., Sboner, A., MacDonald, T.Y., Wang, Y., Sheikh, K.L., Terry, S., Tagawa, S.T.*, et al.* (2011). Molecular characterization of neuroendocrine prostate cancer and identification of new drug targets. Cancer Discov *1*, 487-495.

Ben-Porath, I., Thomson, M.W., Carey, V.J., Ge, R., Bell, G.W., Regev, A., and Weinberg, R.A. (2008). An embryonic stem cell-like gene expression signature in poorly differentiated aggressive human tumors. Nat Genet *40*, 499-507.

Berg, T., Cohen, S.B., Desharnais, J., Sonderegger, C., Maslyar, D.J., Goldberg, J., Boger, D.L., and Vogt, P.K. (2002). Small-molecule antagonists of Myc/Max dimerization inhibit Myc-induced transformation of chicken embryo fibroblasts. Proceedings of the National Academy of Sciences of the United States of America *99*, 3830-3835.

Blackwell, T.K., Kretzner, L., Blackwood, E.M., Eisenman, R.N., and Weintraub, H. (1990). Sequence-specific DNA binding by the c-Myc protein. Science *250*, 1149-1151.

Blackwood, E.M., and Eisenman, R.N. (1991). Max: a helix-loop-helix zipper protein that forms a sequence-specific DNA-binding complex with Myc. Science *251*, 1211-1217.

Blackwood, E.M., Lugo, T.G., Kretzner, L., King, M.W., Street, A.J., Witte, O.N., and Eisenman, R.N. (1994). Functional analysis of the AUG- and CUG-initiated forms of the c-Myc protein. Mol Biol Cell *5*, 597-609.

Blankenberg, D., Von Kuster, G., Coraor, N., Ananda, G., Lazarus, R., Mangan, M., Nekrutenko, A., and Taylor, J. (2010). Galaxy: a web-based genome analysis tool for experimentalists. Curr Protoc Mol Biol *Chapter 19*, Unit 19 10 11-21.

Blow, D.M. (2002). Outline of crystallography for biologists (Oxford ; New York: Oxford University Press).

Bochman, M.L., Paeschke, K., and Zakian, V.A. (2012). DNA secondary structures: stability and function of G-quadruplex structures. Nat Rev Genet *13*, 770-780.

Bouchard, C., Dittrich, O., Kiermaier, A., Dohmann, K., Menkel, A., Eilers, M., and Lüscher, B. (2001). Regulation of cyclin D2 gene expression by the Myc/Max/Mad network: Myc-dependent TRRAP recruitment and histone acetylation at the cyclin D2 promoter. Genes & Development *15*, 2042-2047.

Bouchard, C., Marquardt, J., Brás, A., Medema, R.H., and Eilers, M. (2004). Myc-induced proliferation and transformation require Akt-mediated phosphorylation of FoxO proteins. Embo J *23*, 2830-2840.

Bowers, E.M., Yan, G., Mukherjee, C., Orry, A., Wang, L., Holbert, M.A., Crump, N.T., Hazzalin, C.A., Liszczak, G., Yuan, H.*, et al.* (2010). Virtual ligand screening of the p300/CBP histone acetyltransferase: identification of a selective small molecule inhibitor. Chem Biol *17*, 471-482.

Bradford, M.M. (1976). A rapid and sensitive method for the quantitation of microgram quantities of protein utilizing the principle of protein-dye binding. Anal Biochem *72*, 248-254.

Brenner, C., Deplus, R., Didelot, C., Loriot, A., Vire, E., De Smet, C., Gutierrez, A., Danovi, D., Bernard, D., Boon, T.*, et al.* (2005). Myc represses transcription through recruitment of DNA methyltransferase corepressor. Embo J *24*, 336-346.

Brockmann, M., Poon, E., Berry, T., Carstensen, A., Deubzer, H.E., Rycak, L., Jamin, Y., Thway, K., Robinson, S.P., Roels, F.*, et al.* (2013). Small Molecule Inhibitors of Aurora-A Induce Proteasomal Degradation of N-Myc in Childhood Neuroblastoma. Cancer Cell, 1-15.

Brown, R.V., Danford, F.L., Gokhale, V., Hurley, L.H., and Brooks, T.A. (2011). Demonstration that drug-targeted down-regulation of MYC in non-Hodgkins lymphoma is directly mediated through the promoter G-quadruplex. J Biol Chem *286*, 41018-41027.

Brunger, A.T. (1992). Free R-Value - a Novel Statistical Quantity for Assessing the Accuracy of Crystal-Structures. Nature *355*, 472-475.

Buratowski, S. (2009). Progression through the RNA polymerase II CTD cycle. Molecular cell *36*, 541-546.

Bywater, M.J., Poortinga, G., Sanij, E., Hein, N., Peck, A., Cullinane, C., Wall, M., Cluse, L., Drygin, D., Anderes, K.*, et al.* (2012). Inhibition of RNA polymerase I as a therapeutic strategy to promote cancer-specific activation of p53. Cancer Cell *22*, 51-65.

Cardenas, C., Muller, M., McNeal, A., Lovy, A., Jana, F., Bustos, G., Urra, F., Smith, N., Molgo, J., Diehl, J.A.*, et al.* (2016). Selective Vulnerability of Cancer Cells by Inhibition of Ca(2+) Transfer from Endoplasmic Reticulum to Mitochondria. Cell Rep *14*, 2313-2324.

Chayen, N.E., and Saridakis, E. (2008). Protein crystallization: from purified protein to diffraction-quality crystal. Nat Meth *5*, 147-153.

Chen, L.S., Redkar, S., Bearss, D., Wierda, W.G., and Gandhi, V. (2009). Pim kinase inhibitor, SGI-1776, induces apoptosis in chronic lymphocytic leukemia cells. Blood *114*, 4150-4157.

Chen, R., Keating, M.J., Gandhi, V., and Plunkett, W. (2005). Transcription inhibition by flavopiridol: mechanism of chronic lymphocytic leukemia cell death. Blood *106*, 2513-2519.

Chen, T.C., Hung, Y.C., Lin, T.Y., Chang, H.W., Chiang, I.P., Chen, Y.Y., and Chow, K.C. (2011). Human papillomavirus infection and expression of ATPase family AAA domain containing 3A, a novel anti-autophagy factor, in uterine cervical cancer. Int J Mol Med *28*, 689-696.

Chen, V.B., Arendall, W.B., 3rd, Headd, J.J., Keedy, D.A., Immormino, R.M., Kapral, G.J., Murray, L.W., Richardson, J.S., and Richardson, D.C. (2010). MolProbity: all-atom structure validation for macromolecular crystallography. Acta crystallographica Section D, Biological crystallography *66*, 12-21.

Chen, X., Xu, H., Yuan, P., Fang, F., Huss, M., Vega, V.B., Wong, E., Orlov, Y.L., Zhang, W., Jiang, J.*, et al.* (2008). Integration of external signaling pathways with the core transcriptional network in embryonic stem cells. Cell *133*, 1106-1117.

Cheng, S.W., Davies, K.P., Yung, E., Beltran, R.J., Yu, J., and Kalpana, G.V. (1999). c-MYC interacts with INI1/hSNF5 and requires the SWI/SNF complex for transactivation function. Nat Genet *22*, 102-105.

Cheng, Z., Gong, Y., Ma, Y., Lu, K., Lu, X., Pierce, L.A., Thompson, R.C., Muller, S., Knapp, S., and Wang, J. (2013). Inhibition of BET bromodomain targets genetically diverse glioblastoma. Clin Cancer Res *19*, 1748-1759.

Cheung, A.C., and Cramer, P. (2012). A movie of RNA polymerase II transcription. Cell *149*, 1431-1437.

Chiang, S.F., Huang, C.Y., Lin, T.Y., Chiou, S.H., and Chow, K.C. (2012). An alternative import pathway of AIF to the mitochondria. Int J Mol Med *29*, 365-372.

Chipumuro, E., Marco, E., Christensen, C.L., Kwiatkowski, N., Zhang, T., Hatheway, C.M., Abraham, B.J., Sharma, B., Yeung, C., Altabef, A.*, et al.* (2014). CDK7 inhibition suppresses super-enhancer-linked oncogenic transcription in MYCN-driven cancer. Cell *159*, 1126-1139.

Chou, T.C., and Talalay, P. (1984). Quantitative analysis of dose-effect relationships: the combined effects of multiple drugs or enzyme inhibitors. Advances in enzyme regulation *22*, 27-55.

Christensen, D.J., Chen, Y., Oddo, J., Matta, K.M., Neil, J., Davis, E.D., Volkheimer, A.D., Lanasa, M.C., Friedman, D.R., Goodman, B.K.*, et al.* (2011). SET oncoprotein overexpression in B-cell chronic lymphocytic leukemia and non-Hodgkin lymphoma: a predictor of aggressive disease and a new treatment target. Blood *118*, 4150-4158.

Chung, K.Y., Cheng, I.K., Ching, A.K., Chu, J.H., Lai, P.B., and Wong, N. (2011). Block of proliferation 1 (BOP1) plays an oncogenic role in hepatocellular carcinoma by promoting epithelial-to-mesenchymal transition. Hepatology *54*, 307-318.

Clackson, T., and Wells, J.A. (1995). A hot spot of binding energy in a hormone-receptor interface. Science *267*, 383-386.

Clausen, D.M., Guo, J., Parise, R.A., Beumer, J.H., Egorin, M.J., Lazo, J.S., Prochownik, E.V., and Eiseman, J.L. (2010). In Vitro Cytotoxicity and In Vivo Efficacy, Pharmacokinetics, and Metabolism of 10074-G5, a Novel Small-Molecule Inhibitor of c-Myc/Max Dimerization. Journal of Pharmacology and Experimental Therapeutics *335*, 715-727.

Cogliati, T., Dunn, B.K., Bar-Ner, M., Cultraro, C.M., and Segal, S. (1993). Transfected wild-type and mutant max regulate cell growth and differentiation of murine erythroleukemia cells. Oncogene *8*, 1263-1268.

Cole, M.D., and Cowling, V.H. (2008). Transcription-independent functions of MYC: regulation of translation and DNA replication. Nat Rev Mol Cell Biol *9*, 810-815.

Conacci-Sorrell, M., McFerrin, L., and Eisenman, R.N. (2014). An overview of MYC and its interactome. Cold Spring Harb Perspect Med *4*, a014357.

Conacci-Sorrell, M., Ngouenet, C., and Eisenman, R.N. (2010). Myc-nick: a cytoplasmic cleavage product of Myc that promotes alpha-tubulin acetylation and cell differentiation. Cell *142*, 480-493.

Cuchillo, R., and Michel, J. (2012). Mechanisms of small-molecule binding to intrinsically disordered proteins. Biochem Soc Trans *40*, 1004-1008.

Cunningham, J.T., Moreno, M.V., Lodi, A., Ronen, S.M., and Ruggero, D. (2014). Protein and Nucleotide Biosynthesis Are Coupled by a Single Rate-Limiting Enzyme, PRPS2, to Drive Cancer. Cell *157*, 1088-1103.

D'Andrea, A., Gritti, I., Nicoli, P., Giorgio, M., Doni, M., Conti, A., Bianchi, V., Casoli, L., Sabo, A., Mironov, A.*, et al.* (2016). The mitochondrial translation machinery as a therapeutic target in Myc-driven lymphomas. Oncotarget.

Danciu, T.E., and Whitman, M. (2010). Oxidative stress drives disulfide bond formation between basic helix-loop-helix transcription factors. Journal of cellular biochemistry *109*, 417-424.

Dang, C.V. (2011). Therapeutic targeting of Myc-reprogrammed cancer cell metabolism. Cold Spring Harb Symp Quant Biol *76*, 369-374.

Dang, C.V. (2012). MYC on the path to cancer. Cell *149*, 22-35.

Dang, C.V., Barrett, J., Villa-Garcia, M., Resar, L.M., Kato, G.J., and Fearon, E.R. (1991). Intracellular leucine zipper interactions suggest c-Myc hetero-oligomerization. Mol Cell Biol *11*, 954-962.

Dang, C.V., and Lee, W.M. (1988). Identification of the human c-myc protein nuclear translocation signal. Mol Cell Biol *8*, 4048-4054.

Darnell, J.E., Jr. (2002). Transcription factors as targets for cancer therapy. Nat Rev Cancer *2*, 740-749.

Dauch, D., Rudalska, R., Cossa, G., Nault, J.C., Kang, T.W., Wuestefeld, T., Hohmeyer, A., Imbeaud, S., Yevsa, T., Hoenicke, L.*, et al.* (2016). A MYC-aurora kinase A protein complex represents an actionable drug target in p53-altered liver cancer. Nat Med.

Davis, A.C., Wims, M., Spotts, G.D., Hann, S.R., and Bradley, A. (1993). A null c-myc mutation causes lethality before 10.5 days of gestation in homozygotes and reduced fertility in heterozygous female mice. Genes Dev *7*, 671-682.

Dawson, M.A., Prinjha, R.K., Dittmann, A., Giotopoulos, G., Bantscheff, M., Chan, W.I., Robson, S.C., Chung, C.W., Hopf, C., Savitski, M.M.*, et al.* (2011). Inhibition of BET recruitment to chromatin as an effective treatment for MLL-fusion leukaemia. Nature *478*, 529-533.

Del Poeta, G., Postorino, M., Pupo, L., Del Principe, M.I., Dal Bo, M., Bittolo, T., Buccisano, F., Mariotti, B., Iannella, E., Maurillo, L.*, et al.* (2016). Venetoclax: Bcl-2 inhibition for the treatment of chronic lymphocytic leukemia. Drugs Today (Barc) *52*, 249-260.

Delaunay, A., Isnard, A.D., and Toledano, M.B. (2000). H2O2 sensing through oxidation of the Yap1 transcription factor. Embo J *19*, 5157-5166.

Delmore, J.E., Issa, G.C., Lemieux, M.E., Rahl, P.B., Shi, J., Jacobs, H.M., Kastritis, E., Gilpatrick, T., Paranal, R.M., Qi, J.*, et al.* (2011). BET bromodomain inhibition as a therapeutic strategy to target c-Myc. Cell *146*, 904-917.

Dey, A., Ellenberg, J., Farina, A., Coleman, A.E., Maruyama, T., Sciortino, S., Lippincott-Schwartz, J., and Ozato, K. (2000). A bromodomain protein, MCAP, associates with mitotic chromosomes and affects G(2)-to-M transition. Mol Cell Biol *20*, 6537-6549.

Diederichs, K., and Karplus, P.A. (1997). Improved R-factors for diffraction data analysis in macromolecular crystallography. Nat Struct Biol *4*, 269-275.

Diefenbacher, M.E., Popov, N., Blake, S.M., Schülein-Völk, C., Nye, E., Spencer-Dene, B., Jaenicke, L.A., Eilers, M., and Behrens, A. (2014). The deubiquitinase USP28 controls intestinal homeostasis and promotes colorectal cancer. J Clin Invest.

Druker, B.J. (2002). Inhibition of the Bcr-Abl tyrosine kinase as a therapeutic strategy for CML. Oncogene *21*, 8541-8546.

Druker, B.J., Guilhot, F., O'Brien, S.G., Gathmann, I., Kantarjian, H., Gattermann, N., Deininger, M.W., Silver, R.T., Goldman, J.M., Stone, R.M.*, et al.* (2006). Five-year follow-up of patients receiving imatinib for chronic myeloid leukemia. N Engl J Med *355*, 2408-2417.

Drygin, D., Lin, A., Bliesath, J., Ho, C.B., O'Brien, S.E., Proffitt, C., Omori, M., Haddach, M., Schwaebe, M.K., Siddiqui-Jain, A., *et al.* (2011). Targeting RNA polymerase I with an oral small molecule CX-5461 inhibits ribosomal RNA synthesis and solid tumor growth. Cancer Res *71*, 1418-1430.

Dubois, N.C., Adolphe, C., Ehninger, A., Wang, R.A., Robertson, E.J., and Trumpp, A. (2008). Placental rescue reveals a sole requirement for c-Myc in embryonic erythroblast survival and hematopoietic stem cell function. Development *135*, 2455-2465.

DuBois, S.G., Marachelian, A., Fox, E., Kudgus, R.A., Reid, J.M., Groshen, S., Malvar, J., Bagatell, R., Wagner, L., Maris, J.M., *et al.* (2016). Phase I Study of the Aurora A Kinase Inhibitor Alisertib in Combination With Irinotecan and Temozolomide for Patients With Relapsed or Refractory Neuroblastoma: A NANT (New Approaches to Neuroblastoma Therapy) Trial. J Clin Oncol *34*, 1368-1375.

Durinck, S., Spellman, P.T., Birney, E., and Huber, W. (2009). Mapping identifiers for the integration of genomic datasets with the R/Bioconductor package biomaRt. Nat Protoc *4*, 1184-1191.

Eberhardy, S.R., and Farnham, P.J. (2002). Myc recruits P-TEFb to mediate the final step in the transcriptional activation of the cad promoter. J Biol Chem *277*, 40156-40162.

Edgar, R., Domrachev, M., and Lash, A.E. (2002). Gene Expression Omnibus: NCBI gene expression and hybridization array data repository. Nucleic acids research *30*, 207-210.

Eilers, M. (2016). Personal communication.

Emsley, P., and Cowtan, K. (2004). Coot: model-building tools for molecular graphics. Acta crystallographica Section D, Biological crystallography *60*, 2126-2132.

Emsley, P., Lohkamp, B., Scott, W.G., and Cowtan, K. (2010). Features and development of Coot. Acta crystallographica Section D, Biological crystallography *66*, 486-501.

Ericsson, U.B., Hallberg, B.M., DeTitta, G.T., Dekker, N., and Nordlund, P. (2006). Thermofluor-based high-throughput stability optimization of proteins for structural studies. Anal Biochem *357*, 289-298.

Evans, P.R. (2011). An introduction to data reduction: space-group determination, scaling and intensity statistics. Acta crystallographica Section D, Biological crystallography *67*, 282-292.

Falkenberg, M., Gaspari, M., Rantanen, A., Trifunovic, A., Larsson, N.G., and Gustafsson, C.M. (2002). Mitochondrial transcription factors B1 and B2 activate transcription of human mtDNA. Nat Genet *31*, 289-294.

Fang, H.Y., Chang, C.L., Hsu, S.H., Huang, C.Y., Chiang, S.F., Chiou, S.H., Huang, C.H., Hsiao, Y.T., Lin, T.Y., Chiang, I.P., *et al.* (2010). ATPase family AAA domain-containing 3A is a novel anti-apoptotic factor in lung adenocarcinoma cells. J Cell Sci *123*, 1171-1180.

Farina, A., Faiola, F., and Martinez, E. (2004). Reconstitution of an E box-binding Myc:Max complex with recombinant full-length proteins expressed in Escherichia coli. Protein Expr Purif *34*, 215-222.

Farrell, A.S., and Sears, R.C. (2014). MYC degradation. Cold Spring Harb Perspect Med *4*, a014365-a014365.

Fellmann, C., Zuber, J., McJunkin, K., Chang, K., Malone, C.D., Dickins, R.A., Xu, Q., Hengartner, M.O., Elledge, S.J., Hannon, G.J.*, et al.* (2011). Functional identification of optimized RNAi triggers using a massively parallel sensor assay. Molecular cell *41*, 733-746.

Felsher, D.W. (2010). MYC Inactivation Elicits Oncogene Addiction through Both Tumor Cell-Intrinsic and Host-Dependent Mechanisms. Genes Cancer *1*, 597-604.

Felsher, D.W., and Bishop, J.M. (1999). Reversible tumorigenesis by MYC in hematopoietic lineages. Molecular cell *4*, 199-207.

Fernandez, P.C., Frank, S.R., Wang, L., Schroeder, M., Liu, S., Greene, J., Cocito, A., and Amati, B. (2003). Genomic targets of the human c-Myc protein. Genes Dev *17*, 1115-1129.

Ferre-D'Amare, A.R., Prendergast, G.C., Ziff, E.B., and Burley, S.K. (1993). Recognition by Max of its cognate DNA through a dimeric b/HLH/Z domain. Nature *363*, 38-45.

Fieber, W., Schneider, M.L., Matt, T., Kräutler, B., Konrat, R., and Bister, K. (2001). Structure, function, and dynamics of the dimerization and DNA-binding domain of oncogenic transcription factor v-Myc. J Mol Biol *307*, 1395-1410.

Filippakopoulos, P., and Knapp, S. (2014). Targeting bromodomains: epigenetic readers of lysine acetylation. Nat Rev Drug Discov *13*, 337-356.

Filippakopoulos, P., Qi, J., Picaud, S., Shen, Y., Smith, W.B., Fedorov, O., Morse, E.M., Keates, T., Hickman, T.T., Felletar, I.*, et al.* (2010). Selective inhibition of BET bromodomains. Nature *468*, 1067-1073.

Fiorentino, F.P., Tokgun, E., Sole-Sanchez, S., Giampaolo, S., Tokgun, O., Jauset, T., Kohno, T., Perucho, M., Soucek, L., and Yokota, J. (2016). Growth suppression by MYC inhibition in small cell lung cancer cells with TP53 and RB1 inactivation. Oncotarget.

Fletcher, S., and Prochownik, E.V. (2015). Small-molecule inhibitors of the Myc oncoprotein. Biochim Biophys Acta *1849*, 525-543.

Floc'h, N., Kinkade, C.W., Kobayashi, T., Aytes, A., Lefebvre, C., Mitrofanova, A., Cardiff, R.D., Califano, A., Shen, M.M., and Abate-Shen, C. (2012). Dual targeting of the Akt/mTOR signaling pathway inhibits castration-resistant prostate cancer in a genetically engineered mouse model. Cancer Res *72*, 4483-4493.

Flores, I., Murphy, D.J., Swigart, L.B., Knies, U., and Evan, G.I. (2004). Defining the temporal requirements for Myc in the progression and maintenance of skin neoplasia. Oncogene *23*, 5923-5930.

Frank, S.R., Parisi, T., Taubert, S., Fernandez, P., Fuchs, M., Chan, H.M., Livingston, D.M., and Amati, B. (2003). MYC recruits the TIP60 histone acetyltransferase complex to chromatin. EMBO Rep *4*, 575-580.

Fukazawa, T., Maeda, Y., Matsuoka, J., Yamatsuji, T., Shigemitsu, K., Morita, I., Faiola, F., Durbin, M.L., Soucek, L., and Naomoto, Y. (2010). Inhibition of Myc effectively targets KRAS mutation-positive lung cancer expressing high levels of Myc. Anticancer Res *30*, 4193-4200.

Gabay, M., Li, Y., and Felsher, D.W. (2014). MYC Activation Is a Hallmark of Cancer Initiation and Maintenance. Cold Spring Harbor Perspectives in Medicine *4*, a014241-a014241.

Gallant, P., Shiio, Y., Cheng, P.F., Parkhurst, S.M., and Eisenman, R.N. (1996). Myc and Max homologs in Drosophila. Science *274*, 1523-1527.

Gartel, A.L., Ye, X., Goufman, E., Shianov, P., Hay, N., Najmabadi, F., and Tyner, A.L. (2001). Myc represses the p21(WAF1/CIP1) promoter and interacts with Sp1/Sp3. Proceedings of the National Academy of Sciences of the United States of America *98*, 4510-4515.

Gasteiger, E., Gattiker, A., Hoogland, C., Ivanyi, I., Appel, R.D., and Bairoch, A. (2003). ExPASy: The proteomics server for in-depth protein knowledge and analysis. Nucleic acids research *31*, 3784-3788.

Gaubatz, S., Imhof, A., Dosch, R., Werner, O., Mitchell, P., Buettner, R., and Eilers, M. (1995). Transcriptional Activation by Myc Is under Negative Control by the Transcription Factor Ap-2. Embo J *14*, 1508-1519.

Gebhardt, A. (2016). Personal communication.

Giardine, B., Riemer, C., Hardison, R.C., Burhans, R., Elnitski, L., Shah, P., Zhang, Y., Blankenberg, D., Albert, I., Taylor, J.*, et al.* (2005). Galaxy: a platform for interactive large-scale genome analysis. Genome Res *15*, 1451-1455.

Gilquin, B., Taillebourg, E., Cherradi, N., Hubstenberger, A., Gay, O., Merle, N., Assard, N., Fauvarque, M.O., Tomohiro, S., Kuge, O.*, et al.* (2010). The AAA+ ATPase ATAD3A controls mitochondrial dynamics at the interface of the inner and outer membranes. Mol Cell Biol *30*, 1984-1996.

Goecks, J., Nekrutenko, A., Taylor, J., and Galaxy, T. (2010). Galaxy: a comprehensive approach for supporting accessible, reproducible, and transparent computational research in the life sciences. Genome biology *11*, R86.

Gomez-Roman, N., Grandori, C., Eisenman, R.N., and White, R.J. (2003). Direct activation of RNA polymerase III transcription by c-Myc. Nature *421*, 290-294.

Graff, J.N., Higano, C.S., Hahn, N.M., Taylor, M.H., Zhang, B., Zhou, X., Venkatakrishnan, K., Leonard, E.J., and Sarantopoulos, J. (2016). Open-label, multicenter, phase 1 study of alisertib (MLN8237), an aurora A kinase inhibitor, with docetaxel in patients with solid tumors. Cancer *122*, 2524-2533.

Grand, C.L., Han, H., Munoz, R.M., Weitman, S., Von Hoff, D.D., Hurley, L.H., and Bearss, D.J. (2002). The cationic porphyrin TMPyP4 down-regulates c-MYC and human telomerase reverse transcriptase expression and inhibits tumor growth in vivo. Mol Cancer Ther *1*, 565-573.

Grandori, C., Gomez-Roman, N., Felton-Edkins, Z.A., Ngouenet, C., Galloway, D.A., Eisenman, R.N., and White, R.J. (2005). c-Myc binds to human ribosomal DNA and stimulates transcription of rRNA genes by RNA polymerase I. Nat Cell Biol *7*, 311-318.

Grewal, S.S., Li, L., Orian, A., Eisenman, R.N., and Edgar, B.A. (2005). Myc-dependent regulation of ribosomal RNA synthesis during Drosophila development. Nat Cell Biol *7*, 295-302.

Griffith, M., Griffith, O.L., Coffman, A.C., Weible, J.V., McMichael, J.F., Spies, N.C., Koval, J., Das, I., Callaway, M.B., Eldred, J.M.*, et al.* (2013). DGIdb: mining the druggable genome. Nature methods *10*, 1209-1210.

Gross, M.I., Demo, S.D., Dennison, J.B., Chen, L., Chernov-Rogan, T., Goyal, B., Janes, J.R., Laidig, G.J., Lewis, E.R., Li, J.*, et al.* (2014). Antitumor activity of the glutaminase inhibitor CB-839 in triple-negative breast cancer. Mol Cancer Ther *13*, 890-901.

Guccione, E., Martinato, F., Finocchiaro, G., Luzi, L., Tizzoni, L., Dall' Olio, V., Zardo, G., Nervi, C., Bernard, L., and Amati, B. (2006). Myc-binding-site recognition in the human genome is determined by chromatin context. Nat Cell Biol *8*, 764-770.

Guo, J., Li, T., Schipper, J., Nilson, K.A., Fordjour, F.K., Cooper, J.J., Gordan, R., and Price, D.H. (2014a). Sequence specificity incompletely defines the genome-wide occupancy of Myc. Genome biology *15*, 482.

Guo, J., Parise, R.A., Joseph, E., Egorin, M.J., Lazo, J.S., Prochownik, E.V., and Eiseman, J.L. (2009). Efficacy, pharmacokinetics, tisssue distribution, and metabolism of the Myc-Max disruptor, 10058-F4 [Z,E]-5-[4-ethylbenzylidine]-2-thioxothiazolidin-4-one, in mice. Cancer Chemother Pharmacol *63*, 615-625.

Guo, W., Wisniewski, J.A., and Ji, H. (2014b). Hot spot-based design of small-molecule inhibitors for protein-protein interactions. Bioorg Med Chem Lett *24*, 2546-2554.

Gustafson, W.C., Meyerowitz, J.G., Nekritz, E.A., Chen, J., Benes, C., Charron, E., Simonds, E.F., Seeger, R., Matthay, K.K., Hertz, N.T.*, et al.* (2014). Drugging MYCN through an allosteric transition in Aurora kinase A. Cancer Cell *26*, 414-427.

Hammoudeh, D.I., Follis, A.V., Prochownik, E.V., and Metallo, S.J. (2009). Multiple independent binding sites for small-molecule inhibitors on the oncoprotein c-Myc. J Am Chem Soc *131*, 7390-7401.

Hann, S.R., King, M.W., Bentley, D.L., Anderson, C.W., and Eisenman, R.N. (1988). A non-AUG translational initiation in c-myc exon 1 generates an N-terminally distinct protein whose synthesis is disrupted in Burkitt's lymphomas. Cell *52*, 185-195.

Heckman, K.L., and Pease, L.R. (2007). Gene splicing and mutagenesis by PCR-driven overlap extension. Nat Protoc *2*, 924-932.

Hellman, L.M., and Fried, M.G. (2007). Electrophoretic mobility shift assay (EMSA) for detecting protein-nucleic acid interactions. Nature Protocols *2*, 1849-1861.

Henssen, A., Thor, T., Odersky, A., Heukamp, L., El-Hindy, N., Beckers, A., Speleman, F., Althoff, K., Schafers, S., Schramm, A.*, et al.* (2013). BET bromodomain protein inhibition is a therapeutic option for medulloblastoma. Oncotarget *4*, 2080-2095.

Herbst, A., Hemann, M.T., Tworkowski, K.A., Salghetti, S.E., Lowe, S.W., and Tansey, W.P. (2005). A conserved element in Myc that negatively regulates its proapoptotic activity. EMBO Rep *6*, 177-183.

Herold, S., Wanzel, M., Beuger, V., Frohme, C., Beul, D., Hillukkala, T., Syvaoja, J., Saluz, H.-P., Haenel, F., and Eilers, M. (2002). Negative regulation of the mammalian UV response by Myc through association with Miz-1. Molecular cell *10*, 509-521.

Herter, E.K., Stauch, M., Gallant, M., Wolf, E., Raabe, T., and Gallant, P. (2015). snoRNAs are a novel class of biologically relevant Myc targets. BMC Biol *13*, 25.

Hoffmann, M., Bellance, N., Rossignol, R., Koopman, W.J., Willems, P.H., Mayatepek, E., Bossinger, O., and Distelmaier, F. (2009). C. elegans ATAD-3 is essential for mitochondrial activity and development. PLoS One *4*, e7644.

Holzel, M., Rohrmoser, M., Schlee, M., Grimm, T., Harasim, T., Malamoussi, A., Gruber-Eber, A., Kremmer, E., Hiddemann, W., Bornkamm, G.W.*, et al.* (2005). Mammalian WDR12 is a novel

member of the Pes1-Bop1 complex and is required for ribosome biogenesis and cell proliferation. J Cell Biol *170*, 367-378.

Hu, J., Banerjee, A., and Goss, D.J. (2005). Assembly of b/HLH/z proteins c-Myc, Max, and Mad1 with cognate DNA: importance of protein-protein and protein-DNA interactions. Biochemistry *44*, 11855-11863.

Huang da, W., Sherman, B.T., and Lempicki, R.A. (2009a). Bioinformatics enrichment tools: paths toward the comprehensive functional analysis of large gene lists. Nucleic acids research *37*, 1-13.

Huang da, W., Sherman, B.T., and Lempicki, R.A. (2009b). Systematic and integrative analysis of large gene lists using DAVID bioinformatics resources. Nat Protoc *4*, 44-57.

Huber, W., Carey, V.J., Gentleman, R., Anders, S., Carlson, M., Carvalho, B.S., Bravo, H.C., Davis, S., Gatto, L., Girke, T.*, et al.* (2015). Orchestrating high-throughput genomic analysis with Bioconductor. Nature methods *12*, 115-121.

Hurley, L.H. (2002). DNA and its associated processes as targets for cancer therapy. Nat Rev Cancer *2*, 188-200.

Husnjak, K., Elsasser, S., Zhang, N., Chen, X., Randles, L., Shi, Y., Hofmann, K., Walters, K.J., Finley, D., and Dikic, I. (2008). Proteasome subunit Rpn13 is a novel ubiquitin receptor. Nature *453*, 481-488.

Jaehning, J.A. (2010). The Paf1 complex: platform or player in RNA polymerase II transcription? Biochim Biophys Acta *1799*, 379-388.

Jaenicke, L.A., von Eyss, B., Carstensen, A., Wolf, E., Xu, W., Greifenberg, A.K., Geyer, M., Eilers, M., and Popov, N. (2016). Ubiquitin-Dependent Turnover of MYC Antagonizes MYC/PAF1C Complex Accumulation to Drive Transcriptional Elongation. Molecular cell *61*, 54-67.

Jain, M., Arvanitis, C., Chu, K., Dewey, W., Leonhardt, E., Trinh, M., Sundberg, C.D., Bishop, J.M., and Felsher, D.W. (2002). Sustained loss of a neoplastic phenotype by brief inactivation of MYC. Science *297*, 102-104.

Jang, M.K., Mochizuki, K., Zhou, M., Jeong, H.S., Brady, J.N., and Ozato, K. (2005). The bromodomain protein Brd4 is a positive regulatory component of P-TEFb and stimulates RNA polymerase II-dependent transcription. Molecular cell *19*, 523-534.

Janghorban, M., Farrell, A.S., Allen-Petersen, B.L., Pelz, C., Daniel, C.J., Oddo, J., Langer, E.M., Christensen, D.J., and Sears, R.C. (2014). Targeting c-MYC by antagonizing PP2A inhibitors in breast cancer. Proceedings of the National Academy of Sciences of the United States of America *111*, 9157-9162.

Jiang, H., Bower, K.E., Beuscher, A.E.t., Zhou, B., Bobkov, A.A., Olson, A.J., and Vogt, P.K. (2009). Stabilizers of the Max homodimer identified in virtual ligand screening inhibit Myc function. Mol Pharmacol *76*, 491-502.

Jones, S. (2004). An overview of the basic helix-loop-helix proteins. Genome biology *5*, 226.

Jonkers, I., and Lis, J.T. (2015). Getting up to speed with transcription elongation by RNA polymerase II. Nat Rev Mol Cell Biol *16*, 167-177.

Jung, K.Y., Wang, H., Teriete, P., Yap, J.L., Chen, L., Lanning, M.E., Hu, A., Lambert, L.J., Holien, T., Sundan, A.*, et al.* (2015). Perturbation of the c-Myc-Max protein-protein interaction via synthetic alpha-helix mimetics. J Med Chem *58*, 3002-3024.

Jung, L.A., Gebhardt, A., Koelmel, W., Ade, C.P., Walz, S., Kuper, J., von Eyss, B., Letschert, S., Redel, C., d'Artista, L.*, et al.* (2016). OmoMYC blunts promoter invasion by oncogenic MYC to inhibit gene expression characteristic of MYC-dependent tumors. Oncogene.

Kaatsch, P., Spix, C., Katalinic, A., Hentschel, S., Luttmann, S., Stegmaier, C., Caspritz, S., Christ, M., Ernst, A., Folkerts, J.*, et al.* (2015). Krebs in Deutschland 2011/2012 (Robert Koch-Institut).

Kabsch, W. (2010). Xds. Acta crystallographica Section D, Biological crystallography *66*, 125-132.

Kanazawa, S., Soucek, L., Evan, G., Okamoto, T., and Peterlin, B.M. (2003). c-Myc recruits P-TEFb for transcription, cellular proliferation and apoptosis. Oncogene *22*, 5707-5711.

Kelley, L.A., and Sternberg, M.J. (2009). Protein structure prediction on the Web: a case study using the Phyre server. Nat Protoc *4*, 363-371.

Kelly, K., Cochran, B.H., Stiles, C.D., and Leder, P. (1983). Cell-specific regulation of the c-myc gene by lymphocyte mitogens and platelet-derived growth factor. Cell *35*, 603-610.

Killian, A., Sarafan-Vasseur, N., Sesboue, R., Le Pessot, F., Blanchard, F., Lamy, A., Laurent, M., Flaman, J.M., and Frebourg, T. (2006). Contribution of the BOP1 gene, located on 8q24, to colorectal tumorigenesis. Genes Chromosomes Cancer *45*, 874-881.

Kim, J., Guermah, M., and Roeder, R.G. (2010). The human PAF1 complex acts in chromatin transcription elongation both independently and cooperatively with SII/TFIIS. Cell *140*, 491-503.

Kim, Y.H., Girard, L., Giacomini, C.P., Wang, P., Hernandez-Boussard, T., Tibshirani, R., Minna, J.D., and Pollack, J.R. (2006). Combined microarray analysis of small cell lung cancer reveals altered apoptotic balance and distinct expression signatures of MYC family gene amplification. Oncogene *25*, 130-138.

Kraehn, G.M., Utikal, J., Udart, M., Greulich, K.M., Bezold, G., Kaskel, P., Leiter, U., and Peter, R.U. (2001). Extra c-myc oncogene copies in high risk cutaneous malignant melanoma and melanoma metastases. Br J Cancer *84*, 72-79.

Kress, T.R., Cannell, I.G., Brenkman, A.B., Samans, B., Gaestel, M., Roepman, P., Burgering, B.M., Bushell, M., Rosenwald, A., and Eilers, M. (2011). The MK5/PRAK Kinase and Myc Form a Negative Feedback Loop that Is Disrupted during Colorectal Tumorigenesis. Molecular cell *41*, 445-457.

Kress, T.R., Sabo, A., and Amati, B. (2015). MYC: connecting selective transcriptional control to global RNA production. Nat Rev Cancer *15*, 593-607.

Kretzner, L., Blackwood, E.M., and Eisenman, R.N. (1992a). Myc and Max proteins possess distinct transcriptional activities. Nature *359*, 426-429.

Kretzner, L., Blackwood, E.M., and Eisenman, R.N. (1992b). Transcriptional activities of the Myc and Max proteins in mammalian cells. Curr Top Microbiol Immunol *182*, 435-443.

Krissinel, E., and Henrick, K. (2007). Inference of macromolecular assemblies from crystalline state. J Mol Biol *372*, 774-797.

Kurland, J.F., and Tansey, W.P. (2008). Myc-mediated transcriptional repression by recruitment of histone deacetylase. Cancer Res *68*, 3624-3629.

Kwong, L.N., Costello, J.C., Liu, H., Jiang, S., Helms, T.L., Langsdorf, A.E., Jakubosky, D., Genovese, G., Muller, F.L., Jeong, J.H.*, et al.* (2012). Oncogenic NRAS signaling differentially regulates survival and proliferation in melanoma. Nat Med *18*, 1503-1510.

Laemmli, U.K. (1970). Cleavage of structural proteins during the assembly of the head of bacteriophage T4. Nature *227*, 680-685.

Langmead, B. (2010). Aligning short sequencing reads with Bowtie. Current protocols in bioinformatics / editoral board, Andreas D Baxevanis [et al] *Chapter 11*, Unit 11 17.

Lawrence, M., Huber, W., Pages, H., Aboyoun, P., Carlson, M., Gentleman, R., Morgan, M.T., and Carey, V.J. (2013). Software for computing and annotating genomic ranges. PLoS Comput Biol *9*, e1003118.

Le, A., Lane, A.N., Hamaker, M., Bose, S., Gouw, A., Barbi, J., Tsukamoto, T., Rojas, C.J., Slusher, B.S., Zhang, H.*, et al.* (2012). Glucose-independent glutamine metabolism via TCA cycling for proliferation and survival in B cells. Cell Metab *15*, 110-121.

Lebel, R., McDuff, F.-O., Lavigne, P., and Grandbois, M. (2007). Direct visualization of the binding of c-Myc/Max heterodimeric b-HLH-LZ to E-box sequences on the hTERT promoter. Biochemistry *46*, 10279-10286.

Lee, J.W., Soung, Y.H., Kim, S.Y., Nam, S.W., Park, W.S., Lee, J.Y., Yoo, N.J., and Lee, S.H. (2006). Mutational analysis of MYC in common epithelial cancers and acute leukemias. APMIS *114*, 436-439.

Legouy, E., DePinho, R., Zimmerman, K., Collum, R., Yancopoulos, G., Mitsock, L., Kriz, R., and Alt, F.W. (1987). Structure and expression of the murine L-myc gene. Embo J *6*, 3359-3366.

LeRoy, G., Rickards, B., and Flint, S.J. (2008). The double bromodomain proteins Brd2 and Brd3 couple histone acetylation to transcription. Molecular cell *30*, 51-60.

Li, H., Handsaker, B., Wysoker, A., Fennell, T., Ruan, J., Homer, N., Marth, G., Abecasis, G., Durbin, R., and Genome Project Data Processing, S. (2009). The Sequence Alignment/Map format and SAMtools. Bioinformatics *25*, 2078-2079.

Li, M.Z., and Elledge, S.J. (2007). Harnessing homologous recombination in vitro to generate recombinant DNA via SLIC. Nature methods *4*, 251-256.

Li, M.Z., and Elledge, S.J. (2012). SLIC: a method for sequence- and ligation-independent cloning. Methods in molecular biology *852*, 51-59.

Li, Y., Choi, P.S., Casey, S.C., Dill, D.L., and Felsher, D.W. (2014). MYC through miR-17-92 suppresses specific target genes to maintain survival, autonomous proliferation, and a neoplastic state. Cancer Cell *26*, 262-272.

Lin, C.Y., Loven, J., Rahl, P.B., Paranal, R.M., Burge, C.B., Bradner, J.E., Lee, T.I., and Young, R.A. (2012). Transcriptional amplification in tumor cells with elevated c-Myc. Cell *151*, 56-67.

Lindeman, G.J., Harris, A.W., Bath, M.L., Eisenman, R.N., and Adams, J.M. (1995). Overexpressed max is not oncogenic and attenuates myc-induced lymphoproliferation and lymphomagenesis in transgenic mice. Oncogene *10*, 1013-1017.

Liu, L., Ulbrich, J., Müller, J., Wüstefeld, T., Aeberhard, L., Kress, T.R., Muthalagu, N., Rycak, L., Rudalska, R., Moll, R., *et al.* (2012). Deregulated MYC expression induces dependence upon AMPK-related kinase 5. Nature *483*, 608-612.

Liu, L.F. (1989). DNA topoisomerase poisons as antitumor drugs. Annu Rev Biochem *58*, 351-375.

Liu, Y.C., Li, F., Handler, J., Huang, C.R., Xiang, Y., Neretti, N., Sedivy, J.M., Zeller, K.I., and Dang, C.V. (2008). Global regulation of nucleotide biosynthetic genes by c-Myc. PLoS One *3*, e2722.

Livak, K.J., and Schmittgen, T.D. (2001). Analysis of Relative Gene Expression Data Using Real-Time Quantitative PCR and the 2−ΔΔCT Method. Methods *25*, 402-408.

Lorenzin, F., Benary, U., Baluapuri, A., Walz, S., Jung, L.A., von Eyss, B., Kisker, C., Wolf, J., Eilers, M., and Wolf, E. (2016). Different promoter affinities account for specificity in MYC-dependent gene regulation. Elife *5*.

Loven, J., Hoke, H.A., Lin, C.Y., Lau, A., Orlando, D.A., Vakoc, C.R., Bradner, J.E., Lee, T.I., and Young, R.A. (2013). Selective inhibition of tumor oncogenes by disruption of super-enhancers. Cell *153*, 320-334.

Lu, D. (2015). Personal communication.

Malynn, B.A., de Alboran, I.M., O'Hagan, R.C., Bronson, R., Davidson, L., DePinho, R.A., and Alt, F.W. (2000). N-myc can functionally replace c-myc in murine development, cellular growth, and differentiation. Genes Dev *14*, 1390-1399.

Marchetti, A., Abril-Marti, M., Illi, B., Cesareni, G., and Nasi, S. (1995). Analysis of the Myc and Max interaction specificity with lambda repressor-HLH domain fusions. J Mol Biol *248*, 541-550.

Marcu, K.B. (1987). Regulation of expression of the c-myc proto-oncogene. Bioessays *6*, 28-32.

Marinho, H.S., Real, C., Cyrne, L., Soares, H., and Antunes, F. (2014). Hydrogen peroxide sensing, signaling and regulation of transcription factors. Redox Biol *2*, 535-562.

Marinkovic, D., Marinkovic, T., Mahr, B., Hess, J., and Wirth, T. (2004). Reversible lymphomagenesis in conditionally c-MYC expressing mice. Int J Cancer *110*, 336-342.

Matthews, B.W. (1968). Solvent content of protein crystals. J Mol Biol *33*, 491-497.

Mayer, A., Lidschreiber, M., Siebert, M., Leike, K., Soding, J., and Cramer, P. (2010). Uniform transitions of the general RNA polymerase II transcription complex. Nat Struct Mol Biol *17*, 1272-1278.

McCoy, A.J., Grosse-Kunstleve, R.W., Adams, P.D., Winn, M.D., Storoni, L.C., and Read, R.J. (2007). Phaser crystallographic software. Journal of applied crystallography *40*, 658-674.

McDuff, F.-O., Naud, J.-F., Montagne, M., Sauvé, S., and Lavigne, P. (2009). The Max homodimeric b-HLH-LZ significantly interferes with the specific heterodimerization between the c-Myc and Max b-HLH-LZ in absence of DNA: a quantitative analysis. J Mol Recognit *22*, 261-269.

McKeown, M.R., and Bradner, J.E. (2014). Therapeutic Strategies to Inhibit MYC. Cold Spring Harbor Perspectives in Medicine *4*, a014266-a014266.

McMahon, S.B., Van Buskirk, H.A., Dugan, K.A., Copeland, T.D., and Cole, M.D. (1998). The novel ATM-related protein TRRAP is an essential cofactor for the c-Myc and E2F oncoproteins. Cell *94*, 363-374.

McMahon, S.B., Wood, M.A., and Cole, M.D. (2000). The essential cofactor TRRAP recruits the histone acetyltransferase hGCN5 to c-Myc. Mol Cell Biol *20*, 556-562.

Mertz, J.A., Conery, A.R., Bryant, B.M., Sandy, P., Balasubramanian, S., Mele, D.A., Bergeron, L., and Sims, R.J., 3rd (2011). Targeting MYC dependence in cancer by inhibiting BET bromodomains. Proceedings of the National Academy of Sciences of the United States of America *108*, 16669-16674.

Meyer, N., and Penn, L.Z. (2008). Reflecting on 25 years with MYC. Nat Rev Cancer *8*, 976-990.

Mongiardi, M.P., Savino, M., Bartoli, L., Beji, S., Nanni, S., Scagnoli, F., Falchetti, M.L., Favia, A., Farsetti, A., Levi, A.*, et al.* (2015). Myc and Omomyc functionally associate with the Protein Arginine Methyltransferase 5 (PRMT5) in glioblastoma cells. Sci Rep *5*, 15494.

Mongiardi, M.P., Savino, M., Falchetti, M.L., Illi, B., Bozzo, F., Valle, C., Helmer-Citterich, M., Ferre, F., Nasi, S., and Levi, A. (2016). c-MYC inhibition impairs hypoxia response in glioblastoma multiforme. Oncotarget *7*, 33257-33271.

Montagne, M., Beaudoin, N., Fortin, D., Lavoie, C.L., Klinck, R., and Lavigne, P. (2012). The Max b-HLH-LZ Can Transduce into Cells and Inhibit c-Myc Transcriptional Activities. PLoS ONE *7*, e32172.

Mosmann, T. (1983). Rapid colorimetric assay for cellular growth and survival: application to proliferation and cytotoxicity assays. J Immunol Methods *65*, 55-63.

Mosse, Y.P., Lipsitz, E., Fox, E., Teachey, D.T., Maris, J.M., Weigel, B., Adamson, P.C., Ingle, M.A., Ahern, C.H., and Blaney, S.M. (2012). Pediatric phase I trial and pharmacokinetic study of MLN8237, an investigational oral selective small-molecule inhibitor of Aurora kinase A: a Children's Oncology Group Phase I Consortium study. Clin Cancer Res *18*, 6058-6064.

Mullard, A. (2012). Protein-protein interaction inhibitors get into the groove. Nat Rev Drug Discov *11*, 173-175.

Mullard, A. (2016). Pioneering apoptosis-targeted cancer drug poised for FDA approval. Nat Rev Drug Discov *15*, 147-149.

Muncan, V., Sansom, O.J., Tertoolen, L., Phesse, T.J., Begthel, H., Sancho, E., Cole, A.M., Gregorieff, A., de Alboran, I.M., Clevers, H.*, et al.* (2006). Rapid loss of intestinal crypts upon conditional deletion of the Wnt/Tcf-4 target gene c-Myc. Mol Cell Biol *26*, 8418-8426.

Murre, C., McCaw, P.S., and Baltimore, D. (1989). A new DNA binding and dimerization motif in immunoglobulin enhancer binding, daughterless, MyoD, and myc proteins. Cell *56*, 777-783.

Myant, K., and Sansom, O.J. (2011). Wnt/Myc interactions in intestinal cancer: partners in crime. Exp Cell Res *317*, 2725-2731.

Nair, S.K., and Burley, S.K. (2003). X-ray structures of Myc-Max and Mad-Max recognizing DNA. Molecular bases of regulation by proto-oncogenic transcription factors. Cell *112*, 193-205.

Naldini, L., Blömer, U., Gallay, P., Ory, D., Mulligan, R., Gage, F.H., Verma, I.M., and Trono, D. (1996). In vivo gene delivery and stable transduction of nondividing cells by a lentiviral vector. Science *272*, 263-267.

Nau, M.M., Brooks, B.J., Battey, J., Sausville, E., Gazdar, A.F., Kirsch, I.R., McBride, O.W., Bertness, V., Hollis, G.F., and Minna, J.D. (1985). L-myc, a new myc-related gene amplified and expressed in human small cell lung cancer. Nature *318*, 69-73.

Neidle, S. (2014). Cancer drug design and discovery, Second edition. edn (Amsterdam ; Boston: Elsevier/Academic Press).

Nekludova, L., and Pabo, C.O. (1994). Distinctive DNA conformation with enlarged major groove is found in Zn-finger-DNA and other protein-DNA complexes. Proceedings of the National Academy of Sciences of the United States of America *91*, 6948-6952.

Nesbit, C.E., Tersak, J.M., and Prochownik, E.V. (1999). MYC oncogenes and human neoplastic disease. Oncogene *18*, 3004-3016.

Nicklin, P., Bergman, P., Zhang, B., Triantafellow, E., Wang, H., Nyfeler, B., Yang, H., Hild, M., Kung, C., Wilson, C.*, et al.* (2009). Bidirectional transport of amino acids regulates mTOR and autophagy. In Cell, pp. 521-534.

Nicol, J.W., Helt, G.A., Blanchard, S.G., Jr., Raja, A., and Loraine, A.E. (2009). The Integrated Genome Browser: free software for distribution and exploration of genome-scale datasets. Bioinformatics *25*, 2730-2731.

Nie, Z., Hu, G., Wei, G., Cui, K., Yamane, A., Resch, W., Wang, R., Green, D.R., Tessarollo, L., Casellas, R.*, et al.* (2012). c-Myc Is a Universal Amplifier of Expressed Genes in Lymphocytes and Embryonic Stem Cells. Cell *151*, 68-79.

Niesen, F.H., Berglund, H., and Vedadi, M. (2007). The use of differential scanning fluorimetry to detect ligand interactions that promote protein stability. Nature Protocols *2*, 2212-2221.

Nilsson, J.A., Keller, U.B., Baudino, T.A., Yang, C., Norton, S., Old, J.A., Nilsson, L.M., Neale, G., Kramer, D.L., Porter, C.W.*, et al.* (2005). Targeting ornithine decarboxylase in Myc-induced lymphomagenesis prevents tumor formation. Cancer Cell *7*, 433-444.

Noel, J.K., Iwata, K., Ooike, S., Sugahara, K., Nakamura, H., and Daibata, M. (2013). Development of the BET bromodomain inhibitor OTX015. Mol Cancer Ther *12*.

O'Brien, S.G., Guilhot, F., Larson, R.A., Gathmann, I., Baccarani, M., Cervantes, F., Cornelissen, J.J., Fischer, T., Hochhaus, A., Hughes, T.*, et al.* (2003). Imatinib compared with interferon and low-dose cytarabine for newly diagnosed chronic-phase chronic myeloid leukemia. N Engl J Med *348*, 994-1004.

O'Donnell, K.A., Wentzel, E.A., Zeller, K.I., Dang, C.V., and Mendell, J.T. (2005). c-Myc-regulated microRNAs modulate E2F1 expression. Nature *435*, 839-843.

O'Neil, K.T., Hoess, R.H., and DeGrado, W.F. (1990). Design of DNA-binding peptides based on the leucine zipper motif. Science *249*, 774-778.

Obara, K., Yokoyama, M., Asano, G., and Tanaka, S. (2001). Evaluation of myc and chromosome 8 copy number in colorectal cancer using interphase cytogenetics. Int J Oncol *18*, 233-239.

Oricchio, E., Papapetrou, E.P., Lafaille, F., Ganat, Y.M., Kriks, S., Ortega-Molina, A., Mark, W.H., Teruya-Feldstein, J., Huse, J.T., Reuter, V.*, et al.* (2014). A Cell Engineering Strategy to Enhance the Safety of Stem Cell Therapies. CellReports.

Oster, S.K., Ho, C.S.W., Soucie, E.L., and Penn, L.Z. (2002). The myc oncogene: MarvelouslY Complex. Adv Cancer Res *84*, 81-154.

Ott, C.J., Kopp, N., Bird, L., Paranal, R.M., Qi, J., Bowman, T., Rodig, S.J., Kung, A.L., Bradner, J.E., and Weinstock, D.M. (2012). BET bromodomain inhibition targets both c-Myc and IL7R in high-risk acute lymphoblastic leukemia. Blood *120*, 2843-2852.

Otto, T., Horn, S., Brockmann, M., Eilers, U., Schüttrumpf, L., Popov, N., Kenney, A.M., Schulte, J.H., Beijersbergen, R., Christiansen, H.*, et al.* (2009). Stabilization of N-Myc Is a Critical Function of Aurora A in Human Neuroblastoma. Cancer Cell *15*, 67-78.

Ou, T.M., Lu, Y.J., Zhang, C., Huang, Z.S., Wang, X.D., Tan, J.H., Chen, Y., Ma, D.L., Wong, K.Y., Tang, J.C.*, et al.* (2007). Stabilization of G-quadruplex DNA and down-regulation of oncogene c-myc by quindoline derivatives. J Med Chem *50*, 1465-1474.

Pal, A., Young, M.A., and Donato, N.J. (2014). Emerging potential of therapeutic targeting of ubiquitin-specific proteases in the treatment of cancer. Cancer Res *74*, 4955-4966.

Pan, J., Deng, Q., Jiang, C., Wang, X., Niu, T., Li, H., Chen, T., Jin, J., Pan, W., Cai, X.*, et al.* (2015). USP37 directly deubiquitinates and stabilizes c-Myc in lung cancer. Oncogene *34*, 3957-3967.

Panda, D., Debnath, M., Mandal, S., Bessi, I., Schwalbe, H., and Dash, J. (2015). A Nucleus-Imaging Probe That Selectively Stabilizes a Minor Conformation of c-MYC G-quadruplex and Down-regulates c-MYC Transcription in Human Cancer Cells. Sci Rep *5*, 13183.

Pantoliano, M.W., Petrella, E.C., Kwasnoski, J.D., Lobanov, V.S., Myslik, J., Graf, E., Carver, T., Asel, E., Springer, B.A., Lane, P.*, et al.* (2001). High-density miniaturized thermal shift assays as a general strategy for drug discovery. Journal of biomolecular screening *6*, 429-440.

Park, S., Chung, S., Kim, K.-M., Jung, K.-C., Park, C., Hahm, E.-R., and Yang, C.-H. (2004). Determination of binding constant of transcription factor myc-max/max-max and E-box DNA: the effect of inhibitors on the binding. Biochim Biophys Acta *1670*, 217-228.

Pavri, R., Zhu, B., Li, G., Trojer, P., Mandal, S., Shilatifard, A., and Reinberg, D. (2006). Histone H2B monoubiquitination functions cooperatively with FACT to regulate elongation by RNA polymerase II. Cell *125*, 703-717.

Pelengaris, S., Khan, M., and Evan, G.I. (2002). Suppression of Myc-induced apoptosis in beta cells exposes multiple oncogenic properties of Myc and triggers carcinogenic progression. Cell *109*, 321-334.

Perna, D., Faga, G., Verrecchia, A., Gorski, M.M., Barozzi, I., Narang, V., Khng, J., Lim, K.C., Sung, W.K., Sanges, R.*, et al.* (2012). Genome-wide mapping of Myc binding and gene regulation in serum-stimulated fibroblasts. Oncogene *31*, 1695-1709.

Perumal, D., Kuo, P.Y., Leshchenko, V.V., Jiang, Z., Divakar, S.K., Cho, H.J., Chari, A., Brody, J., Reddy, M.V., Zhang, W.*, et al.* (2016). Dual Targeting of CDK4 and ARK5 Using a Novel Kinase Inhibitor ON123300 Exerts Potent Anticancer Activity against Multiple Myeloma. Cancer Res *76*, 1225-1236.

Peukert, K., Staller, P., Hänel, F., and Eilers, M. (1997). An alternative pathway for gene regulation by Myc. Embo J *16*, 5672-5686.

Pogenberg, V., Ogmundsdottir, M.H., Bergsteinsdottir, K., Schepsky, A., Phung, B., Deineko, V., Milewski, M., Steingrimsson, E., and Wilmanns, M. (2012). Restricted leucine zipper dimerization

and specificity of DNA recognition of the melanocyte master regulator MITF. Genes Dev *26*, 2647-2658.

Popov, N., Wanzel, M., Madiredjo, M., Zhang, D., Beijersbergen, R., Bernards, R., Moll, R., Elledge, S.J., and Eilers, M. (2007). The ubiquitin-specific protease USP28 is required for MYC stability. Nat Cell Biol *9*, 765-774.

Qiu, H., Hu, C., Gaur, N.A., and Hinnebusch, A.G. (2012). Pol II CTD kinases Bur1 and Kin28 promote Spt5 CTR-independent recruitment of Paf1 complex. Embo J *31*, 3494-3505.

Quinlan, A.R., and Hall, I.M. (2010). BEDTools: a flexible suite of utilities for comparing genomic features. Bioinformatics *26*, 841-842.

Rahl, P.B., Lin, C.Y., Seila, A.C., Flynn, R.A., McCuine, S., Burge, C.B., Sharp, P.A., and Young, R.A. (2010). c-Myc regulates transcriptional pause release. Cell *141*, 432-445.

Rahl, P.B., and Young, R.A. (2014). MYC and transcription elongation. Cold Spring Harb Perspect Med *4*, a020990.

Raj, M., Bullock, B.N., and Arora, P.S. (2013). Plucking the high hanging fruit: a systematic approach for targeting protein-protein interactions. Bioorg Med Chem *21*, 4051-4057.

Raturi, A., Gutierrez, T., Ortiz-Sandoval, C., Ruangkittisakul, A., Herrera-Cruz, M.S., Rockley, J.P., Gesson, K., Ourdev, D., Lou, P.H., Lucchinetti, E.*, et al.* (2016). TMX1 determines cancer cell metabolism as a thiol-based modulator of ER-mitochondria Ca2+ flux. J Cell Biol *214*, 433-444.

Raucher, D., and Ryu, J.S. (2015). Cell-penetrating peptides: strategies for anticancer treatment. Trends Mol Med *21*, 560-570.

Redel, C. (2016). Personal communication.

Rhodes, G. (2006). Crystallography made crystal clear : a guide for users of macromolecular models, 3rd edn (Amsterdam ; Boston: Elsevier/Academic Press).

Richon, V.M., Emiliani, S., Verdin, E., Webb, Y., Breslow, R., Rifkind, R.A., and Marks, P.A. (1998). A class of hybrid polar inducers of transformed cell differentiation inhibits histone deacetylases. Proceedings of the National Academy of Sciences of the United States of America *95*, 3003-3007.

Ritchie, M.E., Phipson, B., Wu, D., Hu, Y., Law, C.W., Shi, W., and Smyth, G.K. (2015). limma powers differential expression analyses for RNA-sequencing and microarray studies. Nucleic acids research *43*, e47.

Robinson, M.D., McCarthy, D.J., and Smyth, G.K. (2010). edgeR: a Bioconductor package for differential expression analysis of digital gene expression data. Bioinformatics *26*, 139-140.

Rohrmoser, M., Holzel, M., Grimm, T., Malamoussi, A., Harasim, T., Orban, M., Pfisterer, I., Gruber-Eber, A., Kremmer, E., and Eick, D. (2007). Interdependence of Pes1, Bop1, and WDR12 controls nucleolar localization and assembly of the PeBoW complex required for maturation of the 60S ribosomal subunit. Mol Cell Biol *27*, 3682-3694.

Ruggero, D. (2009). The role of Myc-induced protein synthesis in cancer. Cancer Research *69*, 8839-8843.

Ruggero, D. (2013). Translational control in cancer etiology. Cold Spring Harb Perspect Biol *5*.

Rupp, B. (2010). Biomolecular crystallography : principles, practice, and application to structural biology (New York: Garland Science).

Sabò, A., Kress, T.R., Pelizzola, M., de Pretis, S., Gorski, M.M., Tesi, A., Morelli, M.J., Bora, P., Doni, M., Verrecchia, A*., et al.* (2014). Selective transcriptional regulation by Myc in cellular growth control and lymphomagenesis. Nature *511*, 488-492.

Saldanha, A.J. (2004). Java Treeview--extensible visualization of microarray data. Bioinformatics *20*, 3246-3248.

Sauvé, S., Tremblay, L., and Lavigne, P. (2004). The NMR solution structure of a mutant of the Max b/HLH/LZ free of DNA: insights into the specific and reversible DNA binding mechanism of dimeric transcription factors. J Mol Biol *342*, 813-832.

Savino, M., Annibali, D., Carucci, N., Favuzzi, E., Cole, M.D., Evan, G.I., Soucek, L., and Nasi, S. (2011). The action mechanism of the Myc inhibitor termed Omomyc may give clues on how to target Myc for cancer therapy. PLoS One *6*, e22284.

Schlosser, I., Holzel, M., Murnseer, M., Burtscher, H., Weidle, U.H., and Eick, D. (2003). A role for c-Myc in the regulation of ribosomal RNA processing. Nucleic acids research *31*, 6148-6156.

Schneider, C.A., Rasband, W.S., and Eliceiri, K.W. (2012). NIH Image to ImageJ: 25 years of image analysis. Nature methods *9*, 671-675.

Schrodinger, L. (2015). The PyMOL Molecular Graphics System, Version 1.8.

Schwab, M., Alitalo, K., Klempnauer, K.H., Varmus, H.E., Bishop, J.M., Gilbert, F., Brodeur, G., Goldstein, M., and Trent, J. (1983). Amplified DNA with limited homology to myc cellular oncogene is shared by human neuroblastoma cell lines and a neuroblastoma tumour. Nature *305*, 245-248.

Scognamiglio, R., Cabezas-Wallscheid, N., Thier, M.C., Altamura, S., Reyes, A., Prendergast, A.M., Baumgartner, D., Carnevalli, L.S., Atzberger, A., Haas, S*., et al.* (2016). Myc Depletion Induces a Pluripotent Dormant State Mimicking Diapause. Cell *164*, 668-680.

Sears, R., Leone, G., DeGregori, J., and Nevins, J.R. (1999). Ras enhances Myc protein stability. Molecular cell *3*, 169-179.

Sears, R., Nuckolls, F., Haura, E., Taya, Y., Tamai, K., and Nevins, J.R. (2000). Multiple Ras-dependent phosphorylation pathways regulate Myc protein stability. Genes Dev *14*, 2501-2514.

Sears, R.C. (2004). The life cycle of C-myc: from synthesis to degradation. Cell Cycle *3*, 1133-1137.

Shachaf, C.M., Kopelman, A.M., Arvanitis, C., Karlsson, A., Beer, S., Mandl, S., Bachmann, M.H., Borowsky, A.D., Ruebner, B., Cardiff, R.D*., et al.* (2004). MYC inactivation uncovers pluripotent differentiation and tumour dormancy in hepatocellular cancer. Nature *431*, 1112-1117.

Sheiness, D., and Bishop, J.M. (1979). DNA and RNA from uninfected vertebrate cells contain nucleotide sequences related to the putative transforming gene of avian myelocytomatosis virus. J Virol *31*, 514-521.

Siddiquee, K., Zhang, S., Guida, W.C., Blaskovich, M.A., Greedy, B., Lawrence, H.R., Yip, M.L., Jove, R., McLaughlin, M.M., Lawrence, N.J*., et al.* (2007). Selective chemical probe inhibitor of Stat3, identified through structure-based virtual screening, induces antitumor activity. Proceedings of the National Academy of Sciences of the United States of America *104*, 7391-7396.

Siddiqui-Jain, A., Grand, C.L., Bearss, D.J., and Hurley, L.H. (2002). Direct evidence for a G-quadruplex in a promoter region and its targeting with a small molecule to repress c-MYC transcription. Proceedings of the National Academy of Sciences of the United States of America *99*, 11593-11598.

Siegel, R.L., Miller, K.D., and Jemal, A. (2015). Cancer statistics, 2015. CA Cancer J Clin *65*, 5-29.

Sievers, F., Wilm, A., Dineen, D., Gibson, T.J., Karplus, K., Li, W., Lopez, R., McWilliam, H., Remmert, M., Soding, J.*, et al.* (2011). Fast, scalable generation of high-quality protein multiple sequence alignments using Clustal Omega. Mol Syst Biol *7*, 539.

Sloane, D.A., Trikic, M.Z., Chu, M.L., Lamers, M.B., Mason, C.S., Mueller, I., Savory, W.J., Williams, D.H., and Eyers, P.A. (2010). Drug-resistant aurora A mutants for cellular target validation of the small molecule kinase inhibitors MLN8054 and MLN8237. ACS Chem Biol *5*, 563-576.

Smith, M.J., Charron-Prochownik, D.C., and Prochownik, E.V. (1990). The leucine zipper of c-Myc is required for full inhibition of erythroleukemia differentiation. Mol Cell Biol *10*, 5333-5339.

Sodir, N.M., Swigart, L.B., Karnezis, A.N., Hanahan, D., Evan, G.I., and Soucek, L. (2011). Endogenous Myc maintains the tumor microenvironment. Genes Dev *25*, 907-916.

Soucek, L. (2015). Personal communication.

Soucek, L., Cesareni, G., and Nasi, S. (1998). Design and properties of a Myc derivative that efficiently homodimerizes. Oncogene *17*, 2463-2472.

Soucek, L., Jucker, R., Panacchia, L., Ricordy, R., Tatò, F., and Nasi, S. (2002). Omomyc, a potential Myc dominant negative, enhances Myc-induced apoptosis. Cancer Research *62*, 3507-3510.

Soucek, L., Nasi, S., and Evan, G.I. (2004). Omomyc expression in skin prevents Myc-induced papillomatosis. Cell Death Differ *11*, 1038-1045.

Soucek, L., Whitfield, J., Martins, C.P., Finch, A.J., Murphy, D.J., Sodir, N.M., Karnezis, A.N., Swigart, L.B., Nasi, S., and Evan, G.I. (2008). Modelling Myc inhibition as a cancer therapy. Nature *455*, 679-683.

Soucek, L., Whitfield, J.R., Sodir, N.M., Masso-Valles, D., Serrano, E., Karnezis, A.N., Swigart, L.B., and Evan, G.I. (2013). Inhibition of Myc family proteins eradicates KRas-driven lung cancer in mice. Genes Dev *27*, 504-513.

Spencer, C.A., and Groudine, M. (1991). Control of c-myc regulation in normal and neoplastic cells. Adv Cancer Res *56*, 1-48.

Spotts, G.D., Patel, S.V., Xiao, Q., and Hann, S.R. (1997). Identification of downstream-initiated c-Myc proteins which are dominant-negative inhibitors of transactivation by full-length c-Myc proteins. Mol Cell Biol *17*, 1459-1468.

Staller, P., Peukert, K., Kiermaier, A., Seoane, J., Lukas, J., Karsunky, H., Moroy, T., Bartek, J., Massagué, J., Hänel, F.*, et al.* (2001). Repression of p15INK4b expression by Myc through association with Miz-1. Nat Cell Biol *3*, 392-399.

Steiger, D., Furrer, M., Schwinkendorf, D., and Gallant, P. (2008). Max-independent functions of Myc in Drosophila melanogaster. Nat Genet *40*, 1084-1091.

Strebhardt, K., and Ullrich, A. (2008). Paul Ehrlich's magic bullet concept: 100 years of progress. Nat Rev Cancer *8*, 473-480.

Strieder, V., and Lutz, W. (2002). Regulation of N-myc expression in development and disease. Cancer Lett *180*, 107-119.

Subramanian, A., Tamayo, P., Mootha, V.K., Mukherjee, S., Ebert, B.L., Gillette, M.A., Paulovich, A., Pomeroy, S.L., Golub, T.R., and Lander, E.S. (2005). Gene set enrichment analysis: a knowledge-based approach for interpreting genome-wide expression profiles. Proc Natl Acad Sci USA *102*, 15545-15550.

Sun, M., Schwalb, B., Pirkl, N., Maier, K.C., Schenk, A., Failmezger, H., Tresch, A., and Cramer, P. (2013). Global analysis of eukaryotic mRNA degradation reveals Xrn1-dependent buffering of transcript levels. Molecular cell *52*, 52-62.

Sun, X.X., He, X., Yin, L., Komada, M., Sears, R.C., and Dai, M.S. (2015a). The nucleolar ubiquitin-specific protease USP36 deubiquitinates and stabilizes c-Myc. Proceedings of the National Academy of Sciences of the United States of America *112*, 3734-3739.

Sun, X.X., Sears, R.C., and Dai, M.S. (2015b). Deubiquitinating c-Myc: USP36 steps up in the nucleolus. Cell Cycle *14*, 3786-3793.

Tansey, W.P. (2014). Mammalian MYC Proteins and Cancer. New Journal of Science *2014*, 1-27.

Tavana, O., Li, D., Dai, C., Lopez, G., Banerjee, D., Kon, N., Chen, C., Califano, A., Yamashiro, D.J., Sun, H.*, et al.* (2016). HAUSP deubiquitinates and stabilizes N-Myc in neuroblastoma. Nat Med.

Teng, Y., Ren, X., Li, H., Shull, A., Kim, J., and Cowell, J.K. (2016). Mitochondrial ATAD3A combines with GRP78 to regulate the WASF3 metastasis-promoting protein. Oncogene *35*, 333-343.

Thomas, L.R., Wang, Q., Grieb, B.C., Phan, J., Foshage, A.M., Sun, Q., Olejniczak, E.T., Clark, T., Dey, S., Lorey, S.*, et al.* (2015). Interaction with WDR5 promotes target gene recognition and tumorigenesis by MYC. Molecular cell *58*, 440-452.

Thompson, J.D., Higgins, D.G., and Gibson, T.J. (1994). CLUSTAL W: improving the sensitivity of progressive multiple sequence alignment through sequence weighting, position-specific gap penalties and weight matrix choice. Nucleic acids research *22*, 4673-4680.

Titov, D.V., Gilman, B., He, Q.L., Bhat, S., Low, W.K., Dang, Y., Smeaton, M., Demain, A.L., Miller, P.S., Kugel, J.F.*, et al.* (2011). XPB, a subunit of TFIIH, is a target of the natural product triptolide. Nat Chem Biol *7*, 182-188.

Torre, L.A., Bray, F., Siegel, R.L., Ferlay, J., Lortet-Tieulent, J., and Jemal, A. (2015). Global cancer statistics, 2012. CA Cancer J Clin *65*, 87-108.

Trievel, R.C., and Shilatifard, A. (2009). WDR5, a complexed protein. Nat Struct Mol Biol *16*, 678-680.

van Montfort, R.L., and Workman, P. (2009). Structure-based design of molecular cancer therapeutics. Trends Biotechnol *27*, 315-328.

van Riggelen, J., Muller, J., Otto, T., Beuger, V., Yetil, A., Choi, P.S., Kosan, C., Moroy, T., Felsher, D.W., and Eilers, M. (2010a). The interaction between Myc and Miz1 is required to antagonize TGFbeta-dependent autocrine signaling during lymphoma formation and maintenance. Genes Dev *24*, 1281-1294.

van Riggelen, J., Yetil, A., and Felsher, D.W. (2010b). MYC as a regulator of ribosome biogenesis and protein synthesis. 1-9.

Vennstrom, B., Sheiness, D., Zabielski, J., and Bishop, J.M. (1982). Isolation and characterization of c-myc, a cellular homolog of the oncogene (v-myc) of avian myelocytomatosis virus strain 29. J Virol *42*, 773-779.

Vervoorts, J., Luscher-Firzlaff, J.M., Rottmann, S., Lilischkis, R., Walsemann, G., Dohmann, K., Austen, M., and Luscher, B. (2003). Stimulation of c-MYC transcriptional activity and acetylation by recruitment of the cofactor CBP. EMBO Rep *4*, 484-490.

Vinson, C.R., Sigler, P.B., and McKnight, S.L. (1989). Scissors-grip model for DNA recognition by a family of leucine zipper proteins. Science *246*, 911-916.

Vita, M., and Henriksson, M. (2006). The Myc oncoprotein as a therapeutic target for human cancer. Semin Cancer Biol *16*, 318-330.

Vo, B.T., Wolf, E., Kawauchi, D., Gebhardt, A., Rehg, J.E., Finkelstein, D., Walz, S., Murphy, B.L., Youn, Y.H., Han, Y.G.*, et al.* (2016). The Interaction of Myc with Miz1 Defines Medulloblastoma Subgroup Identity. Cancer Cell *29*, 5-16.

Walsby, E., Lazenby, M., Pepper, C., and Burnett, A.K. (2011). The cyclin-dependent kinase inhibitor SNS-032 has single agent activity in AML cells and is highly synergistic with cytarabine. Leukemia *25*, 411-419.

Walz, S., Lorenzin, F., Morton, J., Wiese, K.E., von Eyss, B., Herold, S., Rycak, L., Dumay-Odelot, H., Karim, S., Bartkuhn, M.*, et al.* (2014). Activation and repression by oncogenic MYC shape tumour-specific gene expression profiles. Nature *511*, 483-487.

Watt, R.A., Shatzman, A.R., and Rosenberg, M. (1985). Expression and characterization of the human c-myc DNA-binding protein. Mol Cell Biol *5*, 448-456.

Weiss, M.S. (2001). Global indicators of X-ray data quality. Journal of applied crystallography *34*, 130-135.

Weiss, M.S., and Hilgenfeld, R. (1997). On the use of the merging R factor as a quality indicator for X-ray data. Journal of applied crystallography *30*, 203-205.

Wells, J.A., and McClendon, C.L. (2007). Reaching for high-hanging fruit in drug discovery at protein-protein interfaces. Nature *450*, 1001-1009.

Westermarck, J., and Hahn, W.C. (2008). Multiple pathways regulated by the tumor suppressor PP2A in transformation. Trends Mol Med *14*, 152-160.

Wiegering, A., Uthe, F.W., Jamieson, T., Ruoss, Y., Huttenrauch, M., Kuspert, M., Pfann, C., Nixon, C., Herold, S., Walz, S.*, et al.* (2015). Targeting Translation Initiation Bypasses Signaling Crosstalk Mechanisms That Maintain High MYC Levels in Colorectal Cancer. Cancer Discov *5*, 768-781.

Wiese, K.E., Haikala, H.M., von Eyss, B., Wolf, E., Esnault, C., Rosenwald, A., Treisman, R., Klefstrom, J., and Eilers, M. (2015). Repression of SRF target genes is critical for Myc-dependent apoptosis of epithelial cells. Embo J *34*, 1554-1571.

Wiese, K.E., Walz, S., von Eyss, B., Wolf, E., Athineos, D., Sansom, O., and Eilers, M. (2013). The Role of MIZ-1 in MYC-Dependent Tumorigenesis. Cold Spring Harbor Perspectives in Medicine *3*, a014290-a014290.

Winn, M.D., Ballard, C.C., Cowtan, K.D., Dodson, E.J., Emsley, P., Evans, P.R., Keegan, R.M., Krissinel, E.B., Leslie, A.G., McCoy, A.*, et al.* (2011). Overview of the CCP4 suite and current developments. Acta crystallographica Section D, Biological crystallography *67*, 235-242.

Winter, G.E., Buckley, D.L., Paulk, J., Roberts, J.M., Souza, A., Dhe-Paganon, S., and Bradner, J.E. (2015). Phthalimide conjugation as a strategy for in vivo target protein degradation. Science *348*, 1376-1381.

Wolf, E., Gebhardt, A., Kawauchi, D., Walz, S., von Eyss, B., Wagner, N., Renninger, C., Krohne, G., Asan, E., Roussel, M.F.*, et al.* (2013). Miz1 is required to maintain autophagic flux. Nature Communications *4*, 1-12.

Wolf, E., Lin, C.Y., Eilers, M., and Levens, D.L. (2014). Taming of the beast: shaping Myc-dependent amplification. Trends Cell Biol, 1-8.

Wolfe, A.L., Singh, K., Zhong, Y., Drewe, P., Rajasekhar, V.K., Sanghvi, V.R., Mavrakis, K.J., Jiang, M., Roderick, J.E., Van der Meulen, J.*, et al.* (2014). RNA G-quadruplexes cause eIF4A-dependent oncogene translation in cancer. Nature *513*, 65-70.

Wu, S.Y., and Chiang, C.M. (2007). The double bromodomain-containing chromatin adaptor Brd4 and transcriptional regulation. J Biol Chem *282*, 13141-13145.

Xiao, Q., Claassen, G., Shi, J., Adachi, S., Sedivy, J., and Hann, S.R. (1998). Transactivation-defective c-MycS retains the ability to regulate proliferation and apoptosis. Genes Dev *12*, 3803-3808.

Yang, Z., Yik, J.H., Chen, R., He, N., Jang, M.K., Ozato, K., and Zhou, Q. (2005). Recruitment of P-TEFb for stimulation of transcriptional elongation by the bromodomain protein Brd4. Molecular cell *19*, 535-545.

Yap, J.L., Wang, H., Hu, A., Chauhan, J., Jung, K.-Y., Gharavi, R.B., Prochownik, E.V., and Fletcher, S. (2013). Pharmacophore identification of c-Myc inhibitor 10074-G5. Bioorg Med Chem Lett *23*, 370-374.

Ye, T., Krebs, A.R., Choukrallah, M.A., Keime, C., Plewniak, F., Davidson, I., and Tora, L. (2011). seqMINER: an integrated ChIP-seq data interpretation platform. Nucleic Acids Res *39*, e35-e35.

Yeh, E., Cunningham, M., Arnold, H., Chasse, D., Monteith, T., Ivaldi, G., Hahn, W.C., Stukenberg, P.T., Shenolikar, S., Uchida, T.*, et al.* (2004). A signalling pathway controlling c-Myc degradation that impacts oncogenic transformation of human cells. Nat Cell Biol *6*, 308-318.

Yin, X., Giap, C., Lazo, J.S., and Prochownik, E.V. (2003). Low molecular weight inhibitors of Myc-Max interaction and function. Oncogene *22*, 6151-6159.

You, W.C., Chiou, S.H., Huang, C.Y., Chiang, S.F., Yang, C.L., Sudhakar, J.N., Lin, T.Y., Chiang, I.P., Shen, C.C., Cheng, W.Y.*, et al.* (2013). Mitochondrial protein ATPase family, AAA domain containing 3A correlates with radioresistance in glioblastoma. Neuro Oncol *15*, 1342-1352.

Zeller, K.I., Jegga, A.G., Aronow, B.J., O'Donnell, K.A., and Dang, C.V. (2003). An integrated database of genes responsive to the Myc oncogenic transcription factor: identification of direct genomic targets. Genome biology *4*, R69.

Zhang, Y., Liu, T., Meyer, C.A., Eeckhoute, J., Johnson, D.S., Bernstein, B.E., Nusbaum, C., Myers, R.M., Brown, M., Li, W.*, et al.* (2008). Model-based analysis of ChIP-Seq (MACS). Genome biology *9*, R137.

Zirath, H., Frenzel, A., Oliynyk, G., Segerström, L., Westermark, U.K., Larsson, K., Munksgaard Persson, M., Hultenby, K., Lehtiö, J., Einvik, C*., et al.* (2013). MYC inhibition induces metabolic changes leading to accumulation of lipid droplets in tumor cells. Proc Natl Acad Sci USA.

Zuber, J., Shi, J., Bradner, J.E., and Lowe, S.W. (2011). RNAi screen identifies Brd4 as a therapeutic target in acute myeloid leukaemia. Nature *478*, 524-528.

7 Appendix

7.1 Abbreviations

Prefixes

p	pico
n	nano
µ	micro
m	milli
c	centi
k	kilo

Units

A	ampere
Å	ångström
Da	dalton
g	gram
h	hour
J	joule
l	liter
m	meter
min	minute
M	mol/l
OD	optical density
s	second
v/v	volume per volume
w/v	weight per volume
°C	degree celsius

Further abbreviations

α	anti
A	adenine
A	alanine, Ala

A_{xxx}	measured by absorbance at xxx nm
aa	amino acid
ABL	Abelson murine leukemia viral oncogene homolog 1, also known as ABL1
ADA	N-(2-Acetamido)iminodiacetic acid
AG	German *Arbeitsgruppe*, English *working group*
ALL	acute lymphoblastic leukemia
AML	acute myeloid leukemia
ANCOVA	analysis of covariances
APS	ammoniumpersulfate
ATCC	American Type Culture Collection
ATP	adenosin-5'-triphosphate
AU	arbitrary unit
b	basic region
b/HLH/Zip	basic helix-loop-helix leucine zipper domain
b2M	β2-microglobulin
BCA	bicinchoninic acid
BCR	breakpoint cluster region
BESSY	Berliner Elektronenspeicherring-Gesellschaft für Synchrotronstrahlung
BET	bromodomain and extra-terminal
bp	base pairs
BrdU	5-bromo-2-deoxyuridine
BSA	bovine serum albumine
C	cytosine
C	cysteine, Cys
Cas	CRISPR associated proteins
CCD	charge-coupled device
CCP4	Collaborative Computational Project, Number 4, 1994
CPM	counts per million
CPP	cell-penetrating peptides
cDNA	complementary DNA
CDK	cyclin-dependent kinase
CDS	coding sequence
CHES	2-(Cyclohexylamino)ethanesulfonic acid
ChIP	chromatin immunoprecipitation
ChIP-seq	chromatin immunoprecipiation followed by deep-sequencing
CI	Combinatory Index
CLL	chronic lymphocytic leukemia
CML	chronic myeloid leukemia
CMV	cyctomegalovirus
CoA	Coenzyme A

cond. [%]	conductivity as in percentage of full range
comp.	competitor
c_{prot}	protein concentration
CRISPR	Clustered regularly interspaced short palindromic repeats
CTD	C-terminal domain (of RNA polymerase II)
Ctrl	control
CV	column volume
D	aspartic acid, Asp
DAVID	Database for Annotation, Visualization and Integrated Discovery
ddH_2O	bidestilled water
DMEM	Dulbecco's Modified Eagle Medium
DMSO	dimethylsulfoxide
DNA	deoxyribonucleic acid
dNTP	deoxyribonucleoside-5'-triphosphate (dATP, dCTP, dGTP, dTTP)
DOX	doxycycline
ds	double-stranded
DTT	dithiothreitol
E	glutamic acid, Glu
E. coli	*Escherichia coli*
E-box	enhancer box
Eμ	immunoglobulin heavy chain enhancer
EC_{50}	half-maximal effective concentration
ECL	enhanced chemoluminescence
EDTA	ethylendiamintetraacetate
e.g.	exempli gratia, for example
EMSA	electrophoretic mobility shift assay
ER	endoplasmic reticulum
ES	enrichment score
ESRF	European Synchrotron Radiation Facility
F	phenylalanine, Phe
for	forward
EGF	epidermal growth factor
FBS	fetal bovine serum
FC	fold change
FDA	U.S. Food and Drug Administration
FDR	false discovery rate
FL	full length
FL	Florida
FLAG	epitope encompassing the DYKDDDDK amino acid sequence
FPLC	fast protein liquid chromatography

FRET	fluorescence resonance energy transfer
g	rcf, relative centrifugal force
G	guanine
G	glycine, Gly
GFP	green fluorescent protein
GO	gene ontology
GSEA	gene set enrichment analysis
GSH	glutathione
GST	glutathione-S-transferase
GTP	guanosine-5'-triphosphate
H	histidine, His
H_2O_2	hydrogen peroxide
HA	human influenza hemagglutinin
HAT	histone acetyl transferase
HeLa	human cervix carcinoma cell line taken from Henrietta Lacks
HDAC	histone deacetylase
HF	high fidelity
hg19	human genome, assembly 19
His_6-tag	hexahistidine tag
HLH	helix-loop-helix
HEPES	2-[4-(2-hydroxyethyl)piperazin-1-yl]ethanesulfonic acid
HGNC	Human Genome Organisation Gene Nomenclature Committee
HRP	horseradish peroxidase
I	isoleucine, Ile
i.a.	inter alia, among other things
IC_{50}	half-maximal inhibitory concentration
i.e.	id est, that is
IEC	ion exchange chromatography
IF	immunofluorescence
IGB	Integrated Genome Browser
IgG	immunoglobulin
IMAC	immobilized metal affinity chromatography
incl.	including
IP	immunoprecipitation
IPTG	isopropyl β-D-1-thiogalactopyranoside
IRES	internal ribosomal entry site
K	lysine, Lys
K	Kelvin
K_d	dissociation constant
L	leucine, Leu

LB	lysogeny broth
lncRNA	long non-coding RNA
M	methionine, Met
Mb	MYC box
MES	2-(N-morpholino)ethanesulfonic acid
miRNA	micro RNA
MOPS	3-Morpholinopropane-1-sulfonic acid
MOI	multiplicity of infection
MR	molecular replacement
MTT	3-(4,5-dimethylthiazol-2-yl)-2,5-diphenyltetrazolium bromide
mRNA	messenger RNA
MWCO	molecular weight cut-off
N	asparagine, Asn
N/A	not applicable, not available
NEM	N-ethylmaleimide
NES	normalized enrichment score
NLS	nuclear localization signal
NP-40	nonidet P-40
NSCLC	non-small-cell lung carcinoma
NTA	nitrilotriacetic acid
OD_{600}	optical density (= absorbance) measured at a wavelength of 600 nm
OHT	4-hydroxytamoxifen
p	phospho
p	probability value (statistics)
P	proline, Pro
PAGE	polyacrylamide gel electrophoresis
PCR	polymerase chain reaction
PDB	Protein Data Bank
PEG	polyethylene glycol
PEI	polyethylenimine
PGK	phosphoglycerate kinase
PIPES	1,4-piperazinediethanesulfonic acid
PMSF	phenylmethylsulfonyl fluoride
PNI	protein-nucleic acid interaction
PPI	protein-protein interaction
PVDF	polyvinylidene difluoride
qPCR	quantitative PCR
R	arginine, Arg
rev	reverse
rmsd	root-mean-square deviation

RNA	ribonucleic acid
RNAi	RNA interfernce
RNAP	RNA polymerase
RNA-seq	RNA-sequencing using next-generation sequencing
RNase	ribonuclease
RPKM	reads per kilobase per million mapped reads
RQI	RNA quality indicator
rRNA	ribosomal RNA
RT	room temperature
S	serine, Ser
S	Svedberg
S1	biosafety level 1 (Schutzstufe 1)
S2	biosafety level 2 (Schutzstufe 2)
SCLC	small-cell lung carcinoma
SD	standard deviation
SD	Superdex
SDS	sodium dodecyl sulfate
SDS-PAGE	SDS polyacrylamide gel electrophoresis
SEC	size-exclusion chromatography
SEM	standard error of the mean
siRNA	small interfering RNA
shRNA	short hairpin RNA
SLIC	sequence and ligation independent cloning
snoRNA	small nucleolar RNA
S-phase	synthesis phase
T	thymine
T	threonine, Thr
$t_{1/2}$	half-life
TAPS	3-[[1,3-dihydroxy-2-(hydroxymethyl)propan-2-yl]amino]propane-1-sulfonic acid
TBE	Tris-borate EDTA buffer
TBS	Tris-buffered saline
TBS-T	Tris-buffered saline with tween-20
TE	Tris-EDTA buffer
TEMED	N,N,N',N'-tetramethylethylendiamine
Tet-On	tetracycline-controlled transcriptional activation technology
T_m	melting temperature
TRD	transregulatory domain
Tris	Tris-(hydroxymethyl)-aminomethan
tRNA	transfer RNA

TSS	transcriptional start site
U	uridine
Ub	ubiquitin
UCSC	University of California, Santa Cruz
UPS	ubiquitin-proteasome system
USA	United States of America
USP	ubiquitin-specific-protease
UTR	untranslated region
V	valine, Val
vs.	versus
W	tryptophan, Trp
WT	wild type
x	fold
Y	tyrosine, Tyr
Zip	leucine zipper
$2F_o-F_c$	observed reflection amplitudes (F_o) - calculated reflection amplitudes (F_c)

7.2 Additional Tables

Table 7.1: Composition of the thermofluor buffer screen
(100 mM buffer each)

Well	Buffer condition	Well	Buffer condition
A1	Citrate pH 4.5	E1	Cacodylate pH 6.0
A2	Bis-Tris pH 7.0	E2	Bis-Tris propane pH 7.0
A3	Imidazole pH 6.5	E3	MOPS pH 7.0
A4	HEPES pH 8.0	E4	Bicine pH 9.0
A5	Tris pH 8.5	E5	Glycylglycine pH 8.5
A6	reference	E6	reference
B1	Acetate pH 4.6	F1	Cacodylate pH 6.5
B2	ADA pH 6.5	F2	PIPES pH 6.5
B3	Imidazole pH 8.0	F3	MOPS pH 7.5
B4	HEPES pH 8.5	F4	Tris pH 7.0
B5	Tris pH 9.0	F5	CHES pH 9.0
B6	reference	F6	water
C1	MES pH 5.5	G1	Bis-Tris pH 5.5
C2	ADA pH 7.0	G2	PIPES pH 7.0
C3	Na/K PO$_4$ pH 6.8	G3	HEPES pH 7.0
C4	Bicine pH 8.0	G4	Tris pH 7.5
C5	TAPS pH 8.0	G5	CHES pH 9.5
C6	reference	G6	water
D1	MES pH 6.5	H1	Bis-Tris pH 6.5
D2	Bis-Tris propane pH 6.0	H2	PIPES pH 7.5
D3	Na/K-PO$_4$ pH 7.55	H3	HEPES pH 7.5
D4	Bicine pH 8.5	H4	Tris pH 8.0
D5	TAPS pH 9.0	H5	CAPS pH 9.8
D6	reference	H6	water

Table 7.2: Statistics for data collection, refinement and anisotropy of the OmoMYC crystal structures.
This table was generated by Wolfgang Kölmel.

A. Data collection and refinement statistics

	Apo structure	DNA bound structure
Data collection and processing		
Wavelength (Å)	1.06448	0.91841
Spacegroup	$P\,4_122$	$P\,2_1$
Unit cell parameters	a = 65.7 Å; b = 65.7 Å; c = 149.5 Å	a = 36.5 Å; b = 95.5 Å; c = 64.9 Å
	$\alpha = 90.0°$; $\beta = 90.0°$; $\gamma = 90.0°$	$\alpha = 90.0°$; $\beta = 105.9°$; $\gamma = 90.0°$
Resolution range (Å)	49.35 – 1.95	47.77 – 2.70
High resolution shell (Å)	2.00 – 1.95	2.83 – 2.70
R_{merge}	0.055 (0.818)	0.116 (0.845)
R_{merge} in top intensity bin	0.025	0.028
R_{meas}	0.061 (0.925)	0.126 (0.919)
$<I/\sigma I>$	17.1 (1.7)	11.9 (2.4)
$CC_{1/2}$	0.999 (0.646)	0.999 (0.593)
Multiplicity	5.4 (4.4)	6.8 (6.6)
Completeness (%)	99.3 (92.9)	99.4 (100.0)
Number of observations	131951 (6892)	79640 (10358)
Number of unique observations	24551 (1569)	11787 (1576)
Refinement		
Resolution range (Å)	49.35 – 1.95	37.95 – 2.70
R_{work}	0.173	0.227
R_{free}	0.194	0.279
Number of reflections	24506	11726
Number of atoms / residues	1390 / 148	2462 / 188
Coordinate error (Å)	0.17	0.40
B factor (Å^2)		
Protein (Chain A/B)	51.90/48.74	79.54/83.44
DNA (Chain C/D)	-	90.73/100.39
Heteroatoms	62.85	-
Water	47.95	-
Deviations from ideal values		
Bond (Å)	0.011	0.006
Angle (°)	1.135	0.776
Chirality (°)	0.053	0.034
Planarity (Å)	0.005	0.004
Dihedral (°)	14.944	23.703
Ramachandran statistics (%)		
Favored	100.0	94.6
Allowed	0.0	4.3
Outlier	0.0	1.1

(The statistics for the highest resolution shell are given in parentheses)

B. Data anisotropy as reported by AIMLESS

Principal axis	Resolution (Å) $CC_{1/2} > 0.5$	Resolution (Å) $<I/\sigma I> > 2.00$
d1	2.47	2.18
d2 (unique b-axis)	2.60	2.37
d3	3.77	3.72

Table 7.3: List of interactions in protein-protein interface of the OmoMYC crystal structures and the MYC/MAX structure.

Numbering of the MYC protein was according to (Nair and Burley, 2003). Distance measurements [Å] were performed on the OmoMYC apo structure and contacts mediated by water molecules were included. An asterisk (*) indicates interactions that cannot be verified with high certainty in the DNA-bound OmoMYC crystal structure due to the lower resolution, (-) indicates that this interaction may be found in the apo-structure only. This table was generated together with Wolfgang Kölmel.

OmoMYC homodimer (PDB code 5I4Z)

Amino acid	Chain	Amin acid	Chain	vice versa B-A	Comment	Distance [Å]	
E22	A	K50	B	x	salt bridge	3.1	
L23	A	L23	B	x	no direct hydrophobic interaction, but part of a hydrophobic pocket	7.6	
L23	A	L49	B	x	hydrophobic interaction	3.7	
S26	A	K50	B	x	hydrogen bond	3.2	*
S26	A	T53	B	x	hydrogen bond, backbone via water	2.8	
F27	A	F27	B	x	hydrophobic interaction	3.6	
F27	A	L49	B	x	hydrophobic interaction	3.8	
L30	A	L30	B	x	hydrophobic interaction	4.1	
L30	A	I56	B	x	hydrophobic interaction	3.8	
L30	A	A52	B	x	hydrophobic interaction	3.9	-
Q33	A	Q60	B		2 hydrogen bonds bridged by water molecules	2.9	
Q33	A	Q60	B	x	hydrogen bond of carbonyl oxygen of Q33 bridged by water	2.6	
I34	A	L37	A	x	hydrophobic interaction	4.0	
I34	B	I56	B	x	no direct hydrophobic interaction, but part of a hydrophobic pocket	4.9	
K45	A	K45	B	x	weak hydrogen bond bridged by water	2.9	
V46	A	E22	B		hydrophobic interaction	4.1	-
V46	A	L23	B	x	hydrophobic interaction	4.0	
L23	A	V46	B		no direct hydrophobic interaction, but part of a hydrophobic pocket	4.3	
L49	A	L49	B	x	hydrophobic interaction	3.6	
A52	A	A52	B	x	no direct hydrophobic interaction, but part of a hydrophobic pocket	5.6	
T53	A	Q33	B	x	hydrophobic interaction	3.7	
Y55	A	Q60	B	x	hydrogen bond	2.5	
Y55	A	I56	B	x	hydrophobic interaction	3.5	
I56	A	I56	B	x	hydrophobic interaction	3.8	
V59	A	V59	B	x	hydrophobic interaction	3.7	
T63	A	T63	B	x	hydrogen bond bridged by water molecules; stabilized by V59	2.7	*
T63	A	L66	B	x	hydrophobic interaction	3.7	
L66	A	L66	B	x	hydrophobic interaction	4.2	
L66	A	I70	B	x	no direct hydrophobic interaction, but part of a hydrophobic pocket	3.6	
I67	A	L66	B	x	hydrophobic interaction	4.3	
E69	A	R74	B		hydrogen bond	3.4	
R74	B	E69	A		salt bridge	2.8	
I70	A	I70	B	x	hydrophobic interaction	3.4	
L73	A	L73	B	x	hydrophobic interaction	4.0	
L73	A	R74	B	x	hydrophobic interaction	4.0	
L73	A	I70	B	x	hydrophobic interaction	3.9	*
N77	A	N77	B	x	hydrogen bond	3.0	
N77	B	K81	B		hydrogen bond	3.4	
L80	A	L80	B	x	hydrophobic interaction	4.0	
L80	A	L84	B	x	hydrophobic interaction	3.8	
L80	A	K81	B	x	hydrophobic interaction	3.9	*
K83	A	R88	B		hydrogen bond bridged by water	2.7	*
K83	A	L84	B	x	hydrophobic interaction	4.0	
L87	A	L87	B	x	hydrophobic interaction	4.0	
L87	A	L84	B	x	hydrophobic interaction	3.6	
L87	A	R88	B	x	hydrophobic interaction	3.8	
C91	A	C91	B	x	disulfide bridge	2.1	
C91	A	A92	B		hydrogen bond, backbone interaction	2.9	

MYC/MAX heterodimer (PDB code 1NKP)

Amino acid	Chain	Amin acid	Chain	vice versa B-A	Comment	Distance [Å]
L917	A	L943	B		hydrophobic interaction	3.9
L917	A	A940	B		no direct hydrophobic interaction, but part of a hydrophobic pocket	4.2
I917	B	V940	A		hydrophobic interaction	3.8
I917	B	L943	A		hydrophobic interaction	3.9
S920	A	D944	B		hydrogen bond	3.0
F921	A	F921	B		hydrophobic interaction	3.6
F921	A	L943	B		hydrophobic interaction	3.9
F921	B	L943	A		hydrophobic interaction	4.0
L924	A	L924	B	x	hydrophobic interaction	4.1
L924	A	L943	B		hydrophobic interaction	3.6
L924	A	I950	B		hydrophobic interaction	3.9
I928	A	I950	B		no direct hydrophobic interaction, but part of a hydrophobic pocket	4.8
V928	B	I950	A		hydrophobic interaction	4.0
I950	A	L924	B		hydrophobic interaction	3.7
L943	A	L924	B		hydrophobic interaction	3.7
Q927	A	R954	B		hydrogen bond + hydrogen bond backbone	2.4
S927	B	Q954	B		hydrogen bond, backbone interaction	3.0
L943	A	L943	B	x	hydrophobic interaction	3.9
A946	A	A946	B		no direct hydrophobic interaction, but part of a hydrophobic pocket	4.7
A946	B	L924	A		no direct hydrophobic interaction, but part of a hydrophobic pocket	4.2
T947	A	S920	B	x	hydrogen bond, backbone interaction via water	2.9
Y949	A	R954	B		hydrogen bond	2.9
Y949	A	I950	B		hydrophobic interaction	3.5
Y949	B	Q954	A		hydrogen bond	3.1
Y949	B	I950	A		hydrophobic interaction	3.7
I950	A	I950	B		hydrophobic interaction	3.8
V953	A	M953	B		hydrophobic interaction	3.4
E957	A	K956	B		salt bridge	3.1
N957	B	V953	A		weak hydrogen bond, backbone interaction	3.2
L960	A	I964	B		hydrophobic interaction	3.9
L960	A	H960	B		hydrophobic interaction	3.6
H960	B	E964	A		hydrogen bond	3.5
I961	A	H960	B		no direct hydrophobic interaction, but part of a hydrophobic pocket	4.3
I964	B	L967	A		hydrophobic interaction	3.5
L967	A	L967	B	x	hydrophobic interaction	4.0
L967	A	K968	B		hydrophobic interaction	3.9
R968	A	L976	B		hydrophobic interaction	3.8
R970	A	E975	B		salt bridge	2.9
R970	A	N971	B		hydrogen bond via water	2.9
R971	A	Q970	B		hydrogen bond	3.0
L974	A	L974	B	x	hydrophobic interaction	3.8
L974	A	V978	B		hydrophobic interaction	4.0
L974	B	L978	A		hydrophobic interaction	4.0
L974	B	K975	A		no direct hydrophobic interaction, but part of a hydrophobic pocket	4.1
E975	B	L974	A		no direct hydrophobic interaction, but part of a hydrophobic pocket	4.1
L978	A	V978	B		hydrophobic interaction	3.4
L978	A	L981	B		hydrophobic interaction	4.0
V978	B	L981	A		hydrophobic interaction	4.0
V978	B	K977	A		hydrophobic interaction	3.7
L978	A	Q977	B		hydrophobic interaction	3.7
L981	A	L981	B	x	no direct hydrophobic interaction, but part of a hydrophobic pocket	4.3

Table 7.4: Solvation free energy values of the protein-protein and protein-DNA interface.
PDBePISA was used to estimate free energies gained upon formation of the indicated interfaces. Total free energy upon binding (ΔiG total) was calculated adding the effect of the interactions (hydrogen bonds (-0.44 kcal/mol per bond), salt bridges (-0.15 kcal/mol per salt bridge) and disulfide bridges (-4.00 kcal/mol per bond) across the interface, as solvation free energy values (ΔiG solvation) do not include the effect of these interactions. Only interactions recognized by PDBePISA were included in the calculation. Addition of ΔiG total values from the protein-protein as well as the protein-DNA interface yielded ΔiG total protein + DNA.

	MYC-MAX + DNA		MAX-MAX + DNA		OmoMYC + DNA		OmoMYC apo
	1NKP		1AN2		5I50		5I4Z
interface	protein-protein	protein-DNA	protein-protein	protein-DNA	protein-protein	protein-DNA	protein-protein
ΔiG solvation [kcal/mol]	-27.6	-30.6	-18.2	-26.6	-32.0	-22.3	-33.3
ΔiG [kcal/mol] protein-protein only	-32.8	-	-22.6	-	-40.6	-	-41.7
ΔiG [kcal/mol] protein-DNA only	-	-42.0	-	-35.4	-	-33.3	-
ΔiG total [kcal/mol] protein + DNA	-74.8		-58.0		-73.9		-

Table 7.5: Rmsd calculations of the different available apo and DNA-bound MYC, MAX and OmoMYC crystal structures.
Table A: Superposition of main chain atoms of the indicated crystal structures. Table B: Superposition of the basic (b) and the helix-loop-helix (HLH) regions, i.e. the DNA-binding region of the MYC, MAX and OmoMYC DNA-bound structures. PDB codes are given in parentheses. Rmsd values of the main chain atoms were calculated using PyMOL.

A.

Model 1 (fixed)	Model 2 (superimposed)	Main chain atoms of residues superimposed	rmsd [Å]
OmoMYC+DNA (5I50)	OmoMYC apo (5I4Z)	19-92	0.600
OmoMYC+DNA (5I50)	MYC-MAX+DNA (1NKP)	Entire range	0.584
OmoMYC+DNA (5I50)	MAX-MAX+DNA (1AN2)	Entire range	1.045
MYC-MAX+DNA (1NKP)	MAX-MAX+DNA (1AN2)	Entire range	0.979

B.

Model 1 (fixed)	Model 2 (superimposed)	Main chain atoms of regions superimposed	rmsd [Å]
OmoMYC+DNA (5I50)	MYC-MAX+DNA (1NKP)	b + HLH	0.426
		b	0.601
OmoMYC+DNA (5I50)	MAX-MAX+DNA (1AN2)	b + HLH	0.876
		b	0.842

Table 7.6: Genes selected as targets for the shRNA screen and information regarding their druggability.
Inhibitor names are given in italics. *:only expert-curated druggability from dGidb included; **: also non-expert curated information from dGidb is included; inh.: inhibitor; dGidb: druggability given in dGidb database.

	gene symbol	protein itself druggalbe*	partner protein druggable**	linked pathway druggable
1	ADRM1	*RA190*		
2	AMPD2	dGidb		
3	ANKRD13B			EGFR
4	ARC			MAPK
5	ASL		*MDLA*: ASS1 inh.	
6	ATAD3A			mitochrondrial dynamics
7	BOP1		*CX-5461*: Pol1 inh.	
8	CDC42EP1			Rho
9	DOHH		*GC7:* deoxyhypusine synthase inh.	
10	FZD8	*OMP-54F28*		
11	GAREML/ FAM59B			MAPK
12	MRPL41		*Tigecycline*	
13	PHLDA2			AKT
14	PIM3	*AZD-1208*		
15	POLRMT	*Tigecycline*		
16	RGS16			Rho
17	SH3GL1			EGFR
18	SLC19A1		*Methotrexate*: DHFR inh.	
19	SLC1A5	*Benzylserine*		
20	SLC4A2	dGidb		
21	SLC52A2		dGidb	
22	SLC7A5	*BCH*		
23	SLCO4A1	*DIDS*		
24	SNAI1	*GN-25*		
25	SPHK1	*SKI-I* (i.a.)		
26	SPNS1	dGidb		
27	SRM		*DFMO*: ODC inh.	

7.3 Acknowledgements

7.4 Publications

Jung, L.A.*, Gebhardt, A.*, Koelmel, W., Ade, C.P., Walz, S., Kuper, J., von Eyss, B., Letschert, S., Redel, C., d'Artista, L., Biankin, A., Zender, L., Sauer, M., Wolf, E., Evan, G., Kisker, C., Eilers, M. (2016). OmoMYC blunts promoter invasion by oncogenic MYC to inhibit gene expression characteristic of MYC-dependent tumors. Oncogene.
*these authors contributed equally

Lorenzin, F., Benary, U., Baluapuri, A., Walz, S., **Jung, L.A.**, von Eyss, B., Kisker, C., Wolf, J., Eilers, M., and Wolf, E. (2016). Different promoter affinities account for specificity in MYC-dependent gene regulation. Elife 5.

Deak, E., Ruster, B., **Keller, L.**, Eckert, K., Fichtner, I., Seifried, E., and Henschler, R. (2010). Suspension medium influences interaction of mesenchymal stromal cells with endothelium and pulmonary toxicity after transplantation in mice. Cytotherapy 12, 260-264. (publication results from work in the Henschler lab)

7.5 Affidavit

I hereby confirm that my thesis entitled "Targeting MYC Function as a Strategy for Tumor Therapy" is the result of my own work. I did not receive any help or support from commercial consultants. All sources and/or materials are listed and specified in the thesis.

Furthermore, I confirm that this thesis has not yet been submitted as part of another examination process neither in identical nor in similar form.

_____   _____

Place, Date   Signature

7.6   Curriculum vitae